Laboratory and field studies of ~~Ice~~ice-nucleating particles from open-lot livestock facilities in Texas

Naruki Hiranuma[1], Brent W. Auvermann[2], Franco Belosi[3], Jack Bush[2], Kimberly M. Cory[1,4], ~~Romy Ullrich-Fösig[5],~~ Dimitrios G. Georgakopoulos[5~~6~~], Kristina Höhler[6~~5~~], Yidi Hou[1], Larissa Lacher[6~~5~~], Harald Saathoff[6~~5~~], Gianni Santachiara[3], Xiaoli Shen[6~~5~~,7], Isabelle Steinke[6~~5~~,8], Romy Ullrich[6], Nsikanabasi S. Umo[6~~5~~], Hemanth S. K. Vepuri[1], Franziska Vogel[6~~5~~], Ottmar Möhler[6~~5~~]

[1]Department of Life, Earth, and Environmental Sciences, West Texas A&M University, Canyon, TX 79016, USA
[2]Texas A&M AgriLife Research, Amarillo, TX 79106, USA
[3]Institute of Atmospheric Sciences and Climate, National Research Council, Bologna, 40129, Italy
[4]Department of Environmental Toxicology, Texas Tech University, Lubbock, TX 79409, USA
[5]Department of Crop Science, Agricultural University of Athens, Athens, 118 55, Greece
[6~~5~~]Institute of Meteorology and Climate Research, Karlsruhe Institute of Technology, Karlsruhe, 76021, Germany
~~[6]Department of Crop Science, Agricultural University of Athens, Athens, 118 55, Greece~~
[7]Department of Earth Atmospheric and Planetary Sciences, Purdue University, West Lafayette, IN 47907, USA
[8]Atmospheric Sciences & Global Change, Pacific Northwest National Laboratory, Richland, WA 99354, USA

Correspondence: Naruki Hiranuma (nhiranuma@wtamu.edu)

Keywords. Ice, Freezing, Cloud, Cattle, Open-Lot Livestock Facility, Soil Dust

Abstract.

In this work, an abundance of ice-nucleating particles (INPs) from livestock facilities was studied through laboratory measurements from cloud simulation chamber experiments and field investigation in the Texas Panhandle. Surface materials from two livestock facilities, one in the Texas Panhandle and another from McGregor, Texas, were selected as dust proxies for laboratory analyses. These two samples possessed different chemical and biological properties. A combination of aerosol interaction and dynamics in the atmosphere (AIDA) measurements and offline ice spectrometry was used to assess the immersion freezing mode ice nucleation ability and efficiency of these proxy samples at temperatures above -29 °C. A dynamic filter processing chamber was also used to complement the freezing efficiencies of submicron and supermicron particles collected from the AIDA chamber. For the field survey, periodic ambient particle sampling took place at four commercial livestock facilities from July 2017 to July 2019. INP concentrations of collected particles were measured using an offline freezing test system, and the data were acquired for temperatures between -5 °C and -25 °C.

Our AIDA laboratory results showed that the freezing spectra of two livestock dust proxies exhibited higher freezing efficiency than previously studied soil dust samples at temperatures below -25 °C. Despite their differences in composition, the freezing efficiencies of both proxy livestock dust samples were comparable to each other. Our dynamic filter processing chamber results showed on average approximately 50% supermicron size dominance in the INPs of both dust proxies. Thus, our laboratory findings suggest the importance of particle size in immersion freezing for these samples, and that the size might be a more important factor for immersion freezing of livestock dust than the composition. From a three-year field survey, we measured a high concentration of ambient INPs of 1,171.6 ± 691.6 L^{-1} (average ± standard error) at -25 °C for aerosol particles collected at the downwind edges of livestock facilities. An obvious seasonal variation in INP concentration, peaking in summer, was observed with the maximum at the same temperature exceeding 10,000 L^{-1} on July 23, 2018. The observed high INP concentrations suggest that a livestock facility is a substantial source of INPs. The INP concentration values from our field survey showed a strong correlation with measured particulate matter mass concentration, which supports the importance of size in ice nucleation of particles from livestock facilities.

~~This study presents a comprehensive investigation of ice-nucleating particles (INPs) from open-lot livestock facilities (OLLFs) in Texas, USA. A three-year field survey (2017 – 2019) was conducted to understand immersion-mode INP abundance from four commercial OLLFs in the Texas Panhandle in different seasons, including summer, spring, and winter. A high concentration of INPs in air, n_{INP}, of 1,171.6 ± 691.6 L^{-1} (average ± standard error) was measured at -25 °C for aerosol particles collected at the downwind edges of these OLLFs. An obvious seasonal variation in n_{INP}, peaking in summer, was observed at OLLFs with the maximum n_{INP} at the same temperature exceeding 10,000 L^{-1} on July 23, 2018. The observed high n_{INP} is an order of magnitude higher than what has been found in previous studies on fertile and agricultural soil dust INPs, and we were able to detect INPs at temperatures as high as -5 °C. Interestingly, the n_{INP} values from our field survey exhibited a strong correlation with measured particulate matter mass concentration ($r = 0.94$; $> 3 \times 10^{-7}$ g L^{-1} in summer), suggesting the importance of large particles in immersion freezing for INPs from OLLF. Motivated by these extremely high INP concentrations, we have conducted a systematic laboratory study at the Aerosol Interaction and Dynamics in the Atmosphere (AIDA) cloud chamber facility to gain further insights into INP propensity and properties of surface materials from two OLLF facilities, one in the Texas Panhandle and another from McGregor, Texas, as OLLF dust proxies. Based on a modern suite of online and offline aerosol particle characterization instruments, we examined the ice nucleation (IN) efficiency of these materials in the temperature range between -7.5 °C and -29°C.~~

~~Our laboratory results showed on average ≈ 50% supermicron size dominance in the INPs of both OLLF dust proxies with a high efficiency of immersion/condensation freezing, as represented by an ice nucleation active surface site density $n_{s,geo}$ (n_{INP} scaled to the total geometric particle surface area) of ≥ 10^{10} m^{-2} at -25 °C. This $n_{s,geo}$ value agrees reasonably well with estimates from our field survey. Therefore, the usage of OLLF surface materials as dust surrogates was verified in our AIDA-controlled laboratory study. Thus agricultural fields, especially OLLF, might represent important INP sources if these particles rise to sufficient height (i.e., cloud altitude) in the atmosphere. New data on the ice nucleation properties of OLLF dust at heterogeneous freezing temperatures above -29 °C were generated. Moreover, we successfully characterized physical, chemical, and biological properties of OLLF dust samples, finding that their IN properties remain unchanged after dry-heating at 100 °C but a subset of analyzed samples are influenced by boiling. Ice crystal residuals, or INPs that remain after the evaporation of water content, were rich in organics and low in salts. These findings imply the importance of heat-insensitive organics in OLLF dust INPs. Surprisingly, no known ice-nucleating microorganisms were found in our OLLF proxy samples. This negative result suggests that proteinaceous and biological ice-nucleating components are not the primary source of INPs from OLLFs. However, more systematic and careful studies are necessary to gain further insight into aerosol and INP properties (e.g., through analyses on ambient samples and ice crystal residuals from multiple seasons). In summary, we developed an INP parameterization for OLLF dust, which contributes to an improved understanding of INP emission and cloud microphysical processes in the supermicron-particle laden region. These OLLF INPs may directly influence the lifetime of supercooled clouds in a unique manner for this region. An application of our IN parameterization is crucial to explore the relationship between INP and supercooled cloud properties over such a predominant agricultural area.~~

1. Introduction

Atmospheric ice-nucleating particles (INPs) are a small subset of aerosol particles that initiate ice crystal formation in supercooled clouds (Vali, 1968; ~~Chapter 9 of~~ Pruppacher and Klett, 2010). While their importance, relevance, and perturbations to cloud and precipitation properties have been revealed by numerous past studies (e.g., Kanji et al., 2017 and references therein), the potential climatic impact of INPs and their representation in numerical models remain under debate (Boucher et al., 2013; Storelvmo, 2017; Zelinka et al., 2020). One of the greatest challenges in the INP research field is the fact that we do not yet understand all INP sources ~~are fast-changing~~ worldwide in part due to the ongoing global climate change (Murray et al., 2021). Thus, it is crucial to identify and characterize any perturbation sources that alter INP abundance and cloud-phase feedback.

Recently, a resurgence of "fertile-and-agricultural soil dust" (soil dust hereafter) INP research has been underway in part because of ~~recent~~ emerging concerns regarding hydrological cycle alter~~n~~ation contributed by modern agricultural practices (Alter et al., 2015; Overpeck and Udall, 2020~~; Alter et al., 2015~~). Moreover, since agricultural practices represent a substantial dust emission source, accounting for up to 25% of total global dust emission (Ginoux et al., 2012), a large amount of INPs are globally anticipated from agricultural activities. Motivated by these reasons as well as by earlier studies on ice nucleation (IN) of surface soil organic and biological samples (Schnell and Vali, 1972; 1973), more recent studies utilized various online and offline instruments. In turn, scientists now have a better understanding of ambient INP concentrations ($n_{INP,}$ per unit volume of air), especially through immersion freezing (i.e., the freezing ~~propensity of INP~~of aerosol particle(s) immersed in a supercooled droplet~~water~~), from different agricultural sources (Conen et al., 2011; Hill et al., 2016; Steinke et al., 2016; Suski et al., 2018). These efforts allow~~ed~~ for first-order~~the first-order~~ estimates of immersion mode n_{INP} from soil dust that is relevant to mixed-phase clouds (O'Sullivan et al., 2014; Tobo et al., 2014; Steinke et al., 2020). For instance, by compiling the data from the Colorado State University continuous flow diffusion chamber and an ice spectrometer, the range of measured soil dust n_{INP} at -20 °C produced by the harvesting of several crops in the High Plains region of the United States from Suski et al. (2018) spanned from ~ 0.3 to 10 L^{-1}. Based on global mean aerosol particle concentrations and immersion mode IN parameterization, O'Sullivan et al. (2014) estimated the simulated n_{INP} at -20 °C and 600 mb to range from ~ 0.01 to 8 L^{-1}. Similarly, Steinke et al. (2020) estimated that soil dust n_{INP} can be as high as approximately~~≈~~ 40 L^{-1} at -20 °C based on their laboratory-derived IN parameterization for soil dust~~s~~ from Northwestern Germany and Wyoming, USA. Overall, these measurements and approximations represent the upper bound of general field-studied n_{INP} from different geographical areas as summarized in Kanji et al. (2017; Fig. 1-10) in the same temperature~~T~~ -range, i.e. ~~~~~0.002 to 60 L^{-1} (see **Sect. ~~3.6~~ 3.2.3** for more detailed comparison discussion).

Agricultural land use ~~is in excess of 50% of~~ accounts for more than 50% of total U.S. land use according to the U.S. Department of Agriculture (Bigelow and Borchers, 2012), and there are > 26,000 "open-lot livestock facilities" (OLLFs) in the U.S. (Drouillard, 2018). The term OLLF is adapted to denote a particular type of animal-feeding operation, in which cattle livestock is raised in outdoor confinement, as distinct from partially or totally enclosed housing, and also as distinct from pasture or free-range production systems (Auvermann et al., 2004). OLLFs are common in semi-arid and arid climates. Contrasted with the alternative production systems typical of wetter and more temperate climates, they (1) are an intensified form of livestock production, generating more marketable product per unit land area with less built infrastructure, (2) make use of the elevated evaporative demand to reduce or eliminate precipitation-generated wastewater that must be controlled under water-quality regulations, and (3) capitalize on the nocturnal cooling characteristic of semi-arid and desert climates to avoid major investments in (and operating costs associated with) ventilation systems while still reducing the incidence and duration of livestock heat stress under most conditions (Auverman, 2001; Pastoor et al., 2012).

In particular, the Texas Panhandle (northern-most counties of Texas; also known as West Texas) is a major contributor to the U.S. cattle production, accounting for 42% of fed beef cattle in the U.S. and 30% of the total cattle population in Texas (> 11 million head, Annamalai et al., 2012; USDA, 2021). Annually, these cattle produce > 5 million tons of manure, which represents a complex microbial habitat containing bacteria and other microorganisms, on an as-collected basis (Von Essen and Auvermann, 2005). In general, cattle manure hosts a wide variety of bovine rumen bacteria (e.g., *Prevotellaceae*, *Clostridiales*), lipoprotein components of certain bacterial cell walls, and non-bacterial fauna of the rumen, such as fungal spores, lichens, fungi, *Plantae*, *Protista*, *Protozoa*, *Chromalveolata*, and *Archaea* (Nagaraja, 2016). Mainly by cattle movements, dried-manure become airborne (Bush et al., 2014). Agricultural dust particles observed at OLLFs have long been known to affect regional air quality because the dust emission ~~-~~flux and 24-hour averaged ground-level dust concentration can be as high as 23.5 $\mu g\ m^{-2}\ s^{-1}$ and 1,200 $\mu g\ m^{-3}$ (Bush et al., 2014; Hiranuma et al., 2011). While there has been no study on the vertical profiles of OLLF dust~~Furthermore~~, our previous study revealed a presence of OLLF-derived particles at 3.5 km downwind of the facility, suggesting their ability to be transported regionally (Hiranuma et al., 2011). Moreover, some recent studies suggest that aerosol particles emitted from agricultural activities might reach cloud heights due to wind erosion, scouring, and other relevant mechanisms (~~Steinke et al., 2020 and references therein;~~ Duniway et al., 2019; Katra, 2020; Steinke et al., 2020 and references therein). Convection and updraft system may also help the vertical transport of aerosol particles in the Southern High Plains region (Li et al., 2017).

Due to the potential to act as a prevalent point source of microbiome-enriched dust particles, ~~in the Southern High Plains region, where a convective cloud and updraft system persists (Li et al., 2017),~~ we hypothesized that an OLLF ~~can~~ could be a source of soil dust INPs. To verify this hypothesis, ~~IN propensities of aerosol particles from OLLFs,~~ IN efficiencies of OLLF proxies, ~~and~~ their physicochemical and biological properties, and IN propensities of ambient particles from OLLFs were studied in both ~~field and~~ laboratory and field settings. Specifically, we examined the immersion mode IN ability of surface-derived material samples aerosolized in a cloud simulation chamber and ambient OLLF dust ~~(~~sampled in the field through~~and analyzed in an~~ offline lab analysis~~setting) and surface-derived material samples aerosolized in the cloud simulation chamber~~. We focused on the immersion mode freezing because recent modeling simulation and remote sensing studies suggest that immersion freezing is the most prominent heterogeneous IN mechanism, ~~accounting for 85 to 99%,~~ through which ice crystals are formed in mixed-phase clouds, accounting for 85 to 99% of ice crystal formation (Hande and Hoose, 2017; Westbrook and Illingworth, 2011). ~~OLLF-emitted particles are known to include substantial amounts of organic materials. Our previous work using Raman micro-spectroscopy revealed that ≈ 96% of ambient aerosol particles sampled at the downwind edge of an OLLF contain brown or black carbon, hydrophobic humic acid, water soluble organics, less soluble fatty acids and carbonaceous materials mixed with salts and minerals (Hiranuma et al., 2011). Recently, organic acids (i.e., long-chain fatty acids) and heat stable organics were found to act as efficient INPs (DeMott et al., 2018; Perkins et al., 2020). However, our knowledge regarding what particular features of OLLF dust trigger immersion freezing at heterogeneous freezing temperatures (*T*s; i.e., size vs. composition) is still lacking. To improve our knowledge, we conducted single-particle composition analyses of different types of OLLF-derived ice crystal residual (ICR) samples. Finally~~To complement the immersion freezing results, we also~~our study~~ attempted to investigate the presence of any known biological INPs by taxonomic identification of the ~~IN-active~~ microbiome~~ and by comparing the IN ability of heat-treated samples to non-heat-treated ones~~. ~~In general, cattle manure hosts a wide variety of bovine rumen bacteria (e.g., *Prevotellaceae*, *Clostridiales*), lipoprotein components of certain bacterial cell walls, and non-bacterial fauna of the rumen, such as fungal spores, lichens, fungi, *Plantae*, *Protista*, *Protozoa*, *Chromalveolata*, and *Archaea* (Nagaraja, 2016). Hence, we examined if any IN-active cattle bovine microorganisms or associated fragments could be identified when aerosolized.~~

2. Materials and Methods

2.~~3~~1. L~~AIDA l~~aboratory study

2.~~2~~1.1. ~~Surface samples for laboratory-based experiments~~Samples

Two types of OLLF surface-derived materials, ~~namely~~ Texas-Dust-01 (TXD01) and Texas-Dust-05 (TXD05), were used ~~as surrogates for dust particles observed at the downwind location of OLLFs in Texas~~for our laboratory study~~. These proxy samples were used in our laboratory study~~ at the ~~Aerosol~~ aerosol ~~Interaction~~ interaction and ~~Dynamics~~ dynamics in the ~~Atmosphere~~ atmosphere (AIDA) facility. TXD01 is a composite sample of surface soils from several OLLFs located in the Texas Panhandle. The other sample (TXD05) originates from a research feedlot in McGregor, TX. Both samples represent a raw surface material composite from feedlot pens, where cattle are fed without antibiotics or probiotics. Soil samples were collected on September 20, 2017. All samples were scooped from the loose dry surface layer of the pens (< 5 cm). Typically, the pen surface layer only extends to a depth of about 5 cm, which represents the depth of hoof penetration into the pen surface (Guo et al., 2011). This surface layer is rich in loose manure, which is a major source of ambient OLLF dust (Bush et al., 2014; von Holdt et al., 2021). All samples were ground and sieved for grain size < 75 µm~~ in grain size~~. They were kept in chemically inert containers at room temperature until analyzed. ~~Physically pulverizing the surface samples simulates the primary emission mechanism and characteristic of OLLFs (Razote et al., 2006; Bush et al., 2014; von Holdt et al., 2021). Dry-heated samples (i.e., ~ 100 °C oven-dried for 12 hours) of each type were analyzed in this study to assess the heat tolerance of INPs. Moreover, wet-boiled samples (i.e., filter samples suspended in pure water and boiled for 20 min; Schiebel, 2017) were also examined for their INP abundance using an offline freezing technique. A summary of our sample physical properties is provided in **Table 2**In addition, we used a single particle mass spectrometer to characterize aerosol particle chemical compositions of our surface samples (presented in **SI Sect.** S**2**)~~.

The physical properties of our samples were characterized by several offline analyses. Bulk density values of both samples were measured using a gas displacement pycnometer (Quantachrome, 1200e Ultrapyc). Nitrogen adsorption-based specific surface area (*SSA*) values, Brunauer-Emmett-Teller (BET) *SSA*, for all samples were also carried out. The Autosorb iQ model 7 gas sorption system (Anton Paar, former Quantachrome Instruments) was used to measure BET *SSA*s in this study. A summary of the physical properties of our samples is provided in **Sect. 3.1.1**. In addition, we used a single-particle mass spectrometer to characterize the aerosol particle chemical compositions of our surface samples in the size range between 200 and 2500 nm presented in Supplemental Information (**SI) Sect. S1**.

~~Briefly, bulk density values of all samples were measured using a gas displacement pychnometer (Quantachrome, 1200e Ultrapyc). As seen, all measured densities are almost identical. There is no systematic difference between non-heated material densities and pre-heated ones, which may be indicative of heat-resistant features, potentially due to pre-exposure to soil *T* on average higher than ambient *T* even at the depth of 150 mm during summer (Cole et al., 2009). Next, geometric specific surface area (*SSA*) values were computed based on AIDA aerosol particle size distribution measurements (i.e., fraction of total surface area concentration to total mass concentration estimated from the size distribution data; see next section and **Table 3**). Additionally, nitrogen adsorption-based *SSA* values, Brunauer-Emmett-Teller (BET) *SSA*, for all samples are also shown in **Table 2**. The Autosorb iQ model 7 gas sorption system (Anton Paar, former Quantachrome Instruments) was used to measure BET *SSA*s in this study. The measured BET *SSA* values of OLLF samples are slightly higher compared to those of previously measured agricultural soil dust samples (0.74 – 2.31 m^2 g^{-1}; O'Sullivan et al., 2014), which suggests that TXD01 and TXD05 are more porous than these previous soil samples, leading to higher BET *SSA*. On average, our geometric *SSA* value (± standard error) is 4.59 ± 0.81 m^2 g^{-1}, which is higher than the BET *SSA* values. As demonstrated in our previous studies, a small *SSA* value is often consistent with the presence of a large aerosol particle population (Hiranuma et al., 2015). Hence, the predominance of larger particles in bulk powders assessed in BET is presumably responsible for the observed differences in these two *SSA* values (**Table2**). Indeed, the particles observed in AIDA were all ≲ 6.5 μm volume equivalent diameter, D_{ve} (**Table 3**), whereas the particles evaluated by BET were up to 75 μm. Therefore, in association with large grain size involved in the BET analysis, bulk samples might have exhibited smaller *SSA* than dry dispersed ones. Furthermore, our *SSA* measurements suggest heat-tolerance in our OLLF samples. We examined BET *SSAs* using two different degassing *Ts* (55 °C and 200 °C) for each sample within ± 10% accuracy of the BET instrument. Geometric *SSAs* of non-heated and heated samples also agreed within given standard errors. Further discussions on representativeness of the surface samples used in this study compared to ambient OLLF soil dust are provided in **Sect. 3**.~~

~~As demonstrated in our previous study, the surface area distribution of ambient OLLF dust peaks in mode diameter at ~ 10 μm (i.e., Fig. 5 of Hiranuma et al., 2011). This mode diameter is larger than surface-derived samples aerosolized and examined in the AIDA chamber (**Table 3**). However, it is cautiously noted that the ambient OLLF dust size distribution is not spatially uniform, and the emitting mechanism itself is not controllable as it highly depends on a unit of mobile livestock. Granting the primacy of hoof action as the decisive emissions mechanism of OLLF dust as described in Bush et al. (2014), a more controlled laboratory experiment has been desired to characterize IN ability of OLLF soil dust. The difference mentioned above and the demand for controllable investigation motivated analyzing IN properties of both bulk samples (< 75 μm-sieved) and aerosolized samples (≲ 6.5 μm).~~ ~~Further results and discussions about representativeness of the surface samples used in this study compared to ambient OLLF soil dust are provided in **Sect. 3**.~~

2.1.2. Cloud simulation chamber experiments

We used the AIDA expansion cloud-simulation chamber (e.g., Möhler et al., 2003) and a set of analytical instruments at the Karlsruhe Institute of Technology to conduct a laboratory campaign named TXDUST01 in 2018. ~~This study aimed at investigating the immersion mode ice-nucleating properties and other characteristics of OLLF dust proxies. We chose the AIDA chamber as our study platform because it simulates ice formation in mixed-phase clouds in a controlled setting with respect to both *T* (± 0.3 °C) and humidity (± 5%; Fahey et al. 2014).This~~ The AIDA chamber generates artificial clouds and activates particles in a simulated atmospheric cloud parcel via expansion cooling. The air volume adjacent to the chamber wall in the 84 m^3 vessel is much smaller ~~in comparison to~~than the actively mixed volume of the vessel. Hence, we neglect the so-called wall effect (e.g., particle wall deposition) in the AIDA. ~~experiment. The AIDA has been applied for the analysis of both ambient and lab-generated INPs and has facilitated characterization of many INP species with the IN efficiency uncertainty of ± 39% (Steinke et al., 2020; Ullrich et al., 2017; Niemand et al., 2012; Hoose and Möhler, 2012).~~ The AIDA measurement uncertainties for temperature, relative humidity (*RH*), and freezing efficiency are ± 0.3 °C (Möhler et al., 2003), ± 5% (Fahey et al., 2014), and ± 35% (Steinke et al., 2011). Note that the AIDA results provided a validation of the other INP spectrometers employed in this study.

An overall AIDA experimental schematic is shown in **Fig. ~~2~~1**. Our OLLF dust proxy sample was injected into the AIDA chamber in an aerosolized form by~~through~~ a rotating brush disperser (PALAS, RGB1000). ~~followed by passing through~~ A~~a~~ series of inertial cyclone impactor stages (50% cut-size diameter ~1 and 5 μm) was deployed between the disperser and the AIDA vessel to limit particle size to < 10 μm in volume equivalent diameter, D_{ve}. Physically pulverizing the surface samples simulates the primary emission mechanism, which justifies the use of RGB1000 and characterization of aerosolized OLLF samples in the AIDA chamber (von Holdt et al., 2021; Razote et al., 2006).

~~Subsequently, t~~The OLLF number concentration and particle size distribution in the AIDA chamber were~~was~~ measured prior to each simulated adiabatic expansion experiment. Specifically, a combination of a scanning mobility particle sizer (SMPS, TSI Inc., Model 3080 differential mobility analyzer and Model 3010 condensation particle counter), an aerosol particle sizer (APS, TSI Inc., Model 3321), and a condensation particle counter (CPC; TSI Inc., Model 3076) measured the ~~collectively measured the total number and size distribution of~~ aerosol particles at a horizontally extended outlet of the AIDA chamber (Möhler et al., 2006).

Table 1 summarizes estimated particle properties from individual AIDA expansion experiments. All lab data associated with this study were archived according to the AIDA experiment number (i.e., TXDUST01_number), and we share these IDs with other associated measurements~~ (e.g., INSEKT)~~. In addition, a~~A~~s seen in **Fig. ~~2~~1**, ~~a set of complementary filter samples of the~~ aerosol particles were sampled on several filter substrates directly from the AIDA chamber ~~was also collected prior to~~before expansion experiments. These filter samples were used for three complementary offline analyses. ~~Afterwards, each particle type (i.e., TXD01 and TXD05) was individually examined for its immersion freezing ability during expansion experiments.~~

~~for three purposes: (1) examining the condensation/immersion freezing ability of aerosol particle collected on nitrocellulose membrane filters (Millipore HABG04700, nominal porosity 0.45 µm) in the dynamic filter processing chamber (DFPC; Santachiara et al., 2010), (2) using them to perform measurements with the IN Spectrometer of the Karlsruhe Institute of Technology (INSEKT; Schiebel, 2017; Schneider et al., 2021), and (3) conducting metagenomics analyses to study biological components of the aerosolized samples. Afterwards, each particle type (i.e., TXD01 and TXD05) was individually examined for its immersion freezing ability during expansion experiments. To complement the AIDA chamber immersion results, INSEKT was used for aerosol particles collected on 47 mm Nuclepore filters (Whatman WHA10417012, pore size 0.2 µm) as well as for < 75 µm sieved-bulk samples collected. The DFPC technique was also used to measure the number concentration, ice-activated fraction, and nucleation efficiency of the INPs under different~~ ~~T~~ ~~conditions and for different particle sizes (i.e., PM$_1$ vs. total) collected on filters. DNA sampling for metagenomics analysis to study biological components of the OLLF bulk samples was also conducted on aerosol particles collected on the Nuclepore filters through an independent inlet.~~

~~Another motivation for using the AIDA facility is its ice-selecting pumped counterflow virtual impactor (IS-PCVI; Hiranuma et al., 2016). As detailed in~~ ~~**Supplemental Information (SI) Sect. S1**~~~~, IS-PCVI separates ICRs from interstitial particles, including cloud droplets, at~~ ~~Ts~~ ~~below -20 °C. Preserving ICRs, which are leftover INPs after the evaporation of water content, by the IS-PCVI is key for elucidating physicochemical identities of INPs. ICRs were collected using TEM grids (Ted Pella Inc., 01844N-F/01896N-F/162-100), and also compared to the total aerosol particles collected directly from the AIDA chamber on Nuclepore™ filters (Whatman, Track-Etched Membranes, 0.2 µm pore size). More detailed information about our IS-PCVI experiments in this study is provided below. Offline single particle analyses were conducted using an electron microscope (JEOL, JSM-6010LA) equipped with an energy dispersive X-ray spectroscopy function. Through this unique capability and subsequent analyses of ICR samples, we obtained detailed information on ICR composition of individual residual particles. In addition, we used a single particle mass spectrometer to characterize aerosol particle chemical compositions of our surface samples (presented in~~ ~~**SI Sect.**~~ ~~S2). Individual details of all lab and field instruments and techniques are introduced in sections below.~~

2.1.3. Ice nucleation spectrometer of the Karlsruhe Institute of Technology

~~**2.4.** Offline immersion freezing experiment techniques~~

~~To assess the ambient~~ ~~n_{INP}~~ ~~through samples collected in the field, we used an offline droplet-freezing assay instrument, the West Texas Cryogenic Refrigerator Applied to Freezing Test system (WT-CRAFT; Vepuri et al., 2021). Briefly, WT-CRAFT enables a simulation of atmospheric immersion freezing using supercooled droplets containing aerosol particles at~~ ~~$T > -25$ °C. WT-CRAFT was a replica of NIPR-CRAFT (Tobo, 2016), but the two systems currently possess different sensitivities to artifact and detectable~~ ~~T~~ ~~ranges as described in Vepuri et al. (2021). In this study, for each ambient sample, we evaluated 70 solution droplets (3 µL each) placed on a hydrophobic Vaseline layer with a cooling rate of 1 °C min^{-1}. All droplets were prepared using filter rinse suspensions with high-performance liquid chromatography (HPLC) grade water. The amount of HPLC water was determined based on the total amount of air sampled through the cross section of filter (~~~~**Table 1**~~~~), which limits the detection capability to 0.05 INP per L of air (standard~~ ~~T~~ ~~and pressure, STP). As described in Vepuri et al. (2021), by optimizing the suspension water volume, the first frozen droplet observed was considered to have 0.05 INP L^{-1} in this study. Each freezing event was determined optically based on the change in droplet brightness when the initially transparent liquid droplets became opaque upon freezing. If the freezing~~ ~~T~~ ~~was not obvious for any droplets, the 8-bit grayscale images were assessed using ImageJ software to determine the~~ ~~T~~ ~~of phase change. After the measurement, we calculated the frozen fraction and estimated the~~ ~~n_{INP}~~ ~~per volume of air as a function of~~ ~~T, $n_{\mathrm{INP}}(T)$~~~~, for every 0.5 °C following the parameterization described in Eqns. 1 – 2 of DeMott et al. (2017). As shown in Hiranuma et al. (2019, i.e., Table S2), the~~ ~~T~~ ~~uncertainty in WT-CRAFT is ± 0.5 °C. The experimental uncertainty is typically represented by 95% binomial confidence intervals (CI95%). While the background freezing contribution of the field blank filter was negligible (< 3%) at -25 °C, we purposely limited our WT-CRAFT data analysis to the~~ ~~T~~ ~~range between 0 °C and -25 °C to eliminate any possible artifacts in our WT-CRAFT data.~~

The IN spectrometer of the Karlsruhe Institute of Technology (INSEKT) system is an~~other~~ offline immersion freezing technique, and ~~As described in Schiebel (2017), the~~ its design and concept ~~of INSEKT~~ are~~is~~ based on the ~~CSU-IS~~Colorado State University ice spectrometer ~~instrument~~ (Hill et al., 2014 and 2016) as described in Schiebel (2017) and Schneider et al. (2021). In this study, INSEKT was used to assess the IN ability of surface OLLF samples collected on 47 mm polycarbonate Nuclepore filters (Whatman, Track-Etched Membranes, 0.2 µm pore) at the AIDA facility. The INSEKT data are especially useful to complement the AIDA chamber immersion results at temperatures above -25 °C. All filter samples were collected ~~from the AIDA chamber prior to individual expansion experiments~~ with a sampling flow rate of 10 L min^{-1}, and a total of ≈ 600 L of air was sampled through a cross-~~-~~section of each ~~47 mm polycarbonate~~ filter (see **Table ~~3~~ 1** for corresponding AIDA experiments). ~~As described in Schiebel (2017), the design and concept of INSEKT is based on the CSU-IS instrument (Hill et al., 2014 and 2016).~~

Filter-collected aerosol particles were suspended in 8 mL filtered nano-pure water, which has a negligible contribution to background freezing (Schneider et al., 2021). The washing water volume was optimized based on the total amount of air sampled through the cross-section of the filter, so that the resulting suspension contained at least 0.015 INP L^{-1} at the upper temperature detection limit of INSEKT. For the INSEKT analysis, ~~aerosol particles were washed off the filter and~~ the resulting suspension ~~is~~ was divided into volumes of 50 µL, which were placed in wells of a sterile PCR tray. It was then placed in an aluminum block thermostated with an ethanol cooling bath (LAUDA RP 890; Lauda), which was cooled down at a rate of 0.33°C min^{-1}. If a well froze upon the presence of an INP, a camera detected the associated brightness change~~s~~. The freezing data were analyzed with a 0.5 °C temperature resolution. The temperature~~T~~ uncertainty of INSEKT was ± 0.5 °C, and the n_{INP} ~~INP concentrations~~ error was estimated ~~by means of~~as the ~~binomial~~ 95% binomial confidence intervals (CI95%)~~CI95%~~ for each sample.

A series of diluted suspensions (×15 to ×225) was consistently analyzed for each sample to acquire INP spectra covering a wide range of heterogeneous freezing temperatures (above -25 °C), which complemented the AIDA results at higher temperatures than AIDA could examine. For the overlapping temperatures, we chose the data exhibiting the minimum CI95% as representative n_{INP} for a given temperature.

We now describe t~~T~~he derivations of n_{INP} based on Vali (1971) ~~is~~ as well as immersion freezing efficiencies~~described in **SI Sect. S4**~~. Initially, we computed the $C_{INP}(T)$ value, which is the nucleus concentration in ultrapure water suspension (L^{-1} water) at a given temperature. This $C_{INP}(T)$ value was calculated as a function of unfrozen fraction, $f_{unfrozen}(T)$ (i.e., the ratio of the number of droplets unfrozen to the total number of droplets) as:

$$C_{INP}(T) = -\frac{\ln\left(f_{unfrozen}(T)\right)}{V_d} \qquad [1]$$

in which, V_d is the volume of the sample in a well (50 μL) for INSEKT. Next, we converted $C_{INP}(T)$ to $n_{INP}(T)$: INP in the unit volume of atmospheric air at standard temperature and pressure (STP), which is 273.15 K and 1013 mb, respectively. The cumulative n_{INP} per unit volume of sample air, described in the previous study DeMott et al. (2017), was then estimated as:

$$n_{INP}(T) = C_{INP}(T) \times (DF) \times \frac{V_l}{V_{air}} \qquad [2]$$

where DF is a serial dilution factor, V_{air} is the sampled air volume, and V_l is the suspension volume. Finally, based on Eqn. 3 of Hiranuma et al. (2015), the INP concentration per unit aerosol particle mass [$n_m(T)$], and INP concentration per unit geometric aerosol particle surface as a function of T [$n_{s,geo}(T)$] was derived as:

$$n_m(T) = \frac{n_{INP}(T)}{M_{ve}} \approx \left(\frac{S_{total}}{M_{total}}\right) n_{s,geo}(T) \qquad [3]$$

where M_{ve} is the mass of a spherical particle of volume equivalent diameter (g), and S_{total}/M_{total} is a geometric specific surface area. The S_{total}/M_{total} value used for this study was derived from particle size distribution measurements from the AIDA chamber (presented in **Table 1**). Niemand et al. (2012) infers that the application of $n_{s,geo}$ is valid for small percentages of IN active fraction (≤ 1%). From the numbers of $N_{total,0}$ given in **Table ~~3~~1** (total number concentration of particles at the initial stage prior to expansion), we examined on average ~ 200,000 L^{-1} aerosol particles in the immersion freezing mode in AIDA. INSEKT typically measures INP counts up to several hundred. Even assuming we evaluate INP up to 2,000 L^{-1}, our INP fraction is 1%. ~~Thus, our n_s parameterization is reasonable.~~We, therefore, conclude that our n_s parameterization introduced in **Sect. 3.1** is reasonable.

~~In this study, filter-collected aerosol particles were suspended in 8 ml filtered nanopure water, which has negligible contribution to background freezing, and used to characterize their IN efficiency (Schneider et al., 2021). Similar to WT-CRAFT, the amount of pure water to generate a stock suspension was adjusted for the first frozen aliquot-well observed to contain ≈ 0.015 INP L^{-1} in this study, based on the total amount of air sampled through the cross section of filter. A series of diluted suspensions (×15 to ×225) was consistently analyzed for each sample to acquire an INP spectra covering a wide range of heterogeneous freezing Ts (-7.5 °C to -25.5 °C). For the overlapping Ts, we chose the data exhibiting the minimum CI95% as representative n_{INP} for given T. In addition, **SI Sect. S3** provides a comparison of our two immersion freezing techniques and results, which are reasonably comparable.~~

2.1.4. Dynamic filter processing chamber

Condensation/immersion mode n_{INP} ~~were~~ was also measured at National Research Council in Bologna ~~CNR-ISAC~~ by means of a dynamic filter processing chamber (DFPC, ~~(~~Santachiara et al., 2010). The DFPC ~~chamber~~ system is a replica of the Langer dynamic developing chamber (Langer and Rogers, 1975). ~~A~~ The systematic temperature uncertainty ~~in terms of T~~ in DFPC is within ± 0.1 °C (Table S1 in Hiranuma et al., 2019). With a water saturation error of ± 0.01, an ice detection error of ± 33%, and the experimental standard deviation, the overall IN efficiency uncertainties of DFPC are estimated to be less than ± 62% for this study. The application of DFPC for immersion freezing has been verified in previous inter-comparison studies (DeMott et al., 2018; Hiranuma et al., 2019).

For the DFPC analyses, aerosol particles were collected on nitrocellulose black gridded membrane filters ~~(0.45 µm porosity, Millipore~~(Millipore HABG04700, nominal porosity 0.45 µm)~~)~~ from the AIDA chamber prior to each expansion experiment (**Table ~~3~~1**). Two parallel samplers employed in this study had an identical sampling flow rate of 2 L min^{-1}, and a total of 100 L of air was sampled for each system. One sampling system collected the total aerosol particles, while another ~~one~~ was equipped with a cyclone impactor (MesaLabs, SCC0732, S/N 13864) to collect only submicron-sized aerosol particles. This impactor was characterized with a cut-off size around 1 µm in aerodynamic diameter (50% cut-off diameter at 0.9 µm) at 2 L min^{-1} flow rate (Kenny, et al., 2000). Therefore, the latter line selectively collected particles smaller than 1 µm aerodynamic diameter.

The cut-size efficiency of this cyclone impactor was tested in the lab against NaCl particles. Particle transmission efficiency along the total sampling line was taken into account by estimating gravitational losses in the horizontal tract of the sampling tube and inertial losses in the bend. At a particle size of 10 µm (larger than what was measured in the AIDA chamber), the overall particle transmission efficiency was higher than 86%. For a particle size of 2 µm, the particle loss is estimated to be ≈ 2.5%. Due to the small loss, we neglected any corrections for aerosol particle counts. After collection, the filters were safely kept in Petri dishes at room temperature~~*T*~~ until the freezing experiments were initiated.

Prior to the DFPC measurement, the sampled filter was inserted onto a metal plate and covered with a smooth surface of paraffin in order to assure good thermal contact between the filter and the supporting substrate. Subsequently, the paraffin was slightly heated and rapidly cooled ~~in order~~ to fill the filter pores. DFPC controlled the temperature~~*T*~~s of the filter and the air, saturated with respect to finely~~-~~ minced ice, with the flow continuously grazing the filter. IN measurements of total aerosol particles, $n_{\mathrm{INP,total}}$, as well as, measurements of PM$_1$ (PM$_x$ = particulate matter smaller than x µm), $n_{\mathrm{INP,PM1}}$, were performed at water supersaturation of 2%, and temperature~~T_{filter}~~ of -18 °C and -22 °C. The supersaturation was calculated theoretically from vapor pressures over ice and water. The exposure time of the filter was 20 min to grow visible ice crystals on INPs at the considered *RH* and temperature~~*T*~~ conditions. The n_{INP} value was calculated by scaling the total counts of ice crystals detected on each filter by the sampled air volume.~~The use of the dynamic chamber is advantageous compared to other techniques as the supersaturation is maintained and less impacted by the effect of hygroscopic particles or ice crystal growth, which might lead to an incomplete activation of the INPs on the filter substrate.~~

2.~~5~~1.5. Extraction of total DNA and metagenomics analysis of sample microbiomes ~~from bulk and aerosolized dust samples~~

~~Total DNA was extracted from Texas dust samples TXD01 and TXD05 prior to and after aerosolization in the AIDA cloud chamber. From bulk samples of dust, total DNA was extracted from 157.1 mg (TXD01) and 128.8 mg (TXD05).~~ To sample aerosolized dust from the AIDA cloud chambers, stainless steel filter holders containing ~~nucleopore~~ 47 mm Nuclepore filters (~~47mm diameter and~~ 0.2 µm pore size) were used. These filters were previously sterilized in a standard vapor autoclave and fitted onto the AIDA cloud chamber for aerosol particle sampling prior to the expansion IN experiment. After the conclusion of the experiments, the holders were removed from the chamber to extract total DNA directly from the N~~n~~ucleopore filters. DNA extractions were performed using the FastDNA® Spin Kit for Soil (MP Biomedicals) as described in the manufacturer's protocol. Filters were aseptically removed from holders and placed in the Lysing Matrix E tube for mechanical cell disruption, which was carried out with the FastPrep® Instrument (MP Biomedicals). The concentration and purity of the extracted DNA were~~was~~ measured by using the Qubit™ 3.0 (Thermo Fisher Scientific). The volume of each sample was 50 – 100 µL.

~~Next, our metagenomics analysis method of total DNA is described.~~ The amplification of phylogenetic marker genes and the metagenomics analysis and sequence processing of amplicons from each dust sample were performed by Eurofins Genomics Germany GmbH using the INVIEW Microbiome Profiling 3.0 protocol in order to identify and classify the microbial population (*Fungi*, *Bacteria*, and *Archaea*) of each sample. To achieve this, the hypervariable regions V1 – V3 and V3 – V5 of the bacterial 16SrRNA gene, the fungal internal transcribed spacer (ITS2) gene, and part of the archaeal 16SrRNA gene were amplified by polymerase chain reactions from each sample using in-house primers. Amplicons were sequenced with the MiSeq next~~-~~-generation sequencing system with the 2 × 300 bp paired-end read module.

2.2~~1~~. Field ~~description~~investigation

2.2.1. Locations

Four commercial OLLFs, ranging from 0.5 to 2.6 km^2 (maximum~~<~~ 45,000 head capacity), located in the Texas Panhandle region were used as the ambient aerosol particle sampling sites. All four sites are located within a 53 km radius of West Texas A&M University in Canyon, Texas. Our experimental layouts at each site, denoted as OLLF-1 to OLLF-4, are shown in **Fig. ~~1~~ 2** (no further specification is provided to protect location privacy). All sites have a capacity greater than 1,000 head, which ~~are~~ is categorized as a large concentrated animal feeding operation facilit~~yies~~ for cattle under the U.S. Environmental Protection Agency's definition (https://www3.epa.gov/npdes/pubs/sector_table.pdf). These OLLFs were selected primarily for the east-west orientation of their feeding and working alleys, which were nearly orthogonal to prevailing south to southwest winds, allowing for downwind and upwind sampling. When south wind prevailed (90° < wind direction < 270°), we used the Northern site as the downwind site. Likewise, the Southern site was used as the downwind site while the north wind was dominant (270° < wind direction < 90°). Our sampling sites represent typical OLLFs, as more than 75% of cattle are produced in large concentrated animal feeding operation facilities in the U.S. (Drouillard, 2018).

2.2.2. Field sampling

~~Aerosol particles were collected to assess immersion freezing properties of “ambient” OLLF samples using offline immersion assays. These~~All field samples were collected using 47 mm Nuclepore filters (~~Whatman, Track-Etched Membranes,~~ 0.2 µm pore) ~~through polycarbonate filter samplers~~. A filter holder was deployed at ~ 1.5 m above the ground. The filter sampling conditions measured locally (during individual sampling activities) are summarized in **Table ~~1~~2**. For the given conditions, the estimated 50% particle transmission of a 1.5 m conductive tube (0.5-inch opening diameter) employed for aerosol samplings was ~ 5 µm (von der Weiden et al., 2009). Our samples were collected in different meteorological seasons, including summers in 2017 – 2019, springs in 2018 and 2019, and winter in 2019, in order to examine the seasonal variation in n_{INP}. All samples were collected when the OLLF pen surface was dry. In 2017, polycarbonate filter samplers were used at both upwind and downwind edges (< 80 m away from OLLF pens) of OLLF-1, 2, and 3 to understand the spatial variation in n_{INP} within facilities (**Fig. ~~1~~2**). Our sampling durations varied, but were up to ~ 4.5 hours, and our final IN propensity results were scaled to the sampled volume of air and suspended water afterward~~s~~ (**Table 2~~1~~**). All filter samples were kept in sterilized tubes refrigerated at 4 °C until the immersion freezing measurements commenced (typically within 24 hours after sampling).

To complement the polycarbonate filter samplers, simultaneous 1-min time-resolved mass concentration measurements of PM_{10} ~~(PM_x = particulate matter smaller than x µm)~~ during individual sampling intervals were also carried out using DustTrak particulate monitors (TSI Inc., Model 8520) equipped with a PM_{10} inlet. ~~Additionally, tapered-element oscillating microbalances (TEOMs; Thermo Scientific Inc., Model 1400ab; Patashnick and Rupprecht, 1991) were deployed at OLLF-1 to continuously monitor PM_{10} mass concentration side-by-side with a polycarbonate filter sampler and DustTrak. With an operating flow rate of 16.7 LPM, our TEOM measured < 1 g m^{-3} of PM with a 5-min time resolution. Two identical TEOMs were deployed at OLLF-1: one at the upwind edge and another at downwind location of OLLF-1 (**Fig. 1**). Both TEOMs ran continuously during the entire 2016 – 2019 study period except for routine maintenance activities.~~ The inlets of DustTrak ~~and TEOMs~~ were maintained at ~ 1.5 m above the ground to be consistent with our polycarbonate filter samplers. ~~It is noteworthy that our TEOM and DustTrak PM_{10} measurements agreed within ± 40% on average.~~

2.2.3. West Texas cryogenic refrigerator applied to freezing test system

To assess the ambient n_{INP} through samples collected in the field, we used an offline droplet-freezing assay instrument, the West Texas ~~Cryogenic~~ cryogenic ~~Refrigerator~~ refrigerator ~~Applied~~ applied to ~~Freezing~~ freezing ~~Test~~ test system (WT-CRAFT; Vepuri et al., 2021). Briefly, WT-CRAFT enables a simulation of atmospheric immersion freezing using supercooled droplets containing aerosol particles at temperatures~~T~~ > -25 °C. WT-CRAFT was a replica of NIPR-CRAFT (Tobo, 2016), but the two systems currently possess different sensitivities to artifacts and detectable temperature~~T~~ ranges as described in Vepuri et al. (2021).

In this study, for each ambient sample, we evaluated 70 solution droplets (3 µL each) placed on a hydrophobic Vaseline layer with a cooling rate of 1 °C min^{-1}. All droplets were prepared using filter rinse suspensions with high-performance liquid chromatography (HPLC)-grade water. The amount of HPLC water volume (i.e., V_l) was determined based on the total amount of air sampled through the ~~cross~~ cross-section of the filter ~~(**Table 1**)~~, which limits the detection capability to 0.05 INP per L of air (~~standard T and pressure,~~ STP). As described in Vepuri et al. (2021), by optimizing the suspension water volume, the first frozen droplet observed was considered to have 0.05 INP L^{-1} in this study. Each freezing event was determined optically based on the change in droplet brightness when the initially transparent liquid droplets became opaque upon freezing. If the freezing temperature~~T~~ was not obvious for any droplets, the 8-bit grayscale images were assessed using ImageJ software to determine the temperature~~T~~ of phase change.

After the measurement, we calculated the frozen fraction and estimated the n_{INP} per volume of air as a function of temperature~~T~~, $n_{\mathrm{INP}}(T)$, for every 0.5 °C ~~following the parameterization described in~~ using Eqns. 1 – 2 (V_d = 3 µL; V_{air} and V_l are provided in **Table 2**) ~~of DeMott et al. (2017)~~. ~~As shown in Hiranuma et al. (2019, i.e., Table S2), t~~The temperature~~T~~ uncertainty and immersion freezing efficiency in WT-CRAFT are~~is~~ ± 0.5 °C and ± 23.5 %, respectively (Vepuri et al., 2021). The experimental uncertainty is typically represented by ~~95% binomial confidence intervals (~~CI95%~~)~~. While the background freezing contribution of the field blank filter was negligible (< 3% activation) at -25 °C, we purposely limited our WT-CRAFT data analysis to the temperature~~T~~ range between 0 °C and -25 °C to eliminate any possible artifacts in our WT-CRAFT data. In addition, **SI Sect. S~~3~~3** provides a comparison of our two immersion freezing techniques and the $n_{\mathrm{INP}}(T)$ results, which are reasonably comparable.

To evaluate the immersion freezing efficiency of ambient aerosol particles collected at OLLFs, we converted our WT-CRAFT-based n_{INP} measurements to ice-nucleating efficiency metrics, such as n_{INP}, n_{m}, and $n_{\mathrm{s,geo}}$ (Eqn 3). The $S_{\mathrm{total}}/M_{\mathrm{total}}$ value used for this study, ~ 0.4 m^2 g^{-1}, is derived from particle size distribution measurements presented in Fig. 3 of Hiranuma et al. (2011).

~~2.6. *n*INP estimation and IN parameterization method~~

~~All IN data from AIDA, WT-CRAFT, INSEKT, and DFPC experiments were converted to and stored in $n_{\mathrm{INP}}(T)$, INP concentration per unit aerosol particle mass [$n_{\mathrm{m}}(T)$], and INP concentration per unit aerosol particle surface as a function of T [$n_{\mathrm{s,geo}}(T)$] (DeMott et al., 2017; Ullrich et al., 2017; Hiranuma et al., 2015). The derivation process of these quantities are summarized in **SI Sect. 4**. These conversions required only scaling measured or estimated $n_{\mathrm{INP}}(T)$ from each method to aerosol particle mass or surface area parameters provided in **Tables 1–3**. Niemand et al. (2012) infers that the application of n_s is valid for small percentages of IN~~

~~active fraction (≤ 1%). From the numbers of $N_{\text{total},0}$ given in **Table 3** (total number concentration of particles at the initial stage prior to expansion), we examined on average ~ 200,000 L^{-1} aerosol particles in the immersion freezing mode in AIDA. Even assuming we evaluate INP up to 2,000 L^{-1}, our INP fraction is 1%. Thus, our n_s parameterization is reasonable.~~

~~A consistent data interpolation method is important to systematically compare immersion freezing data from different IN measurement methodologies. In this study, we present *T*-binned-average IN data (i.e., 0.5 °C bins) for the lab and field IN data. By following the inter-comparison method described in our previous studies (Hiranuma et al., 2015), all lab data were binned/interpolated in a consistent manner using a 0.5 °C resolution data.~~

3. Results and Discussion

3.~~2~~1. Laboratory results

3.1.1. Physical properties of samples

Table 3 summarizes the physical properties of surrogate samples from OLLFs. Additionally, geometric *SSA* values were computed based on aerosol particle size distribution measurements in the AIDA chamber (i.e., a fraction of total surface area concentration to total mass concentration estimated from the size distribution data). The summary of geometric *SSA* values for aerosol particles in each AIDA experiment is summarized in **Table 4**.

As seen in **Table 3**, the measured densities of both sample types are slightly higher than typical grain dust densities (<1.69 g cm^{-3}; Parnell et al., 1986). The action of cattle hooves on the pen can cause compaction of the surface layer, which may result in the higher densities of our samples (Guo et al., 2011). The measured BET *SSA* values of OLLF samples are slightly higher compared to previously measured agricultural soil dust samples (0.74 – 2.31 m^2 g^{-1}; O'Sullivan et al., 2014), which suggests that TXD01 and TXD05 are more porous than these previous soil samples, leading to higher BET *SSA*. Our geometric *SSA* values are higher than the BET *SSA* values. In general, a small *SSA* value is often consistent with the presence of a large aerosol particle population. Hence, the predominance of larger particles in bulk powders assessed in BET is presumably responsible for the observed differences in these two *SSA* values. Indeed, the particles observed in AIDA were all $\lesssim$ 6.5 µm volume equivalent diameter, D_{ve} (**Table 1**) presumably due to the use of cyclone impactor stages after a rotating brush generator, whereas the particles evaluated by BET were up to 75 µm. Therefore, in association with the large grain size involved in the BET analysis, bulk samples might have exhibited smaller *SSA* than dry dispersed ones. As seen in **Table 1**, the mode diameters of TXD01 samples in AIDA were in general smaller than that of TXD05 samples, which is consistent with our *SSA* measurements (see **Tables 3 and 4**).

As demonstrated in our previous study, the surface area distribution of ambient OLLF dust peaks in mode diameter at ≤ 10 µm (Hiranuma et al., 2011). This mode diameter is larger than surface-derived samples aerosolized and examined in the AIDA chamber. However, it is cautiously noted that the ambient OLLF dust size distribution is not spatially uniform, and the emitting mechanism itself is not controllable as it highly depends on a unit of mobile livestock. Granting the primacy of hoof action as the decisive emissions mechanism of OLLF dust as described in Bush et al. (2014), a more controlled laboratory experiment has been needed to characterize IN ability of OLLF soil dust.

3.1.2. AIDA measurements and ~~IN~~ freezing efficiencies of surface materials

~~As shown in **Table 3**, we conducted 10 AIDA experiments to measure IN efficiency of two surface materials; TXD01 and TXD05. Dry-heated samples of each type were also examined: TXD01H and TXD05H.~~ ~~All lab data associated with this study were archived according to the AIDA experiment number (i.e., TXDUST01_number), and we share these IDs with other associated measurements (e.g., INSEKT).~~ ~~As seen in **Table 3**, the mode diameters of TXD01 samples in AIDA were in general smaller than that of TXD05 samples, which is consistent with our *SSA* measurements (see **Table 2**).~~ Shown in **Fig. ~~7~~ 3** are expansion experiment profiles of ~~these~~ all ~~10~~ 6 AIDA expansion experiments ~~with different samples, including TXD01 (i) – (iii), TXD05 (iv) – (vi), TXD01H (vii – viii), and TXD05H (ix – x)~~. These profiles represent data points measured in the chamber over a series of time, such as temperature~~*T*~~ (a), pressure (b), ~~relative humidity (~~*RH*~~,~~ (c), and aerosol particle and hydrometeor concentration (d) for each AIDA experiment. For each~~a~~ cloud formation experiment, the pressure within the chamber was reduced (ΔPressure~~*P*~~ ~ 180 – 290 hPa), causing the temperature~~*T*~~ to drop and a simulated adiabatic 'expansion' to occur. As can be seen, measurements were made ~~by AIDA-simulated immersion freezing~~ at water saturation (*RH* with respect to liquid water around 100%). A droplet-ice threshold typically coincide~~s~~d with ≥ 20 µm D_{ve} ~~(Hiranuma et al., 2016)~~. Thus, the number concentration of > 20 µm D_{ve} ~~AIDA~~ particles measured by a welas optical particle counter (Benz et al., 2005) primarily represents pristine ice crystals formed during the expansion (**Figs. ~~7d~~3d**). The *RH* dropped during some expansions at low temperature~~*T*~~s (**Figs. ~~7c~~3c.iii and ~~7c~~3c.vi**). At these temperature~~*T*~~s, ice crystals grow rather fast at the expense of available water vapor in the AIDA chamber, which causes the observed *RH* drop. Nevertheless, droplets were fully activated within ≈ 100 seconds of each expansion while reaching the peak *RH*, where we see the steep slope of Δ*RH*/Δ*t* in **Fig. ~~7~~3.** Further, as seen in **Fig. ~~7~~3d**, particles of > 20 µm D_{ve} are not increasing and the total aerosol concentration measured by CPC also does not change after the *RH* peak. Thus, all predominant ice formation occurs at or before the *RH* peak through immersion freezing. Lastly, we made sure to only report our IN efficiency at temperature~~*T*~~s higher than ~ -30 °C, corresponding to a saturated condition in the AIDA vessel.

Figure ~~8~~ 4 summarizes our $n_{s,geo}$ spectra of our surface material samples from the AIDA, INSEKT, and DFPC (total aerosol) experiments. For each sample, we compared our experimental dust $n_{s,geo}$ spectra ~~in comparison~~ to six reference soil dust

$n_{s,geo}$ curves~~spectra~~, O14 (England), S16 (Mongolia, Argentina, and Germany), S20 (Northwestern Germany, Wyoming), T14 (Wyoming), T14 (China), and U17 (desert dust samples from Aisa, Canary Island, Israel, and Sahara), available in previously published studies (O'Sullivan et al., 2014; Steinke et al., 2016; 2020; Tobo et al., 2014; Ullrich et al., 2017), as well as our field data (**see Sect. 3.2.3**~~**Fig. 3**~~). ~~Untreated dry samples were assessed by all three techniques. Complementarily, INSEKT was also used to assess immersion freezing efficiency of wet-boiled (i.e., heated) filter samples. As explained in **Sect. 2.4**, a series of diluted samples were examined in INSEKT. We made sure to assess overlapping *T* intervals in a series of measurements to see if $n_{s,geo}$ values from multiple measurements agree within CL95% and, if so, to merge the results together. For each sample, the spectra nearly overlap each other at *T* ~ -25 °C, verifying their comparability and complementing features.~~ As seen in **Fig. ~~8~~4**, our OLLF spectra are comparable to the previous soil dust $n_{s,geo}$ parameterization at relatively low temperatures~~*T*~~ (e.g., the $n_{s,geo}$ value range in orders of magnitude from 10^9 to 10^{10} m^{-2} at around -25 °C). ~~At *T* above -20 °C, the INSEKT results suggest that the bulk TXD01 sample is more active than filter-collected samples beyond the $n_{s,geo}$ uncertainty (**Figs. 8a and 8c**). On the other hand, the INSEKT analyses of TXD05 (**Figs. 8b and 8d**) and all other filter samples did not find a notable difference amongst all samples. Furthermore, the lab-derived~~ The immersion spectra of both surface materials are ~~reasonably comparable to~~located towards the minimum~~ – maximum~~ boundaries of our field $n_{s,geo}$ spectra for temperature~~*T*~~ > -25 °C. While the variability of $n_{s,geo}$ at a single temperature~~*T*~~ could vary by several orders of magnitude for our field data, smaller~~similar~~ variations are found for both lab ~~and field~~ results, implying ~~the similarity of freezing efficiencies~~different properties of our lab and field samples. The difference between our laboratory results and field data is discussed in **Sect. 3.3.1** in more detail. ~~Without scaling to the surface area, n_{INP} spectra exhibited a wide range of INPs over three orders of magnitude; e.g., -25 °C (10.07 to > 10,000 L^{-1}). These~~ Additionally, the similarity of our lab results between TXD01 and TXD05 suggests that ~~(1) there is a difference in the INP abundance between bulk (< 75 µm-sieved) and aerosolized/filtered-samples for TXD01 (≲ 6.5 µm; **Table 3**) presumably due to different properties in particles of these two size subsets (6.5 – 75 µm and ≲ 6.5 µm) and/or different amount of IN-active soil organic matter (Tobo et al, 2014), (2)~~ different physicochemical properties found for our ~~TXD05~~ samples may not impact their INP propensities~~, and (3) TXD05 might be more representative of atmospherically relevant dust (see **Table 2** and **SI Sect. S2**)~~.

3.1.3. Size-segregated analysis

Our DFPC-derived $n_{s,geo}$ values in **Fig. ~~8~~ 4** agreed reasonably well with the INSEKT results at the measured temperature~~*T*~~s within our error ranges. This comparability suggests that freezing ability is similar for condensation and immersion for our surface samples. Besides, several unique characteristics of OLLF INPs were disclosed. For instance, comparability of results from our condensation freezing instrument (DFPC) and immersion freezing assay (INSEKT) was found for both sample types at the overlapped temperatures (18°C and -22°C). A similar observation was previously made for kaolinite particles in Wex et al.(2014). However, as the examined temperatures in our study are limited, the observed equivalence between immersion and condensation freezing for our surface OLLF samples should be cautiously interpreted and may not be conclusive.

More importantly, **Table 5~~4~~** summarizes the comparison of the submicron vs. supermicron INPs for a set of eight samples measured at -18 °C and -22 °C by DFPC. ~~Due to limited range of *T*s and samples assessed by DFPC, we cannot provide any statistical variability of our individual data. But, o~~On average~~,~~ the supermicron INP fraction, given by $[(n_{INP,total} - n_{INP,PM1}) / n_{INP,total}] \times 100$, shows that this fraction contributed 49.7% ± 6.0% (average ± standard error) of the total INP for TXD01 and TXD05 samples at the measured *T*s. This highlights the importance of the large particles, which might dominate the particle surface and mass, ~~coarse fraction~~ in the INP population. Note that we also compared the submicron vs. supermicron $n_{s,geo}$ values. Our PM_1 $n_{s,geo}$ and supermicron $n_{s,geo}$ were virtually identical, implying non-size dependent IN ability across the sizes evaluated in this study (not shown).

Several studies have shown evidence that coarse aerosol particles dominate INPs across the world. DeMott et al. (2010) successfully demonstrated the correlation between immersion-mode n_{INP} and the number concentration of aerosol particles larger than 0.5 µm diameter based on the compilation of field data for more than a decade. ~~, a number of studies have shown the evidence that supermicron aerosol particles dominate INPs across the world. For example,~~ Mason et al. (2016) reported a substantial fraction of supermicron INPs through immersion freezing at a relatively ~~a~~ high temperature~~*T*~~ (> 78% at -15 °C) measured at seven different sites over North America and Europe. Even at -20 °C, the author reported a ~~the~~ fraction of supermicon INPs larger than 50%. Compared to these numbers, our laboratory data show lower fractions, but the INP sources are presumably different. Based on findings from recent studies~~y~~ of size-resolved INPs vs. fluorescent biological particles, these INPs activated at −15 °C are typically thought to be biological (e.g., Huffman et al., 2013; Huang et al., 2021). While there is~~has been~~ more evidence that terrestrial and marine biological particles play an important role in immersion freezing of supermicron-sized particles (e.g., Ladino et al., 2019; Si et al., 2018; Creamean et al., 2018), the atmospheric implication of such rare aerosol species and their overall impact on aerosol-cloud interactions are~~is~~ still under debate. More recently, high IN efficiency by supermicron INPs derived from quartz-rich atmospheric mineral dust~~s~~ has~~have~~ been reported from different locations, including East Asia (Chen et al., 2021) and E~~e~~astern Mediterranean (Reicher et al., 2019). These mineral components usually contribute to IN at low temperature~~*T*~~s. However, there has not been much discussion of large soil dust particles, especially organics, and their contribution to atmospheric ~~ice nucleation~~IN in previous studies. Hence, direct implications of which components contribute to IN at different temperature~~*T*~~s to the observed freezing properties of OLLF particles are~~is~~ still missing. Lastly, while we did not see a systematic increase in~~of~~ supermicron INP fraction as a function of temperature~~*T*~~ as shown in Mason et al. (2016; i.e., supermicron INP fraction at -15 °C larger than at -20 °C), our results in **Table ~~4~~ 5** support that $n_{INP,total}$ is always higher than $n_{INP,PM1}$ for ~~any type of~~ samples used in this study.

~~Interestingly, our comparison between non-heated vs. heated samples indicated no substantial suppression in IN ability by heating, especially for dry-heated samples. This heat-resistant feature of OLLF samples may be due to their pre-exposure to dry, high temperature ambient and soil *T* conditions (Cole et al., 2009). Further, our mass spectrometry analysis on these two subsets revealed no significant deviation in chemical compositions (**SI Sect. S2**~~**S1**~~). Additionally, our metagenomics analysis also found no deviation in terms of bacteria and fungi speciation between dry-heated and non-heat-treated samples as discussed below. A detailed comparison of the non-heat-treated sample to the heated-sample is discussed in **Sect. 3.6** and **SI Sect. S3**.~~

3.1.~~3~~4. Metagenomics analysis

~~**Table 5** summarizes our results of metagenomics analysis. The diversity of the microbiome in the dust samples identified microorganisms common in soil, bovine manure, and inhabitants of the bovine rumen, as expected (detailed in **SI Sect. S5**). Interestingly, no known IN-active species of microorganisms (active at *T*s above -10°C) were detected, although genera of *Bacteria* (*Pseudomonas*) and *Fungi* (*Fusarium*, *Mortierella*) known to include species with IN activity were detected, albeit in negligible numbers. This insignificance of IN-active microbiome and relatively high importance of non-biological supermicron particles as OLLF-INPs are deemed robust. Otherwise, the observed strong mass dependency of OLLF-~~ ~~n_{INP}~~ ~~(**Fig. 5a**) cannot be explained as microorganisms typically contains small mass. We also found very little difference in the bacterial and eukaryotic metagenome in bulk and heat-treated dust samples (no data for *Archaea* were obtained from heat-treated dust samples). Heat treatment of dust samples at 100 °C for 12 hours apparently did not destroy the DNA in our samples, even though most microbial cells were killed. Thus, no notable difference after dry-heating was observed for both TXD01 and TXD05 (**Table 5**). This negative result is important because it agrees with our metagenomics analysis, where no known IN-active bacteria were detected. The diversity of the bacterial microbiome in both samples showed a considerable difference after aerosolization of dust in the AIDA cloud chamber and the subsequent IN experiments in simulated clouds. In aerosolized dust, a significant increase of desiccation-resistant *Actinobacteria* was observed in both samples. Further, we also identified a significant decrease of non-desiccation-resistant *Proteobacteria*, *Firmicutes*, and *Bacteroides* in aerosolized particles (**Table 5**). This result implies that aerosolization and microbial dispersion in the atmosphere may alter microbiome diversity and population, at least for our samples. This unique effect was not observed for *Fungi* and *Archaea* (see **SI Sect. S5** for more details).~~ We examined the diversity of *Archaea*, *Bacteria*, and *Fungi* in TXD01 and TXD05. We analyzed aerosolized particles collected on Nuclepore filters. The results and data of metagenomics analysis are summarized in supplemental **Table S1**. Useful data for *Bacteria* were generated from the amplification and sequencing of the V3 – V5 region of the 16S rDNA phylogenetic marker down to the genus and species level. Data on *Archaea* were generated from TXD05 only. The predominant phyla of *Archaea* consisted of methanogens, colonizers of the bovine rumen, as expected (Fouts et al., 2012) (**Table S1a**). The bacterial fraction of the microbiome was dominated by *Actinobacteria* (the most abundant phylum, common soil inhabitants), *Proteobacteria*, *Firmicutes* (diverse bacterial phyla with species living in the soil as well as in the bovine rumen), and *Bacteroidetes* (common members of the bovine rumen microflora) (Fouts et al., 2012; Chaucheyras-Durand and Ossa, 2014). No known IN-active bacterial species were identified in either sample (Després et al., 2012), although the genus Pseudomonas (containing IN-active species) was detected in low numbers (**Table S1b**). The predominant fungal taxa in our samples belong to *Pezizomycetes* (*Ascomycota*), common soil inhabitants. In this taxon, the coprophilic genus *Ascobolus* was detected in high numbers, as expected (Sarrocco, 2016). The genera *Fusarium* (*Ascomycota-Hypocreales*) and *Mortierella* (*Mucuromycota-Mortierellales*) were also detected in low numbers. These genera contain species with IN activity; however, the phylogenetic analysis did not detect any known IN-active species of these genera (**Table S1c**). Thus, we did not identify any known IN-active microorganisms in our samples. This insignificance of the IN-active microbiome and relatively high importance of non-biological supermicron particles as OLLF-INPs are deemed robust if these particles are emitted as individual, externally mixed particles. Otherwise, the observed strong mass dependency of OLLF-n_{INP} (discussed in **Sect. 3.2** below) cannot be explained as microorganisms typically contain small mass (Hoose et al., 2010).

~~3.4. Ice residual analysis~~

~~A total of 1,259 aerosol and residual particles in the diameter range of 0.2 to 3 μm were assessed through electron microscopy for their physicochemical properties. All of our single particle analyses were carried out with the following parameters: electron beam accelerating voltages of 15 keV, spot size of 50, and working distance of 10 mm. **Table 6** summarizes the size properties of analyzed particles. The number of measured particles was limited depending on the particle availability on each substrate. Nevertheless, we examined at least 100 particles for each sample type, as seen in the table. Out of these particles, the diameter of TXD01 (0.84 μm) particles was on average smaller than TXD05 (1.05 μm). This observation is consistent with our offline particle characterizations (**Table 2**) and the AIDA size measurements (**Table 3**). For the samples used in this study, we could not identify any systematic differences between aerosol particles and residuals in terms of size. Likewise, while we found substantial fractions of supermicron diameter particles in TXD01 (29.2%) and TXD05 (38.8%), there is no obvious enrichment in supermicron population in our ice crystal residuals from this study (**Table 6**).~~

~~Higher aspect ratios in residuals compared to aerosol particles were found for both TXD01 and TXD05 samples. This difference indicates a relative increase in non-spherical particles, that have a higher aspect ratio, in residuals. In short, Hiranuma et al. (2008) found that quasi-spherical OLLF particles were predominantly salt-rich hygroscopic particles, whereas non-spherical~~

~~amorphous particles were found to be organic-dominant with negligible hygroscopicity. Thus, our results suggest the inclusion of non-hygroscopic particles as ice residuals.~~

~~Next, the elemental composition from energy dispersive X-ray spectroscopy analysis revealed some notable differences between aerosol particle samples and residual samples. In this study, we followed the H13 classification scheme to define particle types in the electron microscopy analysis (Hiranuma et al., 2013). Briefly, we semi-quantitatively assessed atomic weight percentage of organic (C, N, O), salt-rich (Na, Mg, K, P), mineral-rich (Al, Si, Ca), and other. We detected carbon in all particles exclusively, but a background signal from polycarbonate substrate film could not be separated and ruled out.~~ ~~**Table 7** shows the summary of particle types based on their elemental compositions for samples used in this study. It should be noted that the "rich" used in the names of particle classes only indicates intensive characteristic peaks in the energy dispersive X-ray spectra, and > 99.9% of particles (except a few aluminosilicate particles) examined in this study were predominantly composed of carbon elements as organics-mixed particles. As seen in the table, an increase in exclusively organic fractions as well as a substantial decrease in salt-rich particles in residuals persisted for both TXD01 and TXD05 samples. The organic type fraction in heated-aerosols is slightly smaller than that in non-heated aerosols. Nevertheless, the increase of organic type fraction for heated-ICRs implies an insignificant heating effect as well as the importance of heat-resistant organics for immersion freezing of OLLF materials. This observation supports the result in~~ ~~**Table 6**~~~~. The reduction in salt-rich particle percentage might be relevant to an increase in aspect ratio (Hiranuma et al., 2008). The observed relative increase in organic-including particles, which might be substantially less hygroscopic compared to salt-rich particles, is also indicative of the predominance of immersion freezing as an IN mechanism of OLLF particles (rather than condensation freezing; Belosi and Santachiara, 2019). Indeed, immersion is a dominant mechanism of IN in mixed-phase clouds (Hande and Hoose, 2017). Regardless, liquid cloud formation might be a prerequisite for activating OLLF particles as ice crystals in the atmosphere.~~

~~Finally, our attempts to analyze the size-resolved abundance of each composition class was not conclusive (not shown), possibly due to limitations in the small population examined. Nonetheless, finding no clear size-dependence of elemental compositions in both total aerosol and residual samples was an important negative result, which is consistent with findings through aerosol single particle spectrometry (~~~~**SI Sect. S2**~~~~).~~

3.2~~1~~. Field results~~Ambient INP spectra~~

3.2.1. Downwind vs. Upwind

~~To evaluate the immersion freezing efficiency of ambient aerosol particles collected at OLLFs, we converted our WT-CRAFT-based $_{INP}$ measurements to ice-nucleating efficiency metrics, such as n_{INP}, n_m, and $n_{s,geo}$ (~~~~**SI Sect. 4**~~~~).~~ Individual ~~values of cumulative~~ PM_{10} mass (derived from DustTrak measurements), n_{INP}, and n_m for each sampling date are provided in **Table ~~1~~6.** On average, an extremely high cumulative n_{INP} at -25 °C of 1,171.6 ± 691.6 L^{-1} (standard error) L^{-1} was found at the downwind site.

Figure ~~3~~5a shows the n_{INP} comparison between downwind samples and upwind samples collected simultaneously at OLLF-1, 2, and 3 in 2017. **Figure 5a** displays individual n_{INP} spectra from each OLLF site. Additionally, **Fig. ~~3b~~ 5b** summarizes the n_{INP} diversity between downwind and upwind in log($n_{INP,downwind}$/$n_{INP,upwind}$), which represents the log-scaled ratio of individual measurements~~ at each OLLF site~~ at given temperature~~T~~s. These n_{INP} ratios are shown only for the temperature~~T~~ range covered by both downwind and upwind data. As can be seen in these two panels, none of the upwind spectra show n_{INP} above -14 °C whereas we detected $n_{INP,downwind}$ at temperature~~T~~s above -10.5 °C, suggesting that the INPs that are ~~active~~ detectable in WT-CRAFT at temperature~~T~~s above -14 °C originate in OLLFs. In fact, across the examined freezing temperature~~T~~s, the downwind spectra from all OLLFs exhibit higher n_{INP} than the upwind spectra; therefore, the log($n_{INP,downwind}$/$n_{INP,upwind}$) values are above zero at temperature~~T~~s below -14 °C.

The source of upwind INPs is unknown. ~~However, because the measured n_{INP} is low at high T, the CI95% error of $n_{INP,upwind}$ at around -15 °C is relatively large as compared to that at a lower T (~~~~**Fig. 3a**~~~~). Hence, the difference between $n_{INP,downwind}$ and $n_{INP,upwind}$ is not conclusive beyond the uncertainty at this T. Furthermore, s~~Since our polycarbonate filter samplers were deployed in the close proximity of livestock pens (< 80 m away as discussed in **Sect. 2.2.2~~1~~**), the influence of soil dust even at an upwind site could not be ruled out depending on local ~~meteorological conditions and~~ livestock activities. Thus, it may be possible that~~ a short episode of~~ resuspended OLLF soil dust results in high n_{INP} at a specific temperature~~T~~ range for the upwind sample. The influence of soil dust from OLLFs on $n_{INP,upwind}$ spectra may be seen around -15 °C (**Fig. 5a**). At this temperature, the $n_{INP,upwind}$ (CI95%) error in a log scale spectrum is relatively large as compared to the lower temperature region, and the difference between $n_{INP,downwind}$ and $n_{INP,upwind}$ is not conclusive beyond the uncertainty around -15 °C. Nonetheless, the downwind n_{INP} values are indeed higher than $n_{INP,upwind}$ (beyond uncertainties) at temperature~~T~~s below -20 °C. At -25 °C, all $n_{INP,downwind}$ values appear to be an order magnitude higher than the upwind ones without any exceptions, indicating that OLLF is a source of a notable amount of INPs across the examined temperature~~T~~ range.

3.2.2. Seasonal variation

Shown in **Fig. ~~4~~ 6** is a compilation of $n_{INP,downwind}$ sorted based on the sampling season (i.e., summer, spring, and winter). Overall, we detected INPs at temperature~~T~~s lower than -5 °C, and the range of $n_{INP,downwind}$ at -20 °C varied in different seasons in 2017 – 2019: summer (5.0 – 421.7 L^{-1}), spring (4.2 – 31.2 L^{-1}), and winter (0.9 – 20.4 L^{-1}). As inferred from **Fig. ~~4~~6**, this seasonality holds true for all investigated temperature~~T~~s. To complement our measurements and observations, more discussion on estimated INPs from an OLLF and their seasonal variability is provided in **SI Sect. S5** and **Table S2**.

The observed seasonal variation in n_{INP} corresponds to the variation~~that~~ in cumulative PM mass (**Table ~~1~~6**). In fact, w~~W~~e observed a prominent linear relationship between aerosol particle mass and INP number concentration (at -25 °C: **Fig. ~~5a~~7a**). Furthermore, the n_m~~n_{INP}~~ values ~~scaled to the mass~~ (~~n_m:~~ **Fig. ~~5b~~7b**) show a nearly constant value (≈ 3×10^9 g^{-1}) at -25 °C (independent of particle mass concentration).

Figure ~~6~~ 8 depicts the $n_{s,geo}$ spectra of aerosol particles from OLLF downwind ambient samples, color-coded with different sampling seasons. As seen in the figure, the seasonal diversity of $n_{s,geo,downwind}$ is less apparent as compared to that of $n_{INP,downwind}$ (**Fig. ~~4~~6**). There is no systematic difference in the range of $n_{INP,downwind}$ in different seasons in 2017 – 2019 at -20 °C: summer ($6.7 \times 10^7 - 2.7 \times 10^9$ m^{-2}), spring ($2.4 \times 10^8 - 2.3 \times 10^9$ m^{-2}), and winter ($1.2 \times 10^8 - 2.9 \times 10^8$ m^{-2}). This observation is consistent with the ascribed ~~prescribed~~ dominance and importance of large particles as soil dust INPs.

Ambient meteorological conditions during the field sampling activities are summarized in **Table 7**. Resuspension of feedlot surface materials is not mainly wind-driven. As mentioned in **Sect. 3.1.1**, cattle movement and hoof action trigger feedlot dust when the air is dry and hot. We performed linear regression analysis for wind speed vs. PM_{10} concentration, and the resulting Pearson correlation coefficient (r) was -0.32. Concerning the high variability of PM_{10} concentrations while sampling, we also examined the relationship between wind speed and cumulative PM mass, and the resulting r was -0.35. In addition, we could not find any relevant statistical correlations between other meteorological parameters (temperature, pressure, and RH) and PM_{10}. We note that precipitation was not considered in this study because we assured to sample aerosol particles when the pen surface was dry (at least several days after precipitation). These results imply the following: (1) ambient meteorological conditions, as summarized in **Table 7~~1~~**, might not be determining factors for n_{INP} for our study sites; (2) there are abundant ~~is a predominance of~~ supermicron INPs from the feedlot **(Sect. 3.1.3)**, which potentially dominates particle mass and OLLF INPs (**Fig. 7**). Overall, our offline measurements of ambient n_{INP} using field filter samples collected in OLLFs show more than several hundred INPs L^{-1} ~~at~~ below -20 °C. More interestingly, there is a notable correlation between INP and ~~ambient aerosol particle mass concentrations~~PM_{10} based on our 2017 – 2019 field study, which indicates the importance of large supermicron aerosol particles as INPs. This ~~motivates~~ result supports the DFPC~~need for further~~ characterization of our OLLF samples in a controlled ~~-~~lab setting ~~in order to identify what particulate size population~~ (i.e., supermicron n_{INP} > submicron n_{INP}~~supermicron vs. submicron~~) ~~and other properties trigger their IN in a controlled lab setting~~.

~~3.5. Estimated INPs released from a OLLF~~

~~Upon confirmation of the comparability between field and lab $n_{s,geo}$ values, we proceeded with ambient n_{INP} estimation based on our field mass concentration data, using the OLLF-1 TEOM PM_{10} data. We elected to use the OLLF-1 data due to their reasonable spatiotemporal coverage (i.e., two identical model TEOMs deployed at the downwind and upwind sites for 2017 – 2019). A summary of TEOM mass concentration data in different seasons over 2017 – 2019 are available in **Table 8**. Frequently, the observed PM_{10} concentration exceeded 10^{-7} g L^{-1}, which is consistent with previous studies (Bush et al., 2014; Hiranuma et al., 2011). On the other hand, the observed mass concentration at the upwind sites was typically substantially lower except for known/recorded interruptions (e.g., a tractor-trailer passing by), resulting in transient increase in mass concentration. As the upwind n_{INP} can be considered non-negligible (see **Sect. 3.1**), we subtracted mass concentrations measured at a nominal upwind edge from the downwind TEOM mass concertation values to compute PM_{10} from OLLF-1. The screened TEOM data were used as ambient particle concentration data to estimate n_{INP} from an OLLF.~~

~~To estimate n_{INP}, we used the $n_{s,geo}$ parameterization given in **SI Sect. S6**. Due to the atmospheric relevance and T coverage extending to -5 °C, we used a fit of ***Field_Median*** in **Table S3** to compute representative $n_{s,geo}$ relevant to OLLF. To convert $n_{s,geo}$ to n_{INP}, we have adapted Equations (1) – (3) in Hiranuma *et al.* (2015). Briefly, the measured mass concentration as well as field *SSA* were used to convert from $n_{s,geo}$ to n_{INP}:~~

~~$n_{INP}(T)(L^{-1}) = n_{s,geo}(T)(m^{-2}) \times Geometric\ SSA \left(\frac{m^2}{g}\right) \times \text{Mass Conc.}\left(\frac{g}{L}\right).$ (1)~~

~~where the geometric *SSA* value for field data, ~ 0.4 m^2 g^{-1}, is derived from particle size distribution measurements presented in Fig. 3 of Hiranuma et al. (2011).~~

~~**Table 8** summarizes the TEOM mass concentrations and estimated annual and seasonal n_{INP} in different seasons over 2017 – 2019. In general, PM_{10} mass concentrations from OLLF-1 (average ± standard errors) were high in meteorological summers ($3.9 \times 10^{-7} \pm 5.6 \times 10^{-8}$ g L^{-1}) and springs ($4.5 \times 10^{-7} \pm 2.4 \times 10^{-7}$ g L^{-1}) as compared to fall ($2.4 \times 10^{-7} \pm 4.4 \times 10^{-8}$ g L^{-1}) and winter ($1.5 \times 10^{-7} \pm 5.3 \times 10^{-8}$ g L^{-1}). A similar trend was found for the upwind PM_{10} mass concentration: summer ($3.4 \times 10^{-8} \pm 9.0 \times 10^{-9}$ g L^{-1}) ≥ spring ($2.8 \times 10^{-8} \pm 9.3 \times 10^{-9}$ g L^{-1}) > fall ($1.8 \times 10^{-8} \pm 5.7 \times 10^{-9}$ g L^{-1}) ≥ winter ($1.4 \times 10^{-8} \pm 7.1 \times 10^{-10}$ g L^{-1}). But, the measured values at the upwind location are consistently an order magnitude lower than that from the downwind location.~~

~~On average, the estimated mean n_{INP} values at -15, -20, and -25 °C in 2016 – 2019 were estimated as 46.8 (±25.3 seasonal standard deviation; same hereafter), 288.1 (± 156.1), and 5,250.9 (± 2,845.6) L^{-1}, respectively. In addition, the median n_{INP} at -15, -20, and -25 °C in 2016 – 2019 were estimated as 14.7 (± 9.2), 90.9 (± 56.4), and 1,656.3 (± 1,028.1) L^{-1}, respectively. As our n_{INP} is linearly scaled to mass concentration (Eqn. 1), estimated n_{INP} showed a similar seasonal variability as seen in mass concentration.~~

~~For instance, at -20 °C, the cumulative n_{INP} averages for each meteorological season over three 2016 – 2019 were estimated as follows: spring (315.4 ± 164.9 L^{-1}) ≥ summer (270.4 ± 39.0 L^{-1}) > fall (165.1 ± 30.8 L^{-1}) ≥ winter (106.9 ± 36.8 L^{-1}). The observed high n_{INP} values were expected for such a high PM$_{10}$ mass concentrations emitted from the cattle feedyard, which represent an important point source of agricultural aerosol particle emission. However, we reemphasize that the IN efficiency of OLLF aerosol particles is somehow similar to other agricultural aerosol particles found in previous studies as discussed in **Sect. 3.2** (**Fig. 8**).~~

~~**Figure 9** displays the TEOM mass concentration time series over 2017 – 2019 as well as cumulative n_{INP} estimated at Ts of -15 °C, -20 °C and -25 °C. The background mass concentration measured at the upwind location (1.7×10^{-8} to 2.6×10^{-8} g L^{-1}) is shown with a red dashed line in **Fig. 9a** and subtracted from the downwind data. The resulting OLLF mass concentration was on average is $4.12 \times 10^{-7} \pm 2.96 \times 10^{-9}$ g L^{-1} (or 411.57 ± 2.96 µg m^{-3}). Annual averages of OLLF mass concentrations are indicated with a blue dashed line in **Fig. 9a**. On average, the downwind concentration exhibited higher mass concentration by more than an order of magnitude. This result implies a constant high particle load from the OLLF, which was also seen by a previous study at the same OLLF (Hiranuma et al., 2011). Seasonal variation is also seen in **Fig. 9a,** as the annual peak of mass concentration (> 10^{-5} g L^{-1}) coincided with summer in each case.~~

~~**Figure 9b** shows associated n_{INP} estimations. As seen in **Fig. 9b**, average estimated INPs at three different Ts, -15 °C, -20 °C, and -25 °C, are shown as a gray dashed line, black dashed line and black solid line, respectively. Our results show that the aerosol particles downwind of a feedlot contain several thousand INPs L^{-1} (median = 1,656 L^{-1}; average = 5,251 L^{-1}) at standard T and pressure (STP) at -25 °C, which is three orders of magnitude higher than typical ambient n_{INP} from continental sources as reported in DeMott et al. (2010). More discussion of OLLF n_{INP} in comparison with previous studies is provided in **Sect. 3.6**.~~

~~Our lab and field measurements-based parameterizations open up further study opportunities to incorporate supermicron INPs from agricultural source in the atmospheric modeling simulation and may provide a hint to reveal the identity of INPs at relatively high Ts (> -15 ºC). Note that the existence of supermicron particles at cloud altitudes is especially non-negligible when we consider atmospheric immersion freezing, which initiates on the surface of a few in a million particles.~~

3.~~6~~2.3. Comparison to previous soil dust IN studies

Figure ~~10~~ 9 summarizes our field measured n_{INP} (**Fig. ~~4~~6**) ~~as well as estimated atmospheric n_{INP}~~ in the temperature~~T~~ range between -5 °C and -25 °C ~~(**Sect. 3.5**)~~ in comparison to the previously reported ambient n_{INP} of soil dust and a compilation of other field-measured n_{INP} from across the world. We ~~purposely selected~~chose to display our estimated n_{INP} with standard deviations and global reference field n_{INP} data from Kanji et al. (2017) at their temperature~~T~~ points (i.e., -15, -20, and -25 °C) to make all comparisons visible in this figure. ~~It is clear that the estimated n_{INP} from OLLF are within OLLF field-measured n_{INP}, implying that our n_{INP} estimation is reasonable and atmospherically relevant.~~ It is ~~also~~ apparent that the OLLF n_{INP} spectra are consistently located above or overlapping with the upper bound of soil dust n_{INP} spectra from previous studies across the temperature~~T~~ range we examined in our field study ~~(i.e., T above -25 °C)~~. Although our INP detection limit of 0.05 L^{-1} in this study is higher than ~~not as good as~~ Suski et al. (2018; ≈ 0.002 L^{-1}), our data exceed their data from crop fields (soybean, sorghum, wheat, and corn) or are at least positioned towards the higher bound of the S18 data points. The observed consistent gap between our OLLF data and previous data holds true even when compared to the globally compiled n_{INP} from multiple field campaigns at -15, -20, and -25 °C (Kanji et al., 2017), indicating that absolute INPs per unit volume at OLLF are much higher than previously investigated field INP sources.

3.3. Laboratory vs. field results

3.3.1. Potential source of discrepancy

~~However, it is important to revisit our IN efficiency discussion included in **Sect. 3.2**. In short, o~~Our laboratory and field-derived $n_{s,\mathrm{geo}}$ values for our ~~derived from surface materials as well as field~~ OFFL samples are comparable to other reference soil and desert dust $n_{s,\mathrm{geo}}$ (**Fig. 4**) ~~(**Fig. 8**)~~. Taken together, ~~Altogether,~~ the observed comparability suggests~~we conclude~~ that OLLF soil dust is an important point ~~-~~source of atmospheric INPs~~, which have comparable or higher IN efficiency compared to formally assessed soil dusts~~. However, there is a deviation between laboratory $n_{s,\mathrm{geo}}$ and that from field investigation beyond uncertainties at temperatures above -22 °C. It is not clear what factors contribute to the observed deviation.

An application of different immersion freezing techniques (i.e., INSEKT and WT-CRAFT for laboratory and field study, respectively) cannot explain the discrepancy. As demonstrated in **Sect. S3**, the immersion freezing results of 50:50 splits of our field-collected filter sample were reproducible via the two techniques. Thus, the system difference can be ruled out of the potential factors triggering the deviation.

Different protocols to preserve laboratory and field samples (i.e., **Sects. 2.1.1 and 2.2.2**) may have impacted our sample properties and INPs. Beall et al. (2020) recently reported that different storage protocols in terms of time and temperature can alter n_{INP} in precipitation samples at relatively high freezing temperatures (i.e., > -19 °C). The authors also noted that “non-heat-labile INPs are generally less sensitive to storage”. This statement is important because our field airborne sample shows heat-stable characteristics (**SI Sect. 4**). However, in part because we have studied a limited number of samples in this study, it is not conclusive whether the difference in storage methods is fully responsible for the suppression of IN efficiency in our surface-collected proxies compared to the airborne sample.

The comparison between the immersion mode freezing ability of ambient OLLF dust sampled in the field and that of surface material samples aerosolized in the cloud simulation chamber shed light on the representativeness of dried, pulverized surface materials as surrogates for ambient dust particles in immersion freezing tests. Previously, Boose et al. (2016) studied immersion freezing abilities of diverse natural dust from nine desert regions around the globe (4 airborne and 11 sieved/milled surface samples) and found that the surface-collected samples tend to contain more efficient INPs than the airborne samples. The authors suggested that mineralogy may play a significant role to explain the observed difference. On the other hand, Kaufmann et al. (2016) found a similar freezing behavior of multiple surface dust samples despite the variation in mineralogy. Both studies noted the necessity of investigating non-mineral compositions. While our laboratory and field samples are different in nature, our organic-predominant samples show a reduction in IN efficiency for surface-collected samples compared to airborne field samples. The observed offset motivates further research in organic INPs.

Microbiomes identified in the OLLF dust proxies from this study (**Sect. 3.1.4**) exhibited different microbiome diversity from our field samples collected on 28 March 2019 and 22, 23, and 24 July 2018, which were previously reported in Vepuri et al. (2021). Dust samples TXD01 and TXD05 in this study were collected in September 2017; TXD01 is a composite sample from many locations of the TX panhandle, TXD05 is from a location in central Texas. Although they are of the same type, open cattle feedlot samples, a multitude of factors including sampling time, sampling methodology, location, cattle races raised in these areas, different feeding strategies, as well as the different total DNA extraction protocols, very likely explain the observed differences in microbiome composition. Nevertheless, they do share some common bacterial taxa, such as the presence of bacteria from the orders *Actinobacteriales*, *Caulobacterales*, and *Burkholderiales*, as well the genus *Marinoscillum*, albeit in low numbers in this study. An important caveat, however, is that we could not find any notable inclusions of known IN-active microbiomes in both sample subsets. While we cannot rule out the possibility of IN from TXD01 and TXD05 samples triggered by biological INPs, our current results do not support it. In the future, we need to carry out an identical metagenomic analysis for ice crystal residual (ICR) samples collected at various temperatures. Extracting enough DNA out of ICR samples would be challenging and is currently not feasible at the AIDA facility. Facilitating a dynamic cooling expansion chamber and collecting ICRs for a prolonged expansion experiment period would be a potential resolution. Future work should include metatranscriptomics (analysis of RNA) to estimate the population size and diversity of live microorganisms, as well as gene expression in the microbial population. More interdisciplinary strategy integrating, dietary, and health-related actions with cattle (e.g., how the diet of cattle, inclusion of antibiotics, and probiotics influence INP abundance in samples of feedlot surface materials) would also be useful.

Identifying heat-stable organic compounds and studying their physicochemical properties may be key to understanding the properties of OLLF INPs. Our chemical composition analysis of laboratory samples (**SI Sect. S1**) indicates that they are exclusively organic in nature in terms of aerosol composition. Further, airborne particles collected in OLLFs are generally known to include substantial amounts of organic materials. For example, our previous work using Raman micro-spectroscopy revealed that ≈ 96% of ambient aerosol particles sampled at the downwind edge of an OLLF contain brown or black carbon, hydrophobic humic acid, water-soluble organics, less soluble fatty acids, and carbonaceous materials mixed with salts and minerals (Hiranuma et al., 2011). Recently, organic acids (i.e., long-chain fatty acids) and heat-stable organics were found to act as efficient INPs (DeMott et al., 2018; Perkins et al., 2020). However, our knowledge regarding what particular organics from OLLFs trigger immersion freezing at heterogeneous freezing temperatures is still lacking. This deficit is another motivation to investigate OLLF-derived ICR samples in the laboratory.

~~One unique aspect of our OLLF samples is their heat tolerance. Previously, Suski et al. (2018) found that heat-treatment (95 °C for 20 min) can suppress the n_{INP} of wheat harvest soil dust sample from Kansas, USA by more than two orders of magnitude at -12 °C. The authors concluded that the decomposition of IN-active heat labile organics and bacteria is responsible for the observed n_{INP} suppression. This result is consistent with the impact of heat treatment on the IN efficiency of soil dust samplew from different regions, such as the one from a lodgepole pine forest in Wyoming, USA (Hill et al., 2016; 105 °C for 20 min) and another from Central Yakutia (Conen et al., 2011; 100 °C for 10 min). Similarly, Tobo et al. (2014) found that the 300 °C combustion can reduce the IN fraction of Wyoming soil dust at -24 °C by the same orders of magnitude as Suski et al. (2018) observed. In contrast, Steinke et al (2016) found no notable effect of heat treatment (~ 110 °C) on the Argentinian soil dust IN efficiency at ~ -24 °C. This heat insensitive nature of Argentinian soil dust may have coincided with its lack of IN-active proteins and/or heat sensitive microbes, which aligns with the absence of known IN-active microbes in our OLLF samples (**Sect. 3.3**). Suppression of $n_{s,\,geo}$ for wet-boiled samples of TXD01H at *T* above -20 °C can be found in **Table 5** and **Fig. 8c**. Nonetheless, the observed consistency in the spectral slopes suggests that lab and field measurements exhibit similar IN above examined *T*s. An example case of the negligible impact of the wet-boiling process on a field OLLF sample is discussed in **SI Sect. S3**. In total, our findings and the observation in Steinke et al. (2016) eliminate proteinaceous and biological ice-nucleating components as the primary source of IN abundance in air. The choice of 100-110 °C for heat treatment seems valid because proteinaceous structures will be destroyed below ~ 100 °C (Steinke et al., 2016). For example, Szyrmer and Zawadzki (1997) found some known cell-free IN-active microbes (e.g., Fusarial nuclei) are stable only up to 60 °C. Other than this study, ice nucleation activity by bacteria (Morris et al., 2004; Christner et al., 2008), fungi (Humphreys et al., 2001), and lichens (Henderson-Begg, et al., 2009) has been shown to be heat-sensitive irreversibly at 100 °C or below. Other soil organic components can be decomposed at *T* between 100 °C and 300 °C (Tobo et al., 2014).~~

3.3.2. Immersion freezing efficiency and parameterizations

The exponential fits for temperature-binned $n_{s,\mathrm{geo}}$ data (i.e., a moving average of every 0.5 °C) of lab and field measurements are summarized in supplemental **Table S3**. This parameterization offers a simple representation of supermicron-dominant INPs from

OLLF, which can act as an important point source of agricultural INPs in a very simple manner. Fit parameters are computationally optimized for the best *r* value, and the resulting parameters for each category are provided in this table. The $n_{s,geo}(T)$ spectral slopes, $\Delta\log(n_{s,geo})/\Delta T$, from this study were also computed. Individual parameterizations are useful to analyze spectra by comparing $\Delta\log(n_{s,geo})/\Delta T$ values. Overall, the range of spectral slope deviations (0.41– 0.52) is higher than what we previously studied in soil dust samples in **Fig. 4** (0.15 – 0.27; S16 – O14), indicating a unique feature of the OLLF dust. We note that offering a universal single parameterization for soil dust-derived INPs is not the scope of this study. As OLLF represents a point source of fresh livestock-generated dust, we expect that it would have different IN efficiency than aged and weathered dust samples.

4. Conclusions

This study aimed at investigating the immersion mode ice-nucleating properties of soil dust from OLLFs in Texas. ~~This study was~~Our investigations were composed of two parts: (1) an AIDA laboratory campaign to investigate the INP propensity and properties of two OLLF soil dust proxies; (~~1~~2) ~~A~~ a multi-year field investigation of immersion-mode INPs from four commercial OLLFs in the Texas Panhandle in 2017 – 2019~~; (2) an AIDA laboratory campaign, which investigated the INP propensity and properties of two OLLF soil dust proxies~~. Our ~~field and~~ laboratory and field findings support that OLLFs are a substantial source of ~~microbiome~~supermicron size ~~-enriched dust~~ particles and organic-rich soil dust INPs.~~, which~~ Overall, the estimated n_{INP} ~~are estimated to~~ exceeds several hundred and several thousand INPs L^{-1} at -20 °C and -25 °C, respectively, in the proximity to the OLLF emission sources.

Our AIDA immersion freezing results for OLLF proxies reasonably agree with the range of previous soil dust $n_{s,geo}$ values at least at temperatures around -25 °C and lower, validating the comparability of our results. However, the INSEKT immersion spectra of both surface materials measured for temperature > -25 °C are lower than previous soil dust outcomes. This difference indicates different properties of our feedlot dust proxies compared to other soil dust samples. Moreover, the importance of large aerosol particles on immersion freezing was verified in our AIDA-based laboratory study. The DFPC offline freezing instrument assessed IN abilities of OLLF dust surrogates with PM_1 and total (> PM_1) size fractions. Our assessment revealed that on average ≈ 50% of OLLF n_{INP} derived from supermicron aerosol particle population in the assessed temperature range between -18 and -22 °C. Thus, our laboratory study showed the potential importance of supermicron aerosol particles from OLLFs as INPs. While our metagenomics analysis does not support the presence of known IN-active microbiomes, more research should be directed to reveal the compositional identities and associated IN abilities of various other animal feeding facility samples.~~The importance of large aerosol particles on immersion freezing, motivated by our field work, was verified in our controlled-AIDA laboratory study, using ground-collected samples from the OLLFs. The DFPC offline freezing instrument assessed IN abilities of OLLF dust surrogates with PM_1 and > PM_1(total) size fractions, and revealed that on average ≈ 50% of OLLF n_{INP} derived from supermicron aerosol particle population in the assessed *T* range between -18 and -22 °C. Besides, several unique characteristics of OLLF INPs were disclosed. For instance, a comparability of results from our condensation freezing instrument (DFPC) and immersion freezing assay (INSEKT) was found. A similar observation was previously made for another composition (mineral dust) in Wex et al. (2014); this similarity suggests that freezing ability is similar for condensation and immersion for our surface OLLF samples. Further, the comparability between immersion mode IN ability of ambient OLLF dust (sampled in the field and analyzed in the offline lab setting) and that of surface material samples aerosolized in the cloud simulation chamber sheds light on the representativeness of dried, pulverized surface materials as surrogates for ambient dust particles in immersion freezing tests (Boose et al., 2016). In short, our AIDA-INSEKT results for OLLF proxies reasonably agree with the range of our field-derived $n_{s,geo}$ values, validating the atmospheric relevance of our lab results (especially TXD05 regardless of varied particle size distributions and sample types; see **Table 3**). Additionally, the observed consistency in the spectral slopes (i.e., **Table 5**) suggests that lab and field measurements exhibit similar IN ability at examined *Ts*.~~

~~Insignificance of dry-heating (100 °C for 24 hours) was demonstrated for both types of OLLF proxies. Previously, Steinke et al (2016) found no notable effect of heat treatment (~ 110 °C) on the Argentinian soil dust IN efficiency at ~ -24 °C. This heat insensitive nature of Argentinian soil dust might have coincided with its lack of IN-active proteins, which align with our lack of known IN-active microbiomes in our OLLF samples (**Sect. 3.3**). While suppression of $n_{s,\,geo}$ for wet-boiled (100 °C for 20 min) samples at *T* above -20 °C was found for both proxies (**Fig. 8**), it is not conclusive how OLLF soil dust is susceptible to heat. An example case of negligible impact of wet-boiling process on a field OLLF sample is discussed in **SI Sect. S3**. In total, our findings and the observation in Steinke et al. (2016) eliminate proteinaceous and biological ice-nucleating components to be considered as the primary source of superb IN abundance from OLLFs. The future sampling of more ambient filters from multiple seasons and systematic analysis of non-heated vs. wet-boiled treatment of ambient samples may provide more conclusive idea of heat resistivity of ambient OLLF-INPs.~~

~~The predominance of organics with salt contents (e.g., potassium) in OLLF particle composition is consistent with our previous study of OLLF soil dust particle composition analyses (Hiranuma et al., 2011). Based on findings from this study, ICR analysis revealed a relative increase in organic inclusion (and decrease in salt inclusion) in residuals, highlighting the importance of organic material in OLLF-derived INPs for atmospheric immersion. Even after dry heating treatment, the increase in organic fraction was found in the ICR of our OLLF samples. Therefore, the investigation of heat-insensitive organics is key to further understand the properties of soil dust INPs, and further research should focus on understanding how organic composition influences IN. Our previous work using Raman micro-spectroscopy revealed that ambient aerosol particles sampled at OLLFs are internally~~

~~mixed with brown or black carbon, hydrophobic humic acid, water soluble organics, less soluble fatty acids, and carbonaceous materials mixed with salts and minerals. But, our current knowledge regarding IN-active organics is still limited.~~

From the first year of our field work, we found that OLLF is a source of INPs that can be active at temperature~~*T*~~s below ~ -5 °C. ~~Briefly, the analysis of log ratio of $n_{\mathrm{INP,downwind}}$ to $n_{\mathrm{INP,upwind}}$ from three different OLLFs consistently shows that~~In short, the INP abundance at the downwind site of each OLLF is an order magnitude higher than at the nominal upwind edge across the examined temperature~~*T*~~ range (≥ -25 °C). This difference between downwind and upwind INPs clearly indicates that a vast majority of INPs found in our field sites (as high as 11,000 INP L^{-1} cumulatively at -25 °C) are from OLLFs~~ (**Table 1**)~~. Over the three years of our field OLLF investigation, there was a clear seasonal variation in n_{INP}. ~~Briefly, s~~Summer n_{INP} at -20 °C from the downwind edge of OLLFs (~~5.0 – 421.7~~up to ≈ 400 L^{-1}) was notably higher than that of spring (~~4.2 – 31.2~~up to ≈30 L^{-1}) and winter (up to ≈ 20~~0.9 – 20.4~~ L^{-1}). The observed seasonal trend persisted for all heterogeneous freezing temperature~~*T*~~s investigated in this study (temperature~~*T*~~ ≥ -25 °C). Interestingly, the observed n_{INP} seasonality strongly correlated to that of PM_{10} mass ($r = 0.94$). This relationship implies the importance of large particles, which dominate aerosol surface area and mass, on IN of OLLF dust. By scaling our n_{INP} to the aerosol particle surface area, we are no longer able to see any clear seasonal variation in $n_{\mathrm{s,geo}}$; thereby, we conclude that the abundance of INP from OLLFs depends on dust quantity at ground-level at a given time, but its IN efficiency is consistent throughout the seasons at least for 2017 – 2019. These findings also suggest that future studies of soil dust INP might need to focus on statistically validating the link between the properties of large supermicron particles and INPs with longer observations from a multitude of regions~~, which might ultimately result in providing a simple IN parameterization for cloud and climate models~~.

~~While we could not rule out the possibility of IN from TXD01 and TXD05 samples triggered by biological INPs, our current results did not support it. In the future, we also need to carry out an identical metagenomic analysis for ICR samples collected at various *T*s. Extracting enough DNA out of ICR samples would be challenging and is currently not feasible at the AIDA facility. Facilitating a dynamic cooling expansion chamber, and collecting ICRs for a prolonged expansion experiment period would be a potential resolution. Moreover, our metagenomics analysis indicated that most microorganisms were alive, but it did not provide any quantitative percentage. Therefore, we must do metatranscriptomics (analysis of RNA) in the future to examine gene expression in the microbial population. More interdisciplinary, collaborative studies (e.g., how the diet of cattle, inclusion of antibiotics, probiotics etc. influence INP abundance in samples of feedlot surface materials) would also be useful.~~ The onsite measurements of size-segregated INPs with a combination of a size-selecting impactor inlet and an online INP monitor will be indeed meaningful to add insights on the importance of large INPs.

Data availability. Original data created for the study will be available in the Supplement upon publication.

Supplement. The supplement related to this article is available online at: www.atmospheric-chemistry-and-physics.net

Author contributions. N.H., N.S.U., B.W.A., and O.M. designed research; N.H., B.W.A., F.B., J.B., K.C., D.G., K.H., Y.H., H.S., X.S., I.S., N.S.U., F.V., L.L., and O.M. performed research; N.H., F.B., R.F., D.G., K.H., Y.H., G.S., X.S., I.S., N.S.U., H.S.K.V., F.V., L.L., and O.M. analyzed data; and N.H., F.B., D.G., and X.S. wrote the paper. N.H. led the revision effort with support of all authors.

Competing interests. The authors declare no conflict of interest.

Acknowledgments. The authors wish to thank the IMK-AAF engineering and infrastructure group (Georg Scheurig, Rainer Buschbacher, Tomasz Chudy, Olga Dombrowski, Jens Nadolny, Frank Schwarz, and Steffen Vogt) for their continued support throughout the TxDUST01 campaign. We also acknowledge Prof. Dr. Thomas Schwartz and Dr.-Ing. Johannes Alexander, Department of Microbiology and Molecular Biology/Institute of Functional Interfaces/Karlsruhe Institute of Technology for valuable technical assistance. The authors acknowledge Hanover Research, Dr. Elise K. Wilbourn, and Dr. Gourihar Kulkarni for the language and technical edition.

Financial support. This project has received funding from the European Union's Horizon 2020 research and innovation programme through the EUROCHAMP-2020 Infrastructure Activity under grant agreement No 730997. This material is based upon work supported by the U.S. Department of Energy, Office of Science, Office of Biological and Environmental Research under Award Number DE-SC-0018979. Naruki Hiranuma and Yidi Hou thank the Killgore Faculty Research and President's Undergraduate Student Research Grants (WT20-034). This work was supported by Alexander von Humboldt – Stiftung (grant No 1188375) through a postdoctoral fellowship for Nsikanabasi S. Umo.

References

Alter, R. E., Fan, Y., Lintner, B. R., and Weaver, C. P.: Observational e~~E~~vidence that Great Plains i~~I~~rrigation h~~H~~as e~~E~~nhanced s~~S~~ummer p~~P~~recipitation i~~I~~ntensity and t~~T~~otals in the Midwestern United States, Journal of Hydrometeorology, 16, 1717–1735, 2015.

Annamalai, K., Sweeten, J. M., Auvermann, B. W., Mukhtar, S., Caperada, S., Engler, C. R., Harman, W., Jn, R., and Deotte, R: Renewable energy and environmental sustainability using biomass from dairy and beef animal production, U.S. Department of Energy Office of Scientific and Technical Information, 1039414, https://doi.org/10.2172/1039414, 2012.

~~Angly, F.E., Dennis, P.G., Skarshewski, A., Vanwonterghem, I., Hugenholtz, P., and Tyson, G. W.: CopyRighter: a rapid tool for improving the accuracy of microbial community profiles through lineage-specific gene copy number correction, Microbiome., 2, 11, https://doi.org/10.1186/2049-2618-2-11, 2014.~~

Auverman, B. W.: Controlling Dust and Odor from Open Lot Livestock Facilities, In: Koelsch et al., Livestock and poultry environmental stewardship (LPES) national curriculum, Midwest Plan Service, Ames, IA, USA, https://lpelc.org/wp-content/uploads/2019/03/LES_42.pdf (last accessed on July 3, 2021), 2001.

Auvermann, B. W., Hiranuma, N., Heflin, K., and Marek, G.: ~~2004.~~ Open-path transmissometry for measurement of visibility impairment by fugitive emissions from livestock facilities, American Society of Agricultural Engineers, 04-4010, https://doi.org/10.13031/2013.17090, https://www.researchgate.net/publication/228888957 (last accessed on March 21, 2021), 2004.

Beall, C. M., Lucero, D., Hill, T. C., DeMott, P. J., Stokes, M. D., and Prather, K. A.: Best practices for precipitation sample storage for offline studies of ice nucleation in marine and coastal environments, Atmos. Meas. Tech., 13, 6473–6486, 2020.

~~Belosi, F. and Santachiara, G.: Laboratory investigation of aerosol coating and capillarity effects on particle ice nucleation in deposition and condensation modes, Atmos. Res., 230, 104633, https://doi.org/10.1016/j.atmosres.2019.104633, 2019.~~

Benz, S., Megahed, K., M¨ohler, O., Saathoff, H., Wagner, R., and Schurath, U.: T-dependent rate measurements of homogeneousice nucleation in cloud droplets using a large atmospheric simulation chamber, J. Photoch. Photobio. A, 176, 208–217, 2005.

Bigelow, D. P. and Borchers, A.: Major uses of land in the United States, 2012. EIB-178, U.S. Department of Agriculture, Economic Research Service, USDA, https://www.ers.usda.gov/webdocs/publications/84880/eib-178.pdf?v=1485.8, (last accessed on July 3, 2021).

Boose, Y., Welti, A., Atkinson, J., Ramelli, F., Danielczok, A., Bingemer, H. G., Plötze, M., Sierau, B., Kanji, Z. A., and Lohmann, U.: Heterogeneous ice nucleation on dust particles sourced from nine deserts worldwide – Part 1: Immersion freezing, Atmos. Chem. Phys., 16, 15075–15095, 2016.

Boucher, O., Randall, D., Artaxo, P., Bretherton, C., Feingold, G., Forster, P., Kerminen, V.-M., Kondo, Y., Liao, H., Lohmann, U., Rasch, P., Satheesh, S. K., Sherwood, S., Stevens, B., and Zhang, X. Y.: Clouds and Aerosols, in: Climate Change 2013: The Physical Science Basis. Contribution of Working Group I to the Fifth Assessment Report of the Intergovernmental Panel on Climate Change, edited by: Stocker, T. F., Qin, D., Plattner, G.-K., Tignor, M., Allen, S. K., Boschung, J., Nauels, A., Xia, Y., Bex, V., and Midgley, P. M., Cambridge University Press, Cambridge, United Kingdom and New York, NY, USA, 571–657, 2013.

Brunauer, S., Emmett, P. H., and Teller, E.: Adsorption of gases in multimolecular layers, J. Am. Chem. Soc., 60, 309–319, 1938.

Bush, J., Heflin, K. R., Marek, G. W., Bryant, T. C., and Auvermann, B. W.: Increasing stocking density reduces emissions of fugitive dust from cattle feedyards, Applied Engineering in Agriculture, 30, 815–824, 2014.

Chaucheyras-Durand, F. and Ossa, F. : Review: The rumen microbiome: Composition, abundance, diversity, and new investigative tools, The Professional Animal Scientist, 30, 1–12, 2014.

Chen, J., Wu, Z., Chen, J., Reicher, N., Fang, X., Rudich, Y., and Hu, M.: Size-resolved atmospheric ice-nucleating particles during East Asian dust events, Atmos. Chem. Phys., 21, 3491–3506, ~~https://doi.org/10.5194/acp-21-3491-2021,~~ 2021.

~~Christner, B. C., Morris, C. E., Foreman, C. M., Cai, R., and Sands, D. C.: Ubiquity of biological ice nucleators in snowfall, Science, 319, 1214. https://doi.org/10.1126/science.1149757, 2008.~~

~~Cole, N. A., Mason, A. M., Todd, R. W., Rhoades, M., and Parker, D. B.: Chemical composition of pen surface layers of beef cattle feedyards, Professional Animal Scientist, 25, 541–552, 2009.~~

Conen, F., Morris, C. E., Leifeld, J., Yakutin, M. V., and Alewell, C.: Biological residues define the ice nucleation properties of soil dust, Atmos. Chem. Phys., 11, 9643–9648, ~~https://doi.org/10.5194/acp-11-9643-2011,~~ 2011.

~~Cory, K. M.: Immersion freezing of non-proteinaceous biological aerosol proxies & Arctic ambient particles, M. S. thesis, West Texas A&M University, https://wtamu-ir.tdl.org/handle/11310/227 (last accessed on March 23, 2021), 66 pp., 2019.~~

Creamean, J. M., Kirpes, R. M., Pratt, K. A., Spada, N. J., Maahn, M., de Boer, G., Schnell, R. C., and China, S.: Marine and terrestrial influences on ice nucleating particles during continuous springtime measurements in an Arctic oilfield location, Atmos. Chem. Phys., 18, 18023–18042, 2018.

DeMott, P. J., Prenni, A. J., Liu, X., Kreidenweis, S. M., Petters, M. D., Twohy, C. H., Richardson, M. S., Eidhammer, T., and Rogers, D. C.: Predicting global atmospheric ice nuclei distributions and their impacts on climate, Proc. Natl. Acad. Sci. U.S.A., 107, 11217–11222, 2010.

DeMott, P. J., Hill, T. C. J., Petters, M. D., Bertram, A. K., Tobo, Y., Mason, R. H., Suski, K. J., McCluskey, C. S., Levin, E. J. T., Schill, G. P., Boose, Y., Rauker, A. M., Miller, A. J., Zaragoza, J., Rocci, K., Rothfuss, N. E., Taylor, H. P., Hader, J. D., Chou, C., Huffman, J. A., Pöschl, U., Prenni, A. J., and Kreidenweis, S. M.: Comparative measurements of ambient atmospheric concentrations of ice nucleating particles using multiple immersion freezing methods and a continuous flow diffusion chamber, Atmos. Chem. Phys., 17, 11227–11245, 2017.

DeMott, P. J., Mason, R. H., McCluskey, C. S., Hill, T. C. J., Perkins, R. J., Desyaterik, Y., Bertram, A. K., Trueblood, J. V., Grassian, V. H., Qiu, Y., Molinero, V., Tobo, Y., Sultana, C. M., Christopher, L., and Prather, K. A.: Ice nucleation by particles containing long-chain fatty acids of relevance to freezing by sea spray aerosols, Environmental Science: Processes & Impacts, 20, 1559–1569, 2018.

Després, V. R., Huffman, J. A., Burrows, S. M., Hoose, C., Safatov, A. S., Buryak, G., Fröhlich-Nowoisky, J., Elbert, W., Andreae, M. O., Pöschl, U., and Jaenicke, R.: Primary biological aerosols in the atmosphere: A review of observations and relevance, Tellus B, 64, 15598, https://doi.org/10.3402/tellusb.v64i0.15598, 2012.

Drouillard, J. S.: Current situation and future trends for beef production in the United States of America - A review, Asian-Australas J Anim Sci., 31, 1007–1016, 2018.

Duniway, M. C., Pfennigwerth, A. A., Fick, S. E., Nauman, T. W., Belnap, J., and Barger, N. N.: Wind erosion and dust from US drylands: a review of causes, consequences, and solutions in a changing world, Ecosphere, 10, https://doi.org/10.1002/ecs2.2650, 2019.

~~Edgar, R. C., Haas, B. J., Clemente, J. C., Quince, C., and Knight, R.: UCHIME improves sensitivity and speed of chimera detection. Bioinformatics, 27, 2194–2200, 2011.~~

~~Eren, A. M., Maignien, L., Sul, W. J., Murphy, L. G., Grim, S. L., Morrison, H. G., and Sogin, M. L.: Oligotyping: differentiating between closely related microbial taxa using 16s rRNA gene data. Methods, Ecol. Evol., 4, 1111–1119, 2013.~~

~~Eren, A. M., Morrison, H. G., Lescault, P. J., Reveillaud, J., Vineis, J. H., and Sogin, M. L.: Minimum entropy decomposition: Unsupervised oligotyping for sensitive partitioning of high-throughput marker gene sequences, The ISME Journal, 9, 968–979, 2015.~~

Fahey, D. W., Gao, R.-S., Möhler, O., Saathoff, H., Schiller, C., Ebert, V., Krämer, M., Peter, T., Amarouche, N., Avallone, L. M., Bauer, R., Bozóki, Z., Christensen, L. E., Davis, S. M., Durry, G., Dyroff, C., Herman, R. L., Hunsmann, S., Khaykin, S. M., Mackrodt, P., Meyer, J., Smith, J. B., Spelten, N., Troy, R. F., Vömel, H., Wagner, S., and Wienhold, F. G.: The AquaVIT-1 intercomparison of atmospheric water vapor measurement techniques, Atmos. Meas. Tech., 7, 3177–3213, ~~https://doi.org/10.5194/amt-7-3177-2014,~~ 2014.

Fouts, D. E., Szpakowski, S., Purushe, J., Torralba, M., Waterman, R. C., MacNeil, M. D., Alexander, L. J., and Nelson, K. E.: Next generation sequencing to define prokaryotic and fungal diversity in the bovine rumen, PLoS One, 7, e48289, https://doi.org/10.1371/journal.pone, 0048289, 2012.

Ginoux, P., Prospero, J. M., Gill, T. E., Hsu, N. C., and Zhao, M.: Global scale attribution of anthropogenic and natural dust sources and their emission rates based on modis deep blue aerosol products, Rev. Geophys., 50, RG3005, https://doi.org/10.1029/2012RG000388, 2012.

Guo, L., Maghirang, R. G., Razote, E. B., Auvermann, B. W.: Laboratory evaluation of dust-control effectiveness of pen surface treatments for cattle feedlots, J. Environ. Qual., 40, 1503–1509, 2011.

Hande, L. B. and Hoose, C.: Partitioning the primary ice formation modes in large eddy simulations of mixed-phase clouds, Atmos. Chem. Phys., 17, 14105–14118, 2017.

~~Henderson-Begg, S. K., Hill, T., Thyrhaug, R., Khan, M., and Moffett, B. F.: Terrestrial and airborne non-bacterial ice nuclei, Atmosph. Sci. Lett., 10: 215–219, https://doi.org/10.1002/asl.241, 2009.~~

Hill, T. C., Moffett, B. F., DeMott, P. J., Georgakopoulos, D. G., Stump, W. L., and Franc, G. D.: Measurement of ice nucleation-active bacteria on plants and in precipitation by quantitative pcr, Appl. Environ. Microbiol., 80, 1256–1267, 2014.

Hill, T. C. J., DeMott, P. J., Tobo, Y., Fröhlich-Nowoisky, J., Moffett, B. F., Franc, G. D., and Kreidenweis, S. M.: Sources of organic ice nucleating particles in soils, Atmos. Chem. Phys., 16, 7195–7211, 2016.

~~Hiranuma, N., Brooks, S. D., Auvermann, B. W., and Littleton, R.: Using environmental scanning electron microscopy to determine the hygroscopic properties of agricultural aerosols, Atmos. Environ., 42, 1983–1994, 2008.~~

Hiranuma, N., Brooks, S. D., Gramann, J., and Auvermann, B. W.: High concentrations of coarse particles emitted from a cattle feeding operation, Atmos. Chem. Phys., 11, 8809–8823, 2011.

~~Hiranuma, N., Brooks, S. D., Moffet, R. C., Glen, A., Laskin, A., Gilles, M. K., Liu, P., Macdonald, A. M., Strapp, J. W., and McFarquhar, G. M.: Chemical characterization of individual particles and residuals of cloud droplets and ice crystals collected on board research aircraft in the ISDAC 2008 study, J. Geophys. Res.-Atmos., 118, 6564–6579, 2013.~~

Hiranuma, N., Augustin-Bauditz, S., Bingemer, H., Budke, C., Curtius, J., Danielczok, A., Diehl, K., Dreischmeier, K., Ebert, M., Frank, F., Hoffmann, N., Kandler, K., Kiselev, A., Koop, T., Leisner, T., Möhler, O., Nillius, B., Peckhaus, A., Rose, D., Weinbruch, S., Wex, H., Boose, Y., DeMott, P. J., Hader, J. D., Hill, T. C. J., Kanji, Z. A., Kulkarni, G., Levin, E. J. T., McCluskey, C. S., Murakami, M., Murray, B. J., Niedermeier, D., Petters, M. D., O'Sullivan, D., Saito, A., Schill, G. P., Tajiri, T., Tolbert, M. A., Welti, A., Whale, T. F., Wright, T. P., and Yamashita, K.: A comprehensive laboratory study on the immersion freezing behavior of illite NX particles: a comparison of 17 ice nucleation measurement techniques, Atmos. Chem. Phys., 15, 2489–2518, 2015.

~~Hiranuma, N., Möhler, O., Kulkarni, G., Schnaiter, M., Vogt, S., Vochezer, P., Järvinen, E., Wagner, R., Bell, D. M., Wilson, J., Zelenyuk, A., and Cziczo, D. J.: Development and characterization of an ice-selecting pumped counterflow virtual impactor (IS-PCVI) to study ice crystal residuals, Atmos. Meas. Tech., 9, 3817–3836, 2016.~~

Hiranuma, N., Adachi, K., Bell, D. M., Belosi, F., Beydoun, H., Bhaduri, B., Bingemer, H., Budke, C., Clemen, H.-C., Conen, F., Cory, K. M., Curtius, J., DeMott, P. J., Eppers, O., Grawe, S., Hartmann, S., Hoffmann, N., Höhler, K., Jantsch, E., Kiselev, A., Koop, T., Kulkarni, G., Mayer, A., Murakami, M., Murray, B. J., Nicosia, A., Petters, M. D., Piazza, M., Polen, M., Reicher, N., Rudich, Y., Saito, A., Santachiara, G., Schiebel, T., Schill, G. P., Schneider, J., Segev, L., Stopelli, E., Sullivan, R. C., Suski, K., Szakáll, M., Tajiri, T., Taylor, H., Tobo, Y., Ullrich, R., Weber, D., Wex, H., Whale, T. F., Whiteside, C. L., Yamashita, K., Zelenyuk, A., and Möhler, O.: A comprehensive characterization of ice nucleation by three different types of cellulose particles immersed in water, Atmos. Chem. Phys., 19, 4823–4849, 2019.

Hoose, C., Kristjánsson, J. E., and Burrows, S. M.: How important is biological ice nucleation in clouds on a global scale? Environ. Res. Lett., 5, 024009, https://doi.org/10.1088/1748-9326/5/2/024009, 2010.

~~Hoose, C. and Möhler, O.: Heterogeneous ice nucleation on atmospheric aerosols: a review of results from laboratory experiments, Atmos. Chem. Phys., 12, 9817–9854, 2012.~~

Huang, S., Hu, W., Chen, J., Wu, Z., Zhang, D., and Fu, P.: Overview of biological ice nucleating particles in the atmosphere, Environment International, 146, 106197, https://doi.org/10.1016/j.envint.2020.106197, 2021.

Huffman, J. A., Prenni, A. J., DeMott, P. J., Pöhlker, C., Mason, R. H., Robinson, N. H., Fröhlich-Nowoisky, J., Tobo, Y., Després, V. R., Garcia, E., Gochis, D. J., Harris, E., Müller-Germann, I., Ruzene, C., Schmer, B., Sinha, B., Day, D. A., Andreae, M. O., Jimenez, J. L., Gallagher, M., Kreidenweis, S. M., Bertram, A. K., and Pöschl, U.: High concentrations of biological aerosol particles and ice nuclei during and after rain, Atmos. Chem. Phys., 13, 6151–6164, 2013.

~~Humphreys, T. L., Castrillo, L. A., and Lee, M. R.: Sensitivity of Partially Purified Ice Nucleation Activity of Fusarium acuminatum SRSF 616, Curr. Microbiol., 42, 330–338, https://doi.org/10.1007/s002840010225, 2001.~~

Kanji, Z. A., Ladino, L. A., Wex, H., Boose, Y., Burkert-Kohn, M., Cziczo, D. J., and Krämer, M.: Overview of ice nucleating particles, Meteorological Monographs, 58, 1.1–~~-~~1.33, 2017.

Kaufmann, L., Marcolli, C., Hofer, J., Pinti, V., Hoyle, C. R., and Peter, T.: Ice nucleation efficiency of natural dust samples in the immersion mode, Atmos. Chem. Phys., 16, 11177–11206, 2016.

Katra, I.: Soil erosion by wind and dust emission in semi-arid soils due to agricultural activities, Agronomy, 10, 89, https://doi.org/10.3390/agronomy10010089, 2020.

Kenny, L. C., Gussman, R., and Meyer, M.: Development of a sharp-cut cyclone for ambient aerosol monitoring applications, Aerosol. Sci. Technol., 32, 338–358, 2000.

Ladino, L. A., Raga, G. B., Alvarez-Ospina, H., Andino-Enríquez, M. A., Rosas, I., Martínez, L., Salinas, E., Miranda, J., Ramírez-Díaz, Z., Figueroa, B., Chou, C., Bertram, A. K., Quintana, E. T., Maldonado, L. A., García-Reynoso, A., Si, M., and Irish, V. E.: Ice-nucleating particles in a coastal tropical site, Atmos. Chem. Phys., 19, 6147–6165, 2019.

Langer, G. and Rodgers, J.: An experimental study of ice nuclei on membrane filters and other substrata, J. Appl. Meteorol., 14, 560–571, 1975.

Li, R., Dong, X., Guo, J., Fu, Y., Zhao, C., Wang, Y., and Min, Q.: The implications of dust ice nuclei effect on cloud top temperature in a complex mesoscale convective system, Sci. Rep.,~~Scientific Reports,~~ 7, 13826, https://doi.org/10.1038/s41598-017-12681-0, 2017.

Mason, R. H., Si, M., Chou, C., Irish, V. E., Dickie, R., Elizondo, P., Wong, R., Brintnell, M., Elsasser, M., Lassar, W. M., Pierce, K. M., Leaitch, W. R., MacDonald, A. M., Platt, A., Toom-Sauntry, D., Sarda-Estève, R., Schiller, C. L., Suski, K. J., Hill, T. C. J., Abbatt, J. P. D., Huffman, J. A., DeMott, P. J., and Bertram, A. K.: Size-resolved measurements of ice-nucleating particles at six locations in North America and one in Europe, Atmos. Chem. Phys., 16, 1637–1651, 2016.

~~Li, R., Dong, X., Guo, J., Fu, Y., Zhao, C., Wang, Y., and Min, Q.: The implications of dust ice nuclei effect on cloud top temperature in a complex mesoscale convective system, Scientific Reports, 7, 13826, https://doi.org/10.1038/s41598-017-12681-0, 2017.~~

Möhler, O., Stetzer, O., Schaefers, S., Linke, C., Schnaiter, M., Tiede, R., Saathoff, H., Krämer, M., Mangold, A., Budz, P., Zink, P., Schreiner, J., Mauersberger, K., Haag, W., Kärcher, B., and Schurath, U.: Experimental investigation of homogeneous freezing of sulphuric acid particles in the aerosol chamber AIDA, Atmos. Chem. Phys., 3, 211–223, 2003.

Möhler, O., Field, P. R., Connolly, P., Benz, S., Saathoff, H., Schnaiter, M., Wagner, R., Cotton, R., Krämer, M., Mangold, A., and Heymsfield, A. J.: Efficiency of the deposition mode ice nucleation on mineral dust particles, Atmos. Chem. Phys., 6, 3007–3021, 2006.

~~Morris, C. E., Georgakopoulos, D. G., and Sands, D. C.: Ice nucleation active bacteria and their potential role in precipitation, J. Phys. IV France, 121, 87–103, https://doi.org/10.1051/jp4:2004121004, 2004.~~

Murray, B. J., Carslaw, K. S., and Field, P. R.: Opinion: Cloud-phase climate feedback and the importance of ice-nucleating particles, Atmospheric Chemistry and Physics, 21, 665–679, 2021.

Nagaraja, T. G.: in Rumenology, edited by: Millen, D., De Beni Arrigoni, M., and Lauritano Pacheco, R., Springer Nature, Cham, Switzerland, pp. 39–61, 2016.

Niemand, M., Moehler, O., Vogel, B., Vogel, H., Hoose, C., Connolly, P., Klein, H., Bingemer, H., DeMott, P., Skrotzki, J., and Leisner, T.: Parameterization of immersion freezing on mineral dust particles: An application in a regional scale model, J. Atmos. Sci., 69, 3077–3092, 2012.

O'Sullivan, D., Murray, B. J., Malkin, T. L., Whale, T. F., Umo, N. S., Atkinson, J. D., Price, H. C., Baustian, K. J., Browse, J., and Webb, M. E.: Ice nucleation by fertile soil dusts: relative importance of mineral and biogenic components, Atmos. Chem. Phys., 14, 1853–1867, 2014.

Overpeck, J. T. and Udall, B.: Climate change and the aridification of North America, Proc. Natl. Acad. Sci. U.S.A., 117, 11856–11858, 2020.

Parnell, C. B., Jones, D. D., Rutherford, R. D., and Goforth, K. J.: Physical properties of five grain dust types, Environ. Health Perspect., 66, 183–188, 1986.

Pastoor, J. W., Loy, D. D., Trenkle, A., and Lawrence, J. D.: Comparing fed cattle performance in open lot and bedded confinement feedlot facilities, The Professional Animal Scientist, 28, 410–416, 2012.

~~Patashnick, H. and Rupprecht, E. G.: Continuous PM-10 measurements using the tapered element oscillating microbalance, Journal of the Air and Waste Management Association, 41, 1079–1083, 1991.~~

Perkins, R. J., Gillette, S. M., Hill, T. C. J., and Demott, P. J.: The labile nature of ice nucleation by Arizona Test Dust, ACS Earth Sp Chem. 4, 133–141, 2020.

~~Phillips, V. T. J., DeMott, P. J., Andronache, C., Pratt, K. A., Prather, K. A., Subramanian, R., and Twohy, C.: Improvements to an empirical parameterization of heterogeneous ice nucleation and its comparison with observations, J. Atmos. Sci., 70, 378–409, 2013.~~

~~Pinnick, R. G., Fernandez, G., Martinez-Andazola, E., Hinds, B. D., Hansen, A. D. A., and Fuller, K.: Aerosol in the arid southwestern United States: Measurements of mass loading, volatility, size distribution, absorption characteristics, black carbon content, and vertical structure to 7 km above sea level, *J. Geophys. Res.*, 98, 2651–2666, 1993.~~

Pruppacher, H. R.~~,~~ and Klett, J. D.: Heterogeneous Nucleation. In Microphysics of Clouds and Precipitation – Second Revised and Enlarged Edition, Kluwer Academic Publishers, Netherland, pp. 287–360, 2010.

Razote, E. B., Maghirang, R. G., Predicala, B. Z., Murphy, J. P., Auvermann, B. W., Harner III, J. P., and Hargrove, W. L.: Laboratory evaluation of the dust emission potential of cattle feedlot surfaces, Transactions of the ASABE, 49, 1117–1124 https://doi.org/10.13031/2013.21729, 2006.

Reicher, N., Budke, C., Eickhoff, L., Raveh-Rubin, S., Kaplan-Ashiri, I., Koop, T., and Rudich, Y.: Size-dependent ice nucleation by airborne particles during dust events in the eastern Mediterranean, Atmos. Chem. Phys., 19, 11143–11158, 2019.

~~Rognes, T., Flouri, T., Nichols, B., Quince, C., and Mahé, F.: VSEARCH: a versatile open source tool for metagenomics, PeerJ. 4, e2584, https://doi.org/10.7717/peerj.2584, 2016.~~

Santachiara, G., Di Matteo, L., Prodi, F., and Belosi, F.: Atmospheric particles acting as ice forming nuclei in different size ranges, Atmos. Res., 96, 266–272, 2010.

Sarrocco, S.: Dung-inhabiting fungi: a potential reservoir of novel secondary metabolites for the control of plant pathogens, Pest. Manag. Sci., 72, 643–652, 2016.

Schiebel, T.: Ice nucleation activity of soil dust aerosols, Ph.D. thesis, Karlsruhe Institute of Technology, https://doi.org/10.5445/IR/1000076327, 131 pp., 2017.

Schneider, J., Höhler, K., Heikkilä, P., Keskinen, J., Bertozzi, B., Bogert, P., Schorr, T., Umo, N. S., Vogel, F., Brasseur, Z., Wu, Y., Hakala, S., Duplissy, J., Moisseev, D., Kulmala, M., Adams, M. P., Murray, B. J., Korhonen, K., Hao, L., Thomson, E. S., Castarède, D., Leisner, T., Petäjä, T., and Möhler, O.: The seasonal cycle of ice-nucleating particles linked to the abundance of biogenic aerosol in boreal forests, Atmos. Chem. Phys., 21, 3899–3918, 2021.

Schnell, R. C.~~,~~ and Vali, G.: Atmospheric Ice Nuclei from Decomposing Vegetation, Nature, 236, 163–165, 1972.

Schnell, R. C.~~,~~ and Vali, G.: World-wide Source of Leaf-derived Freezing Nuclei, Nature, 246, 212–213, 1973.

Si, M., Irish, V. E., Mason, R. H., Vergara-Temprado, J., Hanna, S. J., Ladino, L. A., Yakobi-Hancock, J. D., Schiller, C. L., Wentzell, J. J. B., Abbatt, J. P. D., Carslaw, K. S., Murray, B. J., and Bertram, A. K.: Ice-nucleating ability of aerosol particles and possible sources at three coastal marine sites, Atmos. Chem. Phys., 18, 15669–15685, 2018.

Steinke, I., Möhler, O., Kiselev, A., Niemand, M., Saathoff, H., Schnaiter, M., Skrotzki, J., Hoose, C., and Leisner, T.: Ice nucleation properties of fine ash particles from the Eyjafjallajökull eruption in April 2010, Atmos. Chem. Phys., 11, 12945–12958, 2011.

Steinke, I., Funk, R., Busse, J., Iturri, A., Kirchen, S., Leue, M., Möhler, O., Schwartz, T., Schnaiter, M., Sierau, B., Toprak, E., Ullrich, R., Ulrich, A., Hoose, C., and Leisner, T.: Ice nucleation activity of agricultural soil dust aerosols from Mongolia, Argentina, and Germany, J. Geophys. Res.-Atmos., 121, 13559–13576, 2016.

Steinke, I., Hiranuma, N., Funk, R., Höhler, K., Tüllmann, N., Umo, N. S., Weidler, P. G., Möhler, O., and Leisner, T.: Complex plant-derived organic aerosol as ice-nucleating particles – more than the sums of their parts?, Atmos. Chem. Phys., 20, 11387–11397, ~~https://doi.org/10.5194/acp-20-11387-2020,~~ 2020.

Storelvmo, T.: Aerosol e~~E~~ffects on c~~C~~limate via m~~M~~ixed-p~~P~~hase and i~~I~~ce c~~C~~louds, Annu. Rev. Earth Planet. Sci., 45, 199–222, 2017.

Suski, K. J., Hill, T. C. J., Levin, E. J. T., Miller, A., DeMott, P. J., and Kreidenweis, S. M.: Agricultural harvesting emissions of ice-nucleating particles, Atmos. Chem. Phys., 18, 13755–13771, 2018.

~~Szyrmer, W. and Zawadzki, I.: Biogenic and anthropogenic sources of ice-forming nuclei: A review, Bull. Am. Meteorol. Soc., 78, 209–228, 1997.~~

Tobo, Y., DeMott, P. J., Hill, T. C. J., Prenni, A. J., Swoboda-Colberg, N. G., Franc, G. D., and Kreidenweis, S. M.: Organic matter matters for ice nuclei of agricultural soil origin, Atmos. Chem. Phys., 14, 8521–8531, 2014.

Tobo, Y.: An improved approach for measuring immersion freezing in large droplets over a wide temperature range, Sci. Rep., 6, 32930, https://doi.org/10.1038/srep32930, 2016.

Ullrich, R., Hoose, C., Möhler, O., Niemand, M., Wagner, R., Höhler, K., Hiranuma, N., Saathoff, H., and Leisner, T.: A new icenucleation active site parameterization for desert dust and soot, J. Atmos. Sci., 74, 699–717, 2017.

U.S. Department of Agriculture (USDA): Cattle on feed, the National Agricultural Statistics Service, Agricultural Statistics Board, USDA, https://usda.library.cornell.edu/concern/publications/m326m174z?locale=en#release-items (last accessed on July 3, 2021).

Vali, G.: Ice nucleation relevant to formation of hail, Stormy Weather Group, Ph.D. thesis, McGill University, Montreal, Quebec, Canada, available at https://central.bac-lac.gc.ca/.item?id=TC-QMM-73746&op=pdf&app=Library&oclc_number=894992919 (last accessed on December 21, 2020), 1968.

Vali, G.: Quantitative evaluation of experimental results on the heterogeneous freezing nucleation of supercooled liquids, J. Atmos. Sci., 28, 402–409, 1971.

~~Vali, G., DeMott, P. J., Möhler, O., and Whale, T. F.: Technical Note: A proposal for ice nucleation terminology, Atmos. Chem. Phys., 15, 10263–10270, 2015.~~

Vepuri, H. S. K., Rodriguez, C. A., Georgakopoulos, D. G., Hume, D., Webb, J., Mayer, G. D., and Hiranuma, N.: Ice-nucleating particles in precipitation samples from the Texas Panhandle, Atmos. Chem. Phys., 21, 4503–4520, 2021.

von der Weiden, S.-L., Drewnick, F., and Borrmann, S.: Particle Loss Calculator – a new software tool for the assessment of the performance of aerosol inlet systems, Atmos. Meas. Tech., 2, 479–494, 2009.

Von Essen, S. G. and Auvermann, B. W.: Health effects from breathing air near CAFOs for feeder cattle or hogs, J Agromedicine, 10, 55–64, 2005.

von Holdt, J. R. C., Eckardt, F. D., Baddock, M. C., Hipondoka, M. H. T., and Wiggs, G. F. S.: Influence of sampling approaches on physical and geochemical analysis of aeolian dust in source regions, Aeolian Research, 50, 100684, https://doi.org/10.1016/j.aeolia.2021.100684, 2021.

~~Welti, A., Kanji, Z. A., Lüönd, F., Stetzer, O., and Lohmann, U.: Exploring the mechanisms of ice nucleation on kaolinite: from deposition nucleation to condensation freezing, J. Atmos. Sci. 71, 16–36, 2014.~~

Westbrook, C. D. and Illingworth, A. J.: Evidence that ice forms primarily in supercooled liquid clouds at temperatures > −27°C, Geophys. Res. Lett., 38, L14808, https://doi.org/10.1029/2011GL048021, 2011.

Wex, H., DeMott, P. J., Tobo, Y., Hartmann, S., Rosch, M., Clauss, T., Tomsche, L., Niedermeier, D., and Stratmann, F.: Kaolinite particles as ice nuclei: learning from the use of different kaolinite samples and different coatings, Atmospheric Chemistry and Physics, 14, 5529–5546, 2014.

Zelinka, M. D., Myers, T. A., McCoy, D. T., Po-Chedley, S., Caldwell, P. M., Ceppi, P., Klein, S. A., and Taylor, K. E.: Causes of higher climate sensitivity in CMIP6 models, Geophys. Res. Lett., 47, e2019GL085782, https://doi.org/10.1029/2019gl085782, 2020.

Figures and Tables

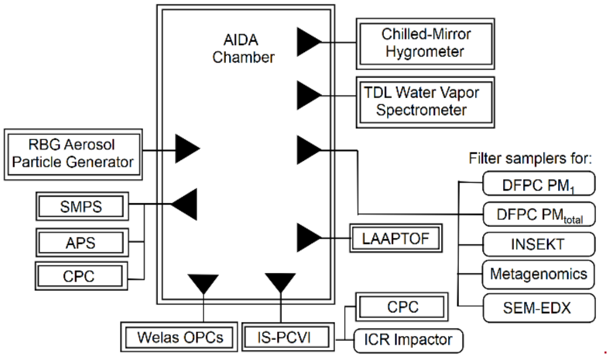

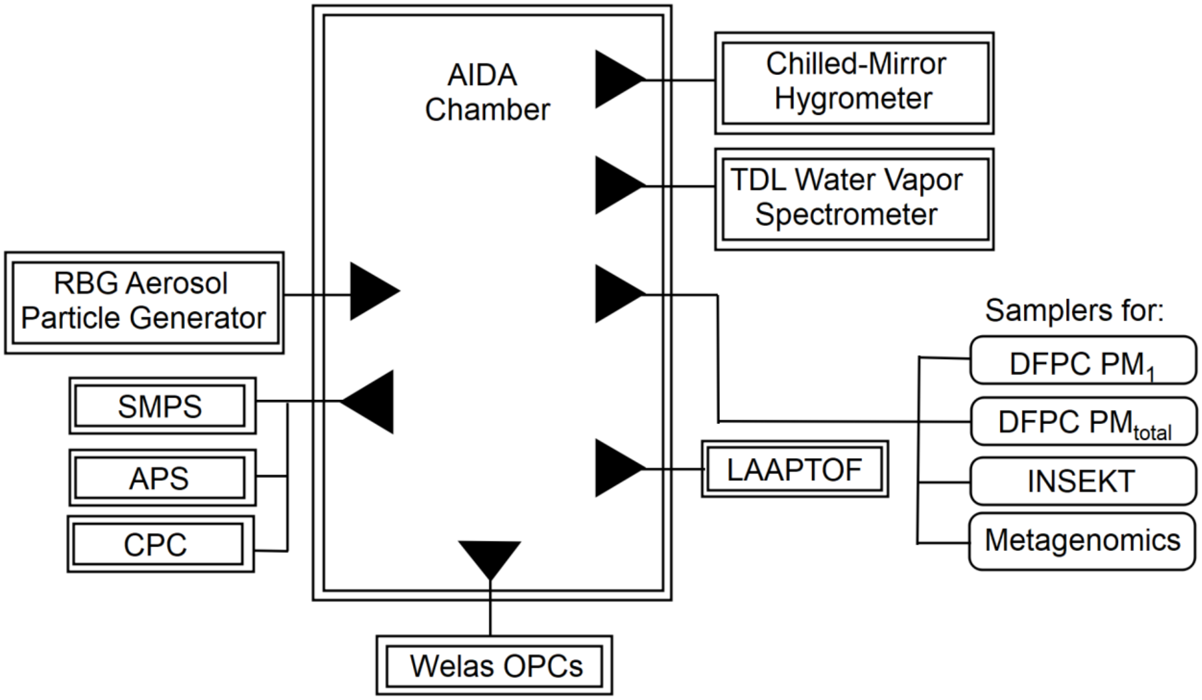

Figure ~~2~~1. Lab experimental schematic of the AIDA facility. All samples were injected using a rotating brush generator (RBG) for aerosol particle generation. Multiple extramural instruments, welas optical particle counters (OPCs), ~~an ice selective pumped counterflow virtual impactor (IS-PCVI),~~ a hygrometer, a tunable diode laser (TDL) spectrometer, a laser ablation aerosol particle time-of-flight mass spectrometer (LAAPTOF; see SI), and aerosol particle counters/sizers (SMPS, APS, CPCs), are connected to the AIDA chamber. Downstream filters and ~~an~~ impactors collected aerosol particles ~~and ice crystal residuals~~ for multiple offline analyses.

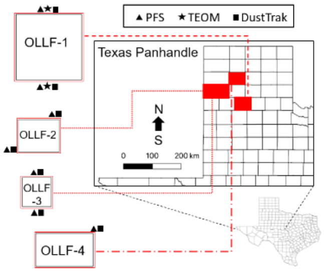

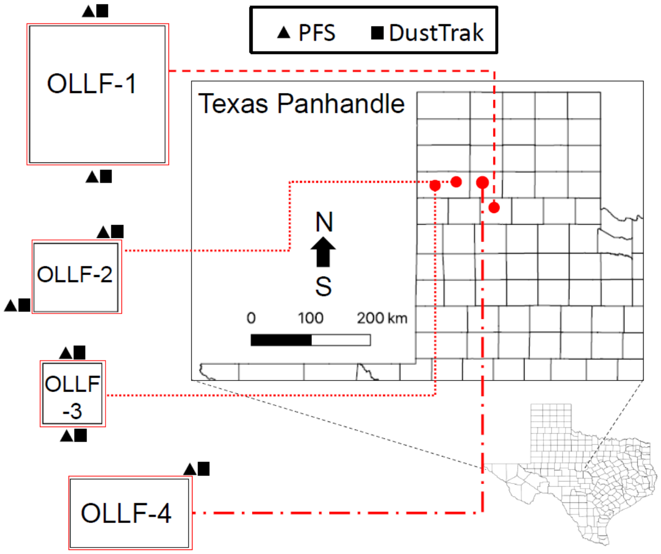

Figure ~~1~~2. Schematic of the field sampling activity at individual sites (only the counties are shown). The dimension of each facility (east – west × north – south) is (1) 1.6 × 1.6 km, (2) 1.0 × 0.8 km, (3) 0.7 × 0.7 km, and (4) 0.8 × 1.4 km. A combination of polycarbonate filter samplers (PFSs) and DustTrak instruments was used at the nominally upwind and downwind edges of OLLF-1 to OLLF-3. ~~Two tapered-element oscillating microbalances (TEOMs) were deployed at OLLF-1 alongside other instruments.~~

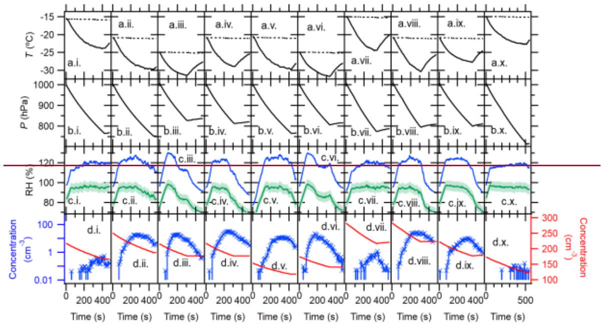

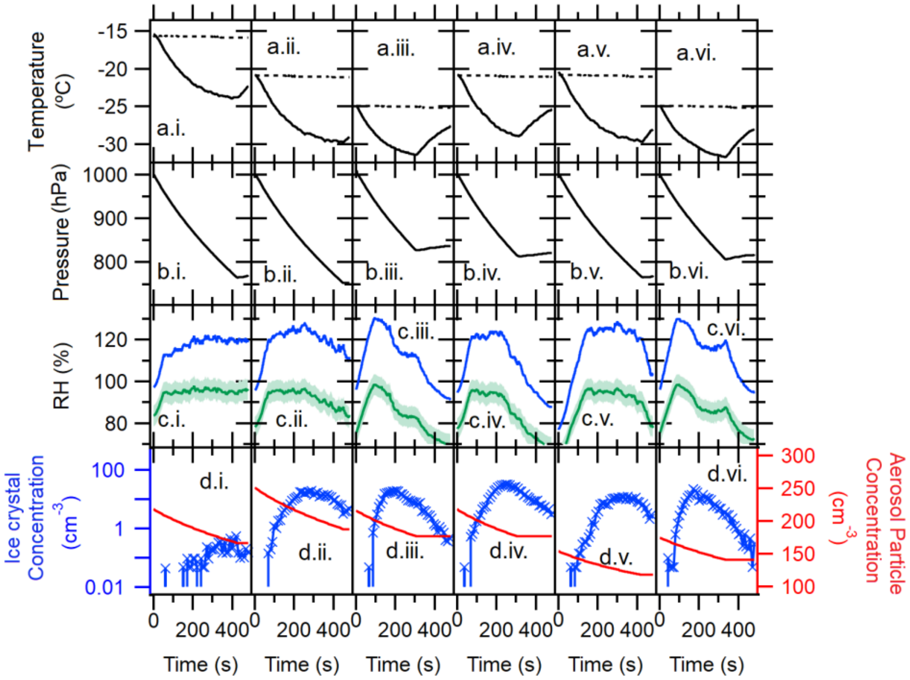

Figure ~~7~~3. Temporal profiles of the AIDA immersion freezing experiment [TXDUST01_07 (i), _08 (ii), _30 (iii), _12 (iv), _13 (v), _32 (vi)~~, _3 (vii), _4 (viii), _16 (ix), _17 (x)~~]. Arrays of alphabetical panels represent the chamber gas temperature~~*T*~~ (solid line) and the chamber wall temperature~~*T*~~ (dashed line) (a), ~~P~~ pressure in the AIDA chamber vessel (b), *RH* with respect to water (green line) and ice (blue line) (c), and aerosol particle concentration ~~initially~~ measured by the CPC (red solid line) as well as number concentration of > 20 μm D_{ve} AIDA particles measured by a welas optical particle counter (blue line) (d). Horizontal numerical panels represent different sample types and AIDA experiments, including TXD01 (i) – (iii) and~~,~~ TXD05 (iv) – (vi)~~, TXD01H (vii – viii), and TXD05H (ix – x)~~. *RH*s were determined with an accuracy of ± 5%, represented as the green shaded area in (c), using the mean gas temperature~~*T*~~ and the mean water vapor concentration.

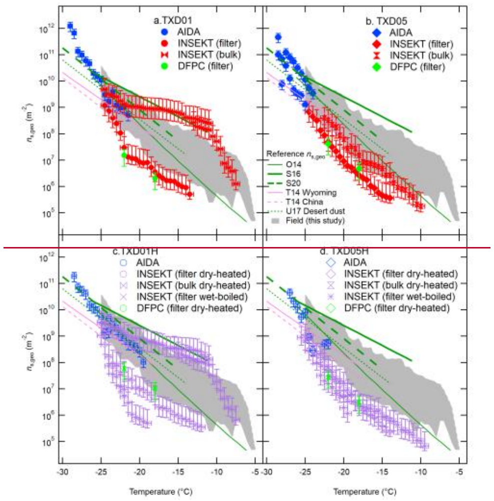

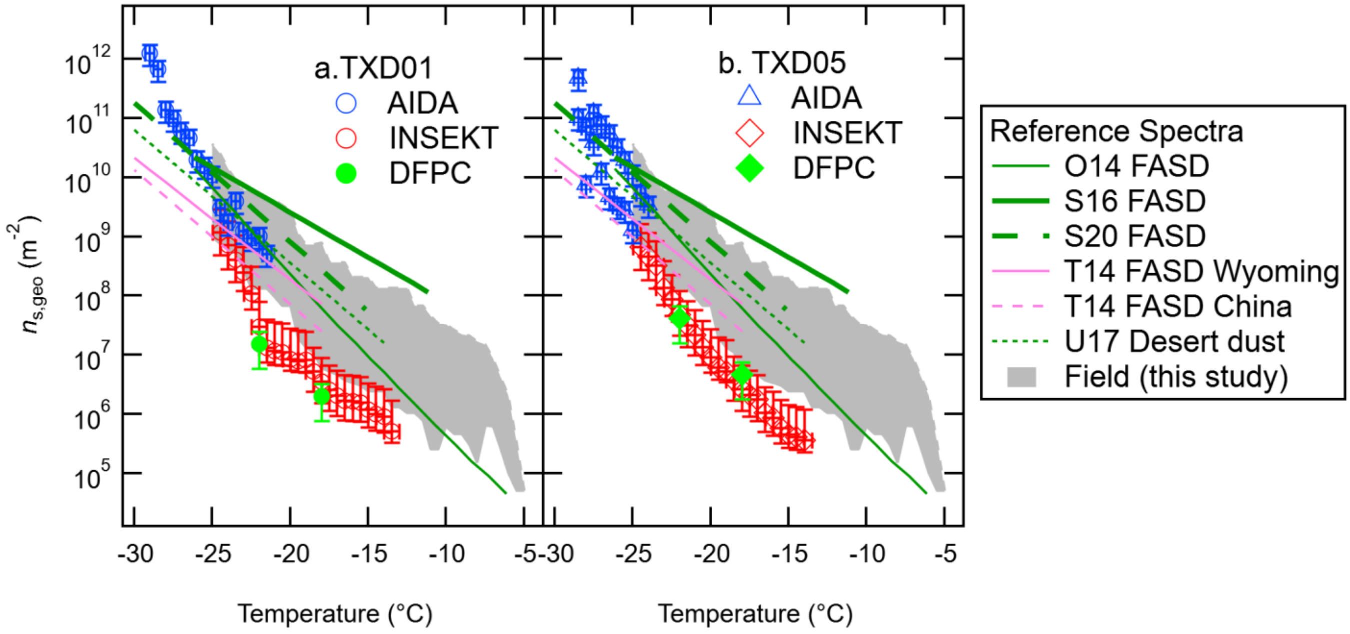

Figure ~~8~~4. IN-active surface-site density, $n_{s,geo}$, of surface materials, TXD01 (a) and~~,~~TXD05 (b)~~, TXD01H (c), and TXD05H (d)~~, was assessed by AIDA, INSEKT, and DFPC (total aerosol particles) as a function of temperature~~T~~. Six reference $n_{s,geo}$ curves for fertile and agricultural soil dust (FASD) ~~soil dust s~~ and desert dust are adapted from O'Sullivan et al. (2014; O14), Steinke et al. (2016; S16), Steinke et al. (2020; S20), Ullrich et al. (2017; U17), and Tobo et al. (2014; T14). The grey-shaded area represents the range of our field $n_{s,geo}$ values at 0.5 °C interval for -5 °C > temperature~~T~~ > -25 °C (**Fig.** ~~6~~8).

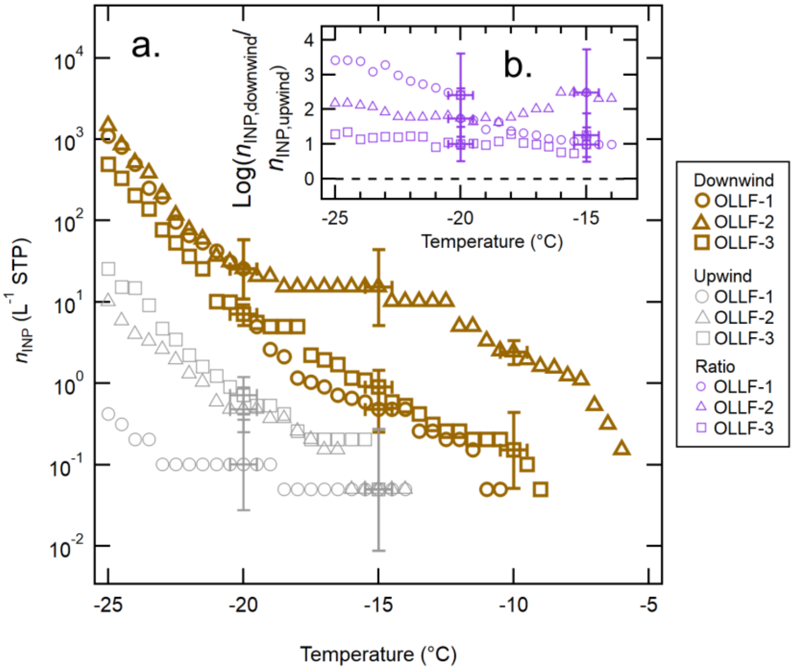

Figure ~~3~~5. The n_{INP} spectra of OLLF aerosol particles from field ambient samples: a comparison of the downwind n_{INP} (brown) to the upwind n_{INP} (grey) from s~~S~~ummer 2017 is shown in (a). Different symbol shapes correspond to individual OLLF sites as indicated in the legend. The uncertainties in temperature~~*T*~~ and n_{sNP} are ± 0.5 °C and ± CI95%, respectively. Error bars are shown at selected temperature~~*T*~~s to make all data points visible. The log-scaled downwind-to-upwind n_{INP} ratios, log($n_{INP,downwind}$/$n_{INP,upwind}$), for the overlapping temperature~~*T*~~ ranges are shown in (b). Note that the uncertainty in this ratio is > 50% due to large CI95% errors for measured n_{INP}. The black dashed line represents the ratio of zero (i.e., no difference between $n_{INP,downwind}$ and $n_{INP,upwind}$).

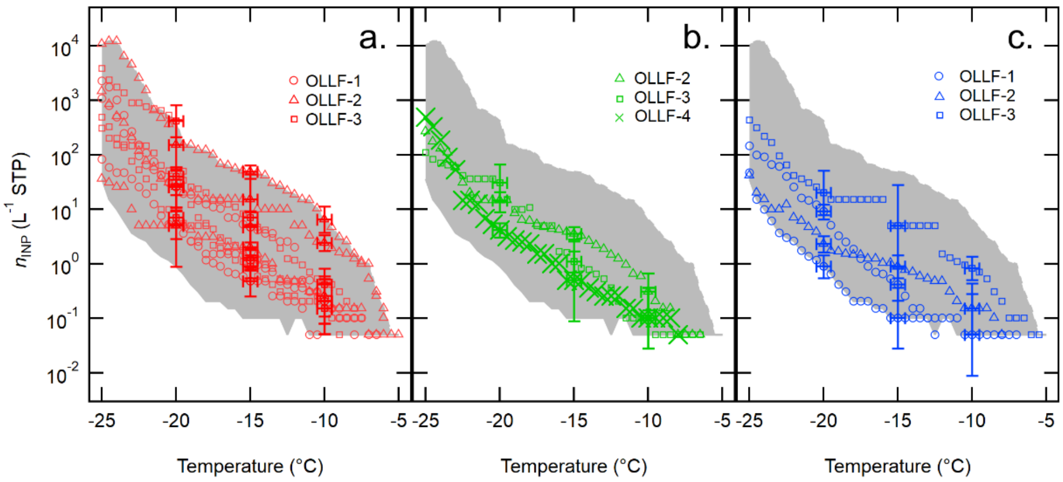

Figure ~~4~~6. Downwind OLLF n_{INP} spectra from 2017 – 2019 sorted based on meteorological seasons are shown; summer (a), spring (b), and winter (c). The uncertainties in temperature~~T~~ and $n_{s,geo}$ are ± 0.5 °C and ± CI95%, respectively, and error bars are shown at -5, -10, and -15 °C. The s~~S~~haded area represents minimum – maximum n_{INP}.

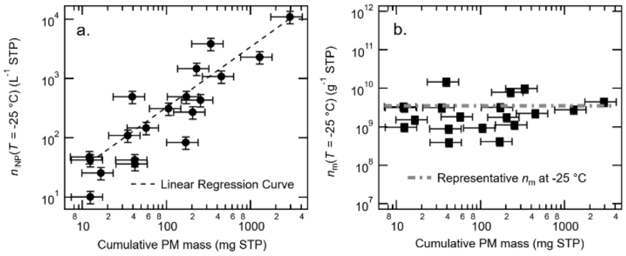

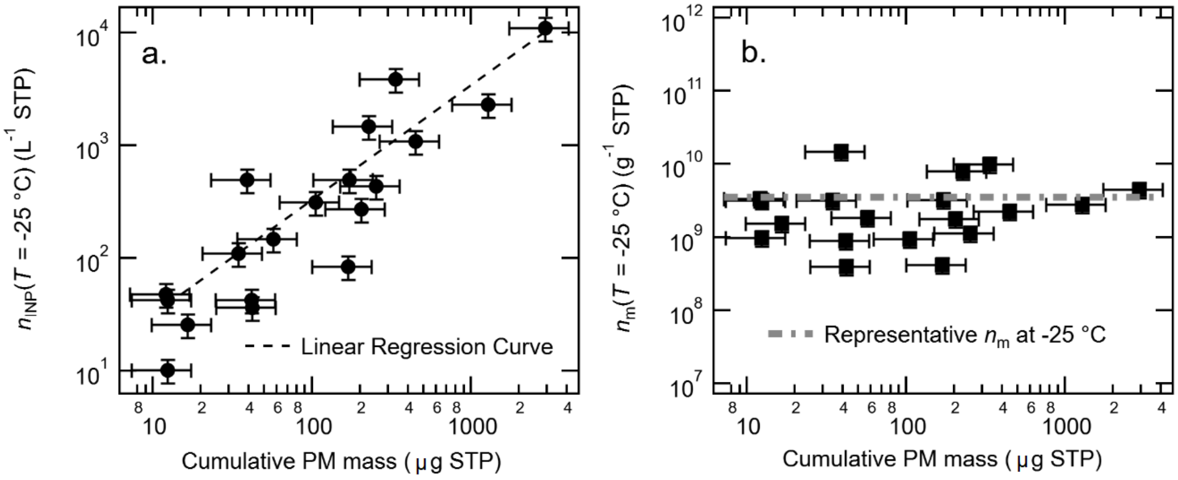

Figure ~~5~~7. Correlation between cumulative PM mass vs. n_{INP} (a) and vs. n_{m} (b) at -25 °C; a linear regression curve in log scale (n_{INP} = 3.51 × Cumulative PM Mass – 2.41; r = 0.94) is shown in (a), and the constant value of representative n_{m} at the given temperature~~T~~ (3.55×10^9 g^{-1}), which is a median n_{m} value of minimum – maximum, is shown in (b). Note the errors in cumulative PM mass are ± 40.4%~~ as discussed in **Sect. 3.1**~~. The uncertainty in n_{INP} and n_{m} is ± 23.5%.

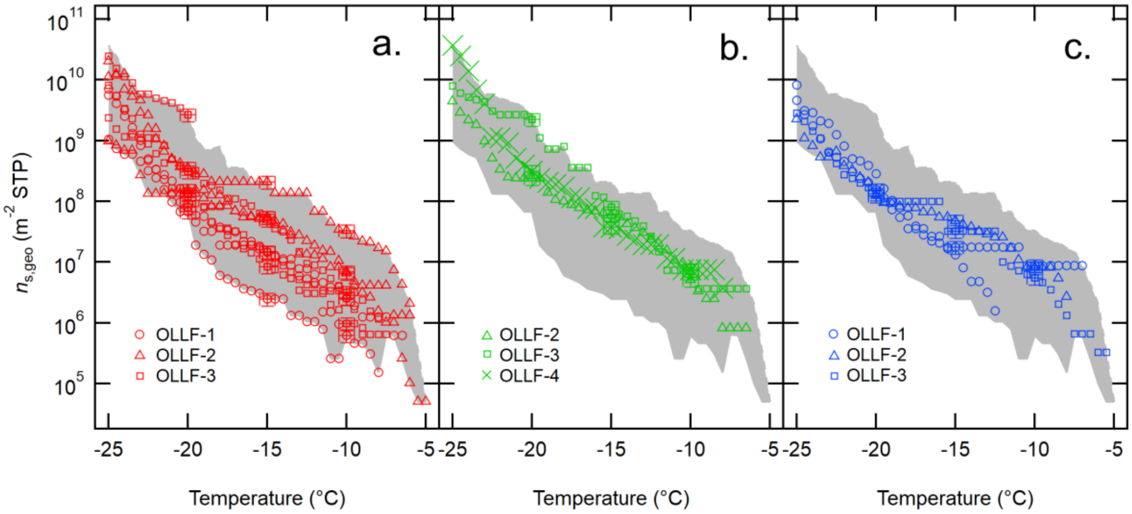

Figure ~~6~~8. The $n_{s,geo}$ spectra of OLLF aerosol particles from field ambient samples collected in 2017 – 2019. All downwind $n_{s,geo}$ spectra from summer (a), spring (b), and winter (c) are shown. Different symbol shapes correspond to individual OLLF sites as indicated in the legend. The uncertainties in temperature~~*T*~~ and $n_{s,geo}$ are ± 0.5 °C and ± 23.5%, respectively, and representing error bars are shown at -5, -10, and -15 °C. The ~~Shaded~~ shaded area represents minimum – maximum $n_{s,geo}$.

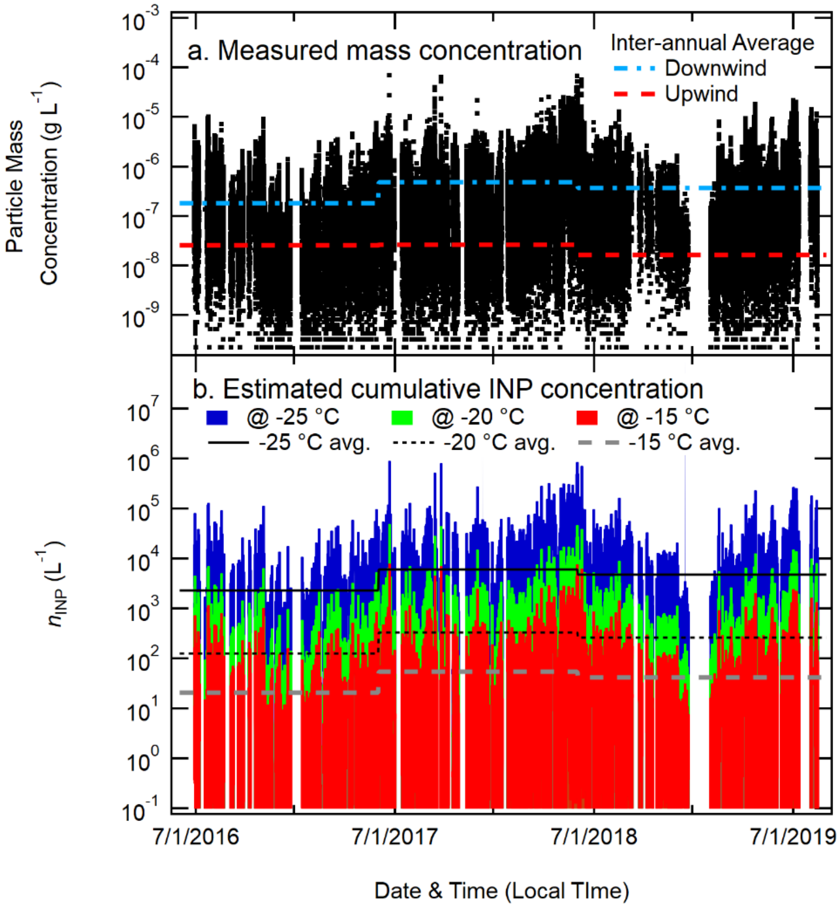

~~**Figure 9**. OLLF INP concentrations. Time-series plot of TEOM mass concentration measured at the downwind side of OLLF-1 (a) and cumulative n_{INP} estimated at *T*s of -15 °C, -20 °C, and -25 °C (b). In Panel a, inter-annual average mass concentrations of aerosol particles from OLLF (blue dashed line) and upwind (red dashed line) are shown (numbers adapted from **Table 8**). In Panel b, likewise, inter-annual average n_{INP} estimated at -15, -20, and -25 °C (reported in **Table 8**) are also shown. Meteorological summer in Texas is used for the beginning and ending time stamps of each year.~~

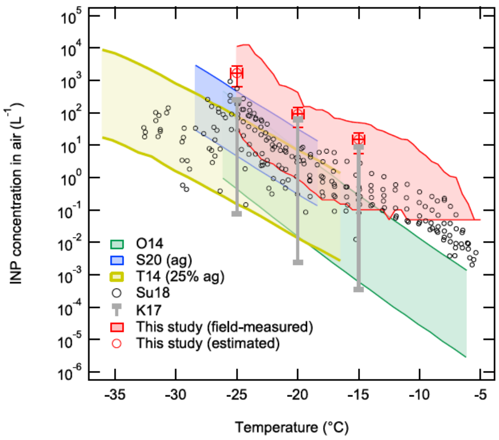

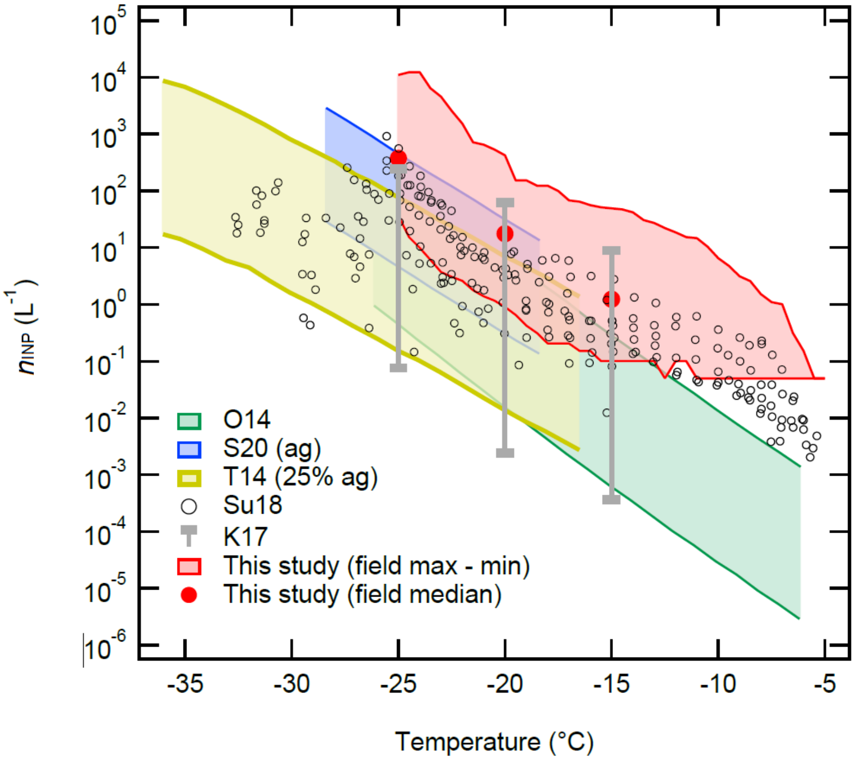

Figure ~~10~~9. The $n_{INP}(T)$ spectra ~~Ambient INP concentrations~~ of soil dust~~s~~ and aerosol particles as a function of temperature~~T~~. The red-shaded area represents the range of our field n_{INP} values at 0.5 °C intervals for -5 °C > temperature~~T~~ > -25 °C from this study (**Fig. ~~6~~4**). The red solid~~open~~ symbols are our ~~estimated~~ median ~~(± standard deviation)~~ at -15, -20, and -25 °C~~ discussed in Sect. 3.5~~. Five reference data are adapted from O'Sullivan et al. (2014 Fig. 9; O14), Steinke et al. (2020 Fig. 3; S20), Tobo et al. (2014 Fig. 6b; T14), Suski et al. (2018 Fig. 1a-d; Su18), and Kanji et al. (2017 Fig. 1-10; K17). Note that we display the maximum and minimum at -15, -20, and -25 °C of K17 in comparison to our estimation.

Table ~~3~~1. Characterization of particle properties: assessed prior to AIDA expansion experiments ~~(H denotes dry-heated)~~.

Experiment ID	Aerosol Particle Type	Mode (Min–Max) Diameter, µm**	$N_{total,0}$, ×10^{3} L^{-1}	$S_{total,0}$, ×10^{-9} m^{2} L^{-1}	$M_{total,0}$, ×10^{-}~~3~~9 ~~g~~µg L^{-1}	~~Geometric SSA, m² g⁻¹~~
	Aerosol Particle Measurements					
TXDUST01_7	TXD01	0.55 (0.10–3.16)	213.7	98.8	18.4	~~5.38~~
TXDUST01_8*	TXD01	0.54 (0.11–2.69)	266.3	115.5	21.1	~~5.46~~
TXDUST01_30	TXD01	0.72 (0.08–6.44)	210.6	119.0	29.7	~~4.01~~
TXDUST01_12*	TXD05	0.67 (0.09–5.14)	199.2	163.5	41.1	~~3.98~~
TXDUST01_13	TXD05	0.71 (0.10–4.71)	155.0	117.2	29.6	~~3.95~~
TXDUST01_32	TXD05	0.84 (0.15–4.37)	163.3	124.9	33.2	~~3.77~~
~~TXDUST01_3*~~	~~TXD01H~~	~~0.53 (0.10–2.69)~~	~~301.1~~	~~130.5~~	~~23.7~~	~~5.51~~
~~TXDUST01_4~~	~~TXD01H~~	~~0.52 (0.08–3.05)~~	~~282.1~~	~~137.1~~	~~23.9~~	~~5.73~~
~~TXDUST01_16*~~	~~TXD05H~~	~~0.78 (0.12–4.95)~~	~~227.4~~	~~195.1~~	~~49.3~~	~~3.96~~
~~TXDUST01_17~~	~~TXD05H~~	~~0.74 (0.12–4.59)~~	~~185.7~~	~~119.7~~	~~29.1~~	~~4.12~~

*~~INSEKT and DFPC s~~Samples for offline analyses (**Sects. 2.1.3 – 2.1.5**) were collected. **Based on the dS/dlogD_{ve} fit; Min–Max values are estimated at 0.1 × 10^{-9} m^{2} L^{-1}; $N_{total,0}$ = total number concentration of particles at the initial stage (t = 0) prior to expansion; $S_{total,0}$ = total surface concentration of particles at the initial stage (t = 0) prior to expansion; $M_{total,0}$ = total mass concentration of particles at the initial stage (t = 0) prior to expansion; D_{ve} = volume equivalent diameter.

Table 2~~1~~. Summary of the ambient aerosol particle filter sampling conditions: UW denotes upwind.

Year	Date	Location	Start Time (Local)	End Time (Local)	Flow Rate (LPM)*	Air Volume, V_{air} (L STP)	Suspension Water Volume, V_l (mL)
2019	20190715	OLLF-1	18:45:00	22:05:00	4.19	838.00	8.74
	20190716	OLLF-2	18:45:00	20:29:00	4.30	447.20	4.66
	20190724	OLLF-3	19:24:00	20:34:00	4.54	317.80	3.31
	20190226	OLLF-1	16:08:00	19:09:00	3.95	714.95	7.45
	20190328	OLLF-2	16:26:00	20:52:00	5.00	1330.00	13.87
	20190420	OLLF-3	17:05:00	21:05:00	4.15	996.00	10.39
	20190116	OLLF-1	16:03:00	19:33:00	3.97	832.65	8.68
	20190117	OLLF-2	15:48:00	19:30:00	3.97	880.23	9.18
	20190118	OLLF-3	15:40:00	18:40:00	3.62	651.60	6.79
2018	20180722	OLLF-1	18:42:00	22:39:00	6.58	1560.00	16.26
	20180723	OLLF-2	18:42:00	22:17:00	5.46	1173.79	12.24
	20180724	OLLF-3	18:20:00	22:13:00	3.65	850.31	8.86
	20180416	OLLF-4	16:53:30	20:06:40	5.99	1158.00	12.10
2017	20170709	OLLF-1	19:32:45	22:26:00	5.28	915.58	9.54
	20170710	OLLF-2	18:06:00	22:06:30	5.10	1227.19	12.79
	20170711	OLLF-3	18:28:00	22:08:00	5.13	1127.99	11.76
	20170709	OLLF-1-UW	19:50:00	22:47:00	5.28	935.24	9.75
	20170710	OLLF-2-UW	18:28:00	22:24:00	5.10	1204.24	12.55
	20170711	OLLF-3-UW	18:41:45	21:54:00	5.12	983.52	10.25

*A mass flow controller or a critical orifice was used to ensure a constant flow throughout each sampling activity. An airflow rate was measured with a flowmeter (TSI Inc., Model 4140).

~~**Table 2**. Properties of OLLF samples: non-heated (TXD01 & TXD05) and dry-heated (TXD01H & TXD05H).~~

~~System~~	~~TXD01~~	~~TXD05~~	~~TXD01H~~	~~TXD05H~~
~~[1]Density, g cm^{-3}~~	~~1.89 ± 0.06~~	~~2.05 ± 0.06~~	~~1.94 ± 0.06~~	~~2.00 ± 0.06~~
~~Geometric *SSA*, m^{2} g^{-1}~~	~~4.95 ± 0.82~~	~~3.97 ± 0.02~~	~~5.62 ± 0.16~~	~~4.04 ± 0.11~~
~~[2]BET-based *SSA*, m^{2} g^{-1}~~	~~3.23 ± 0.20~~	~~2.41 ± 0.20~~	~~3.23 ± 0.32~~	~~2.41 ± 0.24~~

~~[1]With a measurement standard deviation of ± 0.06, our system is capable of measuring densities of other powder samples, such as illite NX (2.91 g cm^{-3}) and fibrous cellulose (1.62 g cm^{-3}). Note that these values are similar to the density values reported by manufacturers for illite NX (2.65 g cm^{-3}) and fibrous cellulose (1.5 g cm).~~

Table 3. Properties of OLLF samples: TXD01 & TXD05.

System	TXD01	TXD05
[1]Density, g cm^{-3}	1.89 ± 0.06	2.05 ± 0.06
Geometric *SSA*, m^{2} g^{-1}	4.95 ± 0.82	3.97 ± 0.02
[2]BET-based *SSA*, m^{2} g^{-1}	3.23 ± 0.20	2.41 ± 0.20

[1]With a measurement standard deviation of ± 0.06, our system is capable of measuring densities of other powder samples, such as illite NX (2.91 g cm^{-3}) and fibrous cellulose (1.62 g cm^{-3}). Note that these values are similar to the density values reported by manufacturers for illite NX (2.65 g cm^{-3}) and fibrous cellulose (1.5 g cm^{-3}). [2]Brunauer et al., 1938.

Table 4. Geometric *SSA* values for individual AIDA expansion experiments.

Experiment ID	Aerosol Particle Type	Geometric *SSA*, m^2 g^{-1}
TXDUST01_7	TXD01	5.38
TXDUST01_8	TXD01	5.46
TXDUST01_30	TXD01	4.01
TXDUST01_12	TXD05	3.98
TXDUST01_13	TXD05	3.95
TXDUST01_32	TXD05	3.77

Table ~~4~~5. DFPC-estimated n_{INP} for TXD01 and TXD05 samples~~: H denotes the dry-heated sample~~. The subscripts of Tot and PM$_1$ represent INP obtained from total aerosol particles and that from PM$_1$ size-segregated aerosol particles, respectively. Standard deviations were derived based on multiple measurements for each sample. ~~Only PM$_{10}$ of TXD01 sample was examined due to the data limitation. This size limit is valid since we observed only < 6.44 µm aerosol particles in AIDA (**Table 3**). Supermicron INP fraction (%) is calculated by [() / $n_{INP,total}$] × 100. Note the change of supermicron INP fraction at two temperatures before and after the dry-heated treatment is due to different total aerosol particles available in AIDA (**Table 3**). A comparison of $n_{s,geo}$ shows a reasonable agreement within the uncertainties reported in **Sect. 2.4**.~~

~~Dust~~	~~n_{INP} x10^{3} (L^{-1}) ± standard dev.~~		~~Supermicron INP fraction (%)~~	
	~~-18 °C~~	~~-22 °C~~	~~-18 °C~~	~~-22 °C~~
~~TXD01$_{Tot}$~~	~~340.0 ± 211.0~~	~~2580.0 ± 698.0~~	~~**26.5**~~	~~**46.5**~~
~~TSD01$_{PM1}$~~	~~250.0 ± 90.0~~	~~1380.0 ± 219.0~~		
~~TXD01H$_{Tot}$~~	~~1266.7 ± 192.5~~	~~7141.7 ± 885.0~~	~~**72.4**~~	~~**60.2**~~
~~TSD01H$_{PM1}$~~	~~350.0 ± 120.0~~	~~2841.7 ± 375.8~~		
~~TXD05$_{Tot}$~~	~~770.0 ± 110.0~~	~~6780.0 ± 426.0~~	~~**58.4**~~	~~**48.4**~~
~~TSD05$_{PM1}$~~	~~320.0 ± 116.0~~	~~3500.0 ± 1066.0~~		
~~TXD05H$_{Tot}$~~	~~508.3 ± 100.0~~	~~4575.0 ± 1080.8~~	~~**60.7**~~	~~**24.6**~~
~~TSD05H$_{PM1}$~~	~~200.0 ± 45.8~~	~~3450.0 ± 715.8~~		

Dust	n_{INP} x10^{3} (L^{-1}) ± standard dev.		Supermicron INP fraction (%)	
	-18 °C	-22 °C	-18 °C	-22 °C
TXD01$_{Tot}$	340.0 ± 211.0	2580.0 ± 698.0	**26.5**	**46.5**
TSD01$_{PM1}$	250.0 ± 90.0	1380.0 ± 219.0		
TXD05$_{Tot}$	770.0 ± 110.0	6780.0 ± 426.0	**58.4**	**48.4**
TSD05$_{PM1}$	320.0 ± 116.0	3500.0 ± 1066.0		

~~**Table 5**. Abundance of major bacterial phyla in dust samples TXD01 and TXD05. Numbers indicate percentage of the OTUs for each phylum in the total bacterial microbiome. The percentage of *Actinobacteria* in the microbiome is increased in aerosolized samples.~~

~~**Taxonomy**~~	~~**Aerosolized TXD01**~~	~~**Aerosolized TXD05**~~
~~*Actinobacteria*~~	~~60.1%~~	~~92.9%~~
~~*Chloroflexi*~~	~~4.0%~~	~~1.1%~~
~~Unclassified~~	~~4.0%~~	~~2.6%~~
~~*Proteobacteria*~~	~~11.4%~~	~~0.6%~~
~~*Firmicutes*~~	~~13.6%~~	~~2.8%~~
~~*Bacteroidetes*~~	~~6.5%~~	~~0.0%~~
~~*Gemmatimonadetes*~~	~~0.4%~~	~~0.0%~~

Table 6. Summary of the ambient aerosol particle mass and immersion freezing properties of all field samples used in this study: UW denotes upwind.

Year	Date	Location	Start Time (Local)	End Time (Local)	Cumulative PM mass (μg STP)†	n_{INP}@ -25°C (L^{-1} STP)	n_{m}@ -25°C (g^{-1} STP)
2019	20190715	OLLF-1	18:45:00	22:05:00	168.20	8.38E+01	4.18E+08
	20190716	OLLF-2	18:45:00	20:29:00	41.92	3.66E+01	3.91E+08
	20190724	OLLF-3	19:24:00	20:34:00	105.00	3.11E+02	9.42E+08
	20190226	OLLF-1	16:08:00	19:09:00	57.22	1.48E+02	1.84E+09
	20190328	OLLF-2	16:26:00	20:52:00	204.55	2.72E+02	1.77E+09
	20190420	OLLF-3	17:05:00	21:05:00	34.50	1.10E+02	3.18E+09
	20190116	OLLF-1	16:03:00	19:33:00	12.02	4.78E+01	3.31E+09
	20190117	OLLF-2	15:48:00	19:30:00	41.53	4.22E+01	8.94E+08
	20190118	OLLF-3	15:40:00	18:40:00	251.77~~8~~	4.35E+02	1.13E+09
2018	20180722	OLLF-1	18:42:00	22:39:00	1281.10~~0~~	2.31E+03	2.81E+09
	20180723	OLLF-2	18:42:00	22:17:00	2917.86~~9~~	1.10E+04	4.43E+09
	20180724	OLLF-3	18:20:00	22:13:00	334.15	3.87E+03	9.84E+09
	20180416	OLLF-4	4:53:30	8:06:40	38.92	4.93E+02	1.47E+10
2017	20170709	OLLF-1	19:32:45	22:26:00	445.33	1.09E+03	2.25E+09
	20170710	OLLF-2	18:06:00	22:06:30	226.47~~5~~	1.48E+03	8.00E+09
	20170711	OLLF-3	18:28:00	22:08:00	171.52	4.92E+02	3.23E+09
	20170709	OLLF-1-UW	19:50:00	22:47:00	12.39~~4~~	4.22E+01	3.18E+09
	20170710	OLLF-2-UW	18:28:00	22:24:00	12.40	1.01E+01	9.78E+08
	20170711	OLLF-3-UW	18:41:45	21:54:00	16.53	2.57E+01	1.53E+09

~~*A mass flow controller or a critical orifice was used to ensure a constant flow throughout each sampling activity. An air flow rate was measured with a flowmeter (TSI Inc., Model 4140).~~ †Cumulative values of the mass collected on a filter were estimated by integrating DustTrak mass data, sampling time, and flow rate.

Table 7. Summary of the ambient conditions during field sampling activities: UW denotes upwind.

Year	Date	Location	Start Time (Local)	End Time (Local)	Wind Speed (MPH)	Wind Direction (degree)	Temperature (°C)	Pressure (mb)	*RH* (%)
2019	20190715	OLLF-1	18:45:00	22:05:00	3.6 ± 1.3	157.9 ± 13.9	30.1 ± 3.2	1015.6 ± 0.2	42.0 ± 10.8
	20190716	OLLF-2	18:45:00	20:29:00	10.6 ± 1.7	186.4 ± 4.3	34.3 ± 0.9	1015.9 ± 0.2	27.8 ± 1.7
	20190724	OLLF-3	19:24:00	20:34:00	10.1 ± 1.3	147.5 ± 6.6	28.9 ± 0.8	1020.6 ± 0.1	31.6 ± 1.4
	20190226	OLLF-1	16:08:00	19:09:00	11.2 ± 4.3	207.9 ± 13.2	20.5 ± 2.7	1014.8 ± 0.2	14.3 ± 2.9
	20190328	OLLF-2	16:26:00	20:52:00	8.7 ± 3.3	217.2 ± 6.7	23.5 ± 3.6	1012.7 ± 0.2	26.5 ± 6.8
	20190420	OLLF-3	17:05:00	21:05:00	10.2 ± 2.9	197.2 ± 19.1	27.0 ± 2.9	1009.0 ± 0.4	16.6 ± 5.0
	20190116	OLLF-1	16:03:00	19:33:00	16.6 ± 2.8	256.0 ± 6.8	16.5 ± 1.9	1014.7 ± 0.4	30.3 ± 3.1
	20190117	OLLF-2	15:48:00	19:30:00	8.7 ± 1.8	188.3 ± 11.6	14.6 ± 2.9	1017.4 ± 0.3	30.2 ± 5.6
	20190118	OLLF-3	15:40:00	18:40:00	23.3 ± 2.5	319.4 ± 33.1	11.5 ± 3.9	1005.3 ± 2.2	41.1 ± 21.8
2018	20180722	OLLF-1	18:42:00	22:39:00	5.7 ± 1.6	170.7 ± 11.0	33.4 ± 4.3	1015.7 ± 0.3	17.8 ± 5.8
	20180723	OLLF-2	18:42:00	22:17:00	5.1 ± 3.9	83.6 ± 21.1	28.8 ± 2.4	1022.4 ± 0.8	39.0 ± 5.1
	20180724	OLLF-3	18:20:00	22:13:00	7.9 ± 1.9	136.6 ± 12.0	28.9 ± 1.4	1023.3 ± 0.6	38.1 ± 2.6
	20180416	OLLF-4	16:53:30	20:06:40	12.1 ± 4.0	216.2 ± 8.3	29.5 ± 1.8	1009.9 ± 0.1	5.6 ± 0.8
2017	20170709	OLLF-1	19:32:45	22:26:00	9.3 ± 2.9	160.5 ± 10.1	27.9 ± 2.9	1017.0 ± 0.4	52.8 ± 13.1
	20170710	OLLF-2	18:06:00	22:06:30	10.3 ± 3.0	183.8 ± 9.0	31.6 ± 2.7	1015.5 ± 0.3	30.8 ± 5.1
	20170711	OLLF-3	18:28:00	22:08:00	6.4 ± 1.7	172.0 ± 10.9	29.9 ± 2.5	1015.2 ± 0.4	26.6 ± 6.0
	20170709	OLLF-1-UW	19:50:00	22:47:00	9.6 ± 2.8	160.4 ±9.4	27.1 ± 2.7	1017.2 ± 0.5	56.1 ± 12.3
	20170710	OLLF-2-UW	18:28:00	22:24:00	10.0 ± 3.0	182.6 ± 8.1	30.9 ± 2.9	1015.5 ± 0.4	32.1 ± 5.6
	20170711	OLLF-3-UW	18:41:45	21:54:00	6.2 ± 1.7	172.6 ± 10.8	30.0 ± 2.3	1015.2 ± 0.4	26.1 ± 5.4

~~**Table 6**. Summary of particle size properties through electron microscopy.~~

~~Sample Type~~	~~Measured Particles~~	~~*Diameter (μm)~~		~~**Aspect Ratio~~		~~Spermicron Size Fraction (%)~~
		~~Average~~	~~Std. Error~~	~~Average~~	~~Std. Error~~	
~~TXD01 aerosol~~	~~159~~	~~0.80~~	~~0.03~~	~~1.46~~	~~0.04~~	~~27.7%~~
~~TXD01 residual~~	~~185~~	~~0.87~~	~~0.03~~	~~1.56↑~~	~~0.04~~	~~29.2%~~
~~TXD01H dry-heated aerosol~~	~~162~~	~~0.82~~	~~0.03~~	~~1.42~~	~~0.03~~	~~26.5%~~
~~TXD01H dry-heated residual~~	~~126~~	~~0.90~~	~~0.04~~	~~1.48↑~~	~~0.05~~	~~33.3%~~
~~TXD01 cumulative~~	~~632~~	~~**0.84**~~	~~0.02~~	~~1.48~~	~~0.02~~	~~29.2%~~
~~TXD05 aerosol~~	~~194~~	~~0.99~~	~~0.03~~	~~1.37~~	~~0.03~~	~~44.3%~~
~~TXD05 residual~~	~~164~~	~~1.17~~	~~0.03~~	~~1.49↑~~	~~0.03~~	~~56.7%~~
~~TXD05H dry-heated aerosol~~	~~100~~	~~1.23~~	~~0.04~~	~~1.41~~	~~0.05~~	~~64.0%~~
~~TXD05H dry-heated residual~~	~~169~~	~~0.90~~	~~0.03~~	~~1.49↑~~	~~0.04~~	~~27.8%~~
~~TXD05 cumulative~~	~~627~~	~~**1.05**~~	~~0.02~~	~~1.44~~	~~0.02~~	~~38.8%~~

~~*Average of 2-D cross sections. **Ratio of cross sections (i.e., longer cross section/shorter cross section).~~

~~**Table 7**. Summary of particle composition types through energy dispersive X-ray spectroscopy.~~

~~Particle Type~~	~~TXD01 Abundance (%)~~				~~TXD05 Abundance (%)~~			
	~~Aerosol~~	~~Residual~~	~~Dry-heated Aerosol~~	~~Dry-heated Residual~~	~~Aerosol~~	~~Residual~~	~~Dry-heated Aerosol~~	~~Dry-heated Residual~~
~~Organic~~	~~5.0~~	~~7.6↑~~	~~3.1~~	~~9.5↑~~	~~8.2~~	~~9.1↑~~	~~3.0~~	~~11.2↑~~
~~Salt-rich~~	~~34.6~~	~~10.3↓~~	~~35.8~~	~~4.0↓~~	~~22.2~~	~~4.9↓~~	~~15.0~~	~~10.1↓~~
~~Mineral-rich~~	~~57.2~~	~~77.8~~	~~56.2~~	~~70.6~~	~~68.0~~	~~82.9~~	~~79.0~~	~~74.6~~
~~Other~~	~~3.1~~	~~4.3~~	~~4.9~~	~~15.9~~	~~1.5~~	~~3.0~~	~~3.0~~	~~4.1~~

~~**Table 8.** Inter-annual and seasonal PM_{10} mass concentrations from OLLF-1 as well as estimated n_{INP}.~~

	~~PM_{10} Mass Concentration (g L^{-1})~~		~~Estimated $n_{INP}(T)$ (L^{-1})~~		
	~~*OLLF~~	~~Upwind~~	~~T = -15 °C~~	~~T = -20 °C~~	~~T = -25 °C~~
~~**2016 – 2017**~~	~~**1.8E-07**~~	~~**2.6E-08**~~	~~**20.7**~~	~~**127.5**~~	~~**2323.4**~~
~~Summer~~	~~3.7E-07~~	~~5.2E-08~~	~~42.3~~	~~260.5~~	~~4747.7~~
~~Fall~~	~~1.6E-07~~	~~2.8E-08~~	~~18.1~~	~~111.7~~	~~2036.3~~

~~Winter~~	-	~~6.3E-08~~	~~1.5E-08~~	~~7.2~~	~~44.2~~	~~806.2~~
~~Spring~~	-	~~1.6E-07~~	~~2.1E-08~~	~~17.7~~	~~108.9~~	~~1985.5~~
~~**2017 – 2018**~~	-	~~**4.8E-07**~~	~~**2.6E-08**~~	~~**54.6**~~	~~**336.4**~~	~~**6133.0**~~
~~Summer~~	-	~~3.0E-07~~	~~2.3E-08~~	~~33.8~~	~~208.5~~	~~3801.1~~
~~Fall~~	-	~~3.1E-07~~	~~1.9E-08~~	~~35.4~~	~~218.2~~	~~3978.3~~
~~Winter~~	-	~~2.5E-07~~	~~1.3E-08~~	~~27.9~~	~~171.7~~	~~3129.6~~
~~Spring~~	-	~~9.2E-07~~	~~4.6E-08~~	~~104.1~~	~~641.3~~	~~11690.9~~
~~**2018 – 2019**~~	-	~~**3.7E-07**~~	~~**1.7E-08**~~	~~**42.3**~~	~~**260.7**~~	~~**4752.5**~~
~~Summer~~	-	~~4.9E-07~~	~~2.6E-08~~	~~55.6~~	~~342.3~~	~~6240.6~~
~~Fall~~	-	~~2.4E-07~~	~~7.9E-09~~	~~26.8~~	~~165.3~~	~~3013.0~~
~~Winter~~	-	~~1.5E-07~~	~~1.3E-08~~	~~17.0~~	~~104.8~~	~~1910.2~~
~~Spring~~	-	~~2.8E-07~~	~~1.6E-08~~	~~31.8~~	~~195.8~~	~~3570.0~~

~~*Upwind concentration is subtracted.~~ - - - -

Supplemental~~ry~~ Information (SI) for

Ice-nucleating particles from open-lot livestock facilities in Texas

Naruki Hiranuma[a,1], Brent W. Auvermann[b], Franco Belosi[c], Jack Bush[b], Kimberly M. Cory[a,d], ~~Romy Ullrich-Fösig[e],~~ Dimitrios G. Georgakopoulos[e~~f~~], Kristina Höhler[f~~e~~], Yidi Hou[a], Larissa Lacher[f~~e~~], Harald Saathoff[f~~e~~], Gianni Santachiara[c], Xiaoli Shen[f~~e~~,g], Isabelle Steinke[f~~e~~,h], Romy Ullrich[f], Nsikanabasi S. Umo[f~~e~~], Hemanth S. K. Vepuri[a], Franziska Vogel[f~~e~~], Ottmar Möhler[f~~e~~]

[a]Department of Life, Earth, and Environmental Sciences, West Texas A&M University, Canyon, TX 79016; [b]Texas A&M AgriLife Research, Amarillo, TX 79106; [c]Institute of Atmospheric Sciences and Climate, National Research Council, Bologna, Italy 40129; [d]Department of Environmental Toxicology, Texas Tech University, Lubbock, TX 79409; [e]Department of Crop Science, Agricultural University of Athens, Athens, Greece 118 55; [f~~e~~]Institute of Meteorology and Climate Research, Karlsruhe Institute of Technology, Karlsruhe, Germany 76021; [f]Department of Crop Science, Agricultural University of Athens, Athens, Greece 118 55; [g]Department of Earth Atmospheric and Planetary Sciences, Purdue University, West Lafayette, IN 47907; [h] Atmospheric Sciences & Global Change, Pacific Northwest National Laboratory, Richland, WA 99354

[1]To whom correspondence should be addressed. E-mail: nhiranuma@wtamu.edu.

This PDF file includes:

Supplementary text S1 to S6
Figures S1 to S5
Tables S1 to S3
SI References

~~S1. Ice-selecting pumped counterflow virtual impactor (IS-PCVI) sampling~~

~~The IS-PCVI is a custom-built instrument that can accommodate a substantially larger counterflow in comparison to commercially available PCVIs (e.g., Boulter et al., 2006). Such a large counterflow allows the IS-PCVI to have critical cut-off sizes of larger than 10 μm (more than twice as large as regular PCVIs) and, therefore, to inertially separate ice crystals from droplets found in mixed-phase clouds. As described in Hiranuma et al. (2016), the development of the IS-PCVI was guided by computation fluid dynamics simulations, and performance was verified in the lab using the AIDA chamber. Verifications include its transmission efficiencies (≈ 93%; See Fig. 7) and cut-sizes up to ~ 30 μm, ice phase separation based on the cut-size, validation of the evaporation section as part of the IS-PCVI outlet, performance of the interstitial particle sampling and minimum artifact detection (up to 5%).~~

~~**Table S1** summarizes the IS-PCVI properties used in four AIDA experiments during the TXDUST AIDA laboratory campaign. We selected these four experiments to focus on analyzing ice crystal residuals of each sample (i.e., TXD01, TXD01H, TXD05, and TXD05H) due to their similar critical cut-size and/or experimental conditions. The flow conditions in the IS-PCVI were chosen to ascertain the critical cut-size of ice crystals >24 μm diameter, which can be estimated based on Fig. 9 of Hiranuma et al. (2016). During the TXDUST01 campaign, the output flow of IS-PCVI was constant at 2.5 LPM, while the input and counter flows were slightly varied as listed in **Table S1**. Nonetheless, we used a moderate virtual concentration factor (i.e., Output/Input > 25) to ensure we collected a reasonable amount of ice crystal residuals on the substrates deployed downstream of IS-PCVI. **Fig. S1** shows temporal profiles of IS-PCVI experimental parameters during four AIDA cloud simulation experiments, in which ice crystal residuals were characterized and sampled. The number concentration of particles above a droplet-ice threshold size in the AIDA chamber was measured by the welas optical particle counter (Benz et al., 2005). These numbers virtually agreed with our residual count measured by a condensation particle counter (CPC, TSI Inc., Model 3076) after IS-PCVI (**Figs. 2 and S1d**). This comparability validated our choice of flow setting as well as the resulting critical cut-size of IS-PCVI (> 24 μm).~~

~~**Table S1**. Characterization of IS-PCVI properties during the AIDA expansion experiments. The critical cut-size of ice crystals was determined by the conditions of the input flow, output flow, effective counterflow (ECF), counterflow (CF), counterflow-to-input ratio, and pump flow.~~

				~~IS-PCVI properties~~						
~~Exp. ID~~	~~Reference time (CET)~~	~~Aerosol particle type~~	~~Cloud type~~	~~Input (LPM)~~	~~Output (LPM)~~	~~ECF (LPM)~~	~~CF (LPM)~~	~~CF/Input ratio~~	~~Pump (LPM)~~	~~critical cut-size (µm)~~
~~TXDUST01_08~~	~~10/11/2018 11:30:00~~	~~TXD01~~	~~Mixed-Phase~~	~~70.0~~	~~2.5~~	~~7.0~~	~~9.5~~	~~0.136~~	~~77.0~~	~~24.0~~
~~TXDUST01_04~~	~~10/9/2018 11:11:00~~	~~TXD01_Dry-Heated~~	~~Mixed-Phase~~	~~50.0~~	~~2.5~~	~~6.5~~	~~9.0~~	~~0.180~~	~~56.5~~	~~29.4~~
~~TXDUST01_12~~	~~10/15/2018 11:14:00~~	~~TXD05~~	~~Mixed-Phase~~	~~70.0~~	~~2.5~~	~~7.0~~	~~9.5~~	~~0.136~~	~~77.0~~	~~24.0~~
~~TXDUST01_31~~	~~10/26/2018 8:38:00~~	~~TXD05_Dry-Heated~~	~~Mixed-Phase~~	~~70.0~~	~~2.5~~	~~7.0~~	~~9.5~~	~~0.136~~	~~77.0~~	~~24.0~~

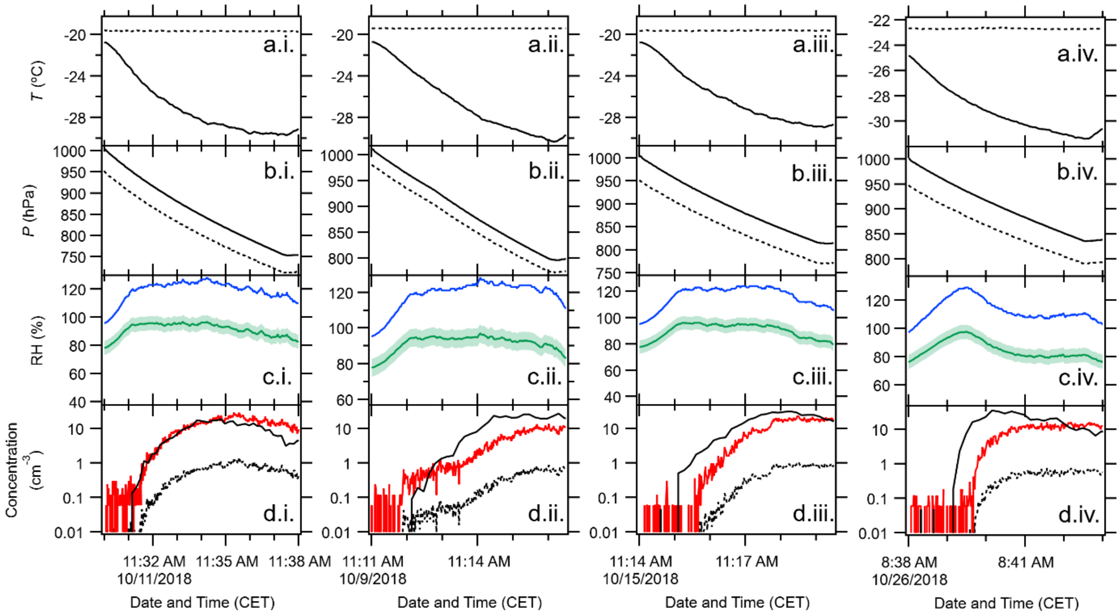

~~**Figure S1**. Temporal plots of the AIDA freezing experiments. Arrays of alphabetical panels represent the chamber gas *T*(solid line) and the IS-PCVI nozzle *T* (dashed line) (a), *P* in the AIDA chamber (solid line) and the IS-PCVI (dashed line) (b), *RH* with respect to water (green line) and ice (blue line) (c), and residuals measured by the CPC (red solid line) and corrected residual concentration according to Eqn. (6) of Hiranuma et al. (2016) (black dashed line) (d). In Panel (d), the number concentration of AIDA particles that have sizes above a droplet-ice threshold size (black solid line) is also shown. Horizontal numerical panels represent different sample types and AIDA experiments, including TXD01 (TXDUST01_08) (i), dry-heated TXD01 (TXDUST01_04) (ii), TXD05 (TXDUST01_12) (iii), and dry-heated TXD05 (TXDUST01_31) (iv). *RHs* were determined with an accuracy of ± 5% using the mean gas *T* and the mean water vapor concentration. Note that the minimum detection of CPC is 0.1 cm^{-3}, and only negligible background particle concentration was observed prior to each expansion. The counterflow to input flow ratios of 0.180 (ii) and 0.136 (i, iii and iv) correspond to critical ice particle cut-sizes of ≥ 24 μm volume-equivalent diameter, according to Fig. 9 of Hiranuma et al. (2016), transmitting pristine ice crystals downstream of the IS-PCVI.~~

~~S2~~S1. Chemical composition analysis

~~Single ~~Single-particle mass spectra of dry dispersed TXD particles in the size range between 200 and 2500 nm (vacuum aerodynamic diameter) were measured in the lab using a laser ablation aerosol particle time-of-flight mass spectrometer (LAAPTOF; AeroMegt GmbH) (Shen et al., 2018; 2019). ~~Both untreated and heat-treated samples were examined. ~~The powder particles were generated by powder dispersion using a rotating brush generator (PALAS GmbH, RBG1000), where a small volume~~s~~ of dry ~~TXD ~~samples ~~were ~~was dispersed by dry synthetic air.

The averaged mass spectra of TXD01 and TXD05 are shown in **Fig. ~~S2~~S1**. ~~We found no significant alternations in chemical composition and size distribution after dry-heating treatment; thereby, only spectra measured for the non-treated samples are shown. Nonetheless, this negative result supports the heat tolerance of TXD particles. ~~In general, the mass spectra of the dry dispersed particles showed high signals of organic markers at mass-to-charge ratio, m/z, of +44 ($COO/C_2H_6N^+$), -26 ($CN/C_2H_2^-$), -42 ($CNO/C_2H_2O^-$), -45 ($COOH^-$), -59 (CH_2COOH^-), -71 (CCH_2COOH^-), +30 ($NO/CH_3NH/CH_2O^+$), +58 (C_2H_5-NH-CH_2^+), and +59 ($(CH_3)_3N^+$). These are typical markers for organic acids and amine-containing particles. For example, peaks at m/z of +44 can be attributed to $COO/CH2NO^+$ derived from organic compounds/~~nitrogen ~~nitrogen-containing organic compounds (Schneider et al., 2011). It should be noted that m/z 44 can also be contributed by SiO^+, which is a silicon marker (Silva and Prather, 2000). Further, -45 ($COOH^-$), -59 (CH_2COOH^-), and -71 (CCH_2COOH^-) are the markers for carboxylic acids. ~~Peak ~~The peak at m/z of +30 can be attributed to NO^+ arising from nitrate, ammonium (Murphy et al., 2006; Shen et al., 2018), and CH_3NH^+ from amines (Silva and Prather, 2000; Schmidt et al., 2017). The other amine markers at +58 ($C_2H_5NHCH_2^+$) and +59 ($(CH_3)_3N^+$) were identified by previous studies (e.g., Angelino et al., 2001; Pratt et al., 2009; Schmidt et al., 2017).

For the inorganic markers, the characteristic ions were found on the peaks at m/z +23 (Na^+), +24 (Mg^+), +27 (Al^+), +28 (Si^+), +39 (K^+), +40 (Ca^+), +44 (SiO^+), +56 (CaO/Fe^+), +64/66 (Zn^+), -97 (HSO_4^-),+30 (NO^+), -63 (PO_2^-), -79 (PO_3^-), and -95 (PO_4^-). Calcium and sodium are used as additives in the diet fed to the cattle, and they also exist in the unpaved road dust (National Research Council, 2000; Ocsay et al., 2006). Manure is a source of ammonium and phosphate. Minor fractions of other salts and mineral dust constituents found in this work~~,~~ were also identified in the field samples (Hiranuma et al., 2011 and references therein). As mentioned above, +30 NO^+ can arise from ammonium (Murphy et al., 2006; Shen et al., 2018). In addition, -63 (PO_2^-), -79 (PO_3^-), and -95 (PO_4^-) are phosphate markers (Schmidt et al., 2017; Zawadowicz et al., 2017). However, our inorganic quantification is inconclusive, and the result may deviate from other quantitative composition analyses.

Comparing TXD01 to TXD05, we found that TXD01 had more intensive phosphate (-63, -79) and potassium (+39) compared to TXD05 (**Fig. ~~S2~~S1**). In particular, phosphate intensity was a few times higher than TDX05. On the other hand, TXD05 had ~~a ~~higher signals of sodium- and nitrogen-containing compounds as well as stronger amine markers, i.e., m/z +30 (NO/CH_3NH^+) and +58 (C_2H_5-NH-CH_2^+), than TXD01.

A more detailed analysis of the individual mass spectra revealed several distinct particle types. Using a combination of the fuzzy c-means clustering (Shen et al., 2019) and the marker peak search method based on the above-mentioned and other characteristic ions, we found several distinct composition classes, such as "~~Potassium ~~Potassium-rich," "Potassium and ~~phosphate ~~phosphate-rich," "Potassium, sodium, and ammonium rich," "Amine rich," and "Mineral and ~~Metal ~~Metal-rich." We note that the "rich" used here only indicates intensive characteristic peaks in the mass spectra rather than a large mass fraction. **Figure ~~S3~~ S2** shows the fuzzy classification results. As can be seen, there was no notable ~~size ~~size-dependent composition for ~~any ~~both sample types. ~~No obvious change in chemical compositions and size distribution was found after dry-heating treatment. A slight decrease in organic-potassium mixtures was found for dry-heated particle samples in comparison to non-heated ones, but the difference was insignificant. ~~A significant amount of carboxylic acid groups (i.e., m/z -45 and -71) was found in each particle. These prevalent organic markers suggest that, regardless of the classification, TXD are predominantly organic in nature. This organic predominance as well as the substantial inclusion of salts (e.g., potassium) are consistent with our previous study of TXD particles' composition (Hiranuma et al., 2011). We also note that our LAAPTOF aerosol particle chemical composition analysis was not intended to find ice nucleation (IN) ~~-~~active composition. Ice-nucleating particles (INPs) generally represent a small subset of aerosol particles (roughly one per million, even at low temperature~~T~~s). Thus, examining aerosol particle chemical composition cannot be directly linked to the role of chemistry in IN. In other words, aerosol particle composition does not necessarily represent INP composition. ~~A complementary elemental composition of ice crystal residuals is discussed in the main manuscript. But~~However, aerosol particle composition data are important for understanding the general chemical compositions of our samples.

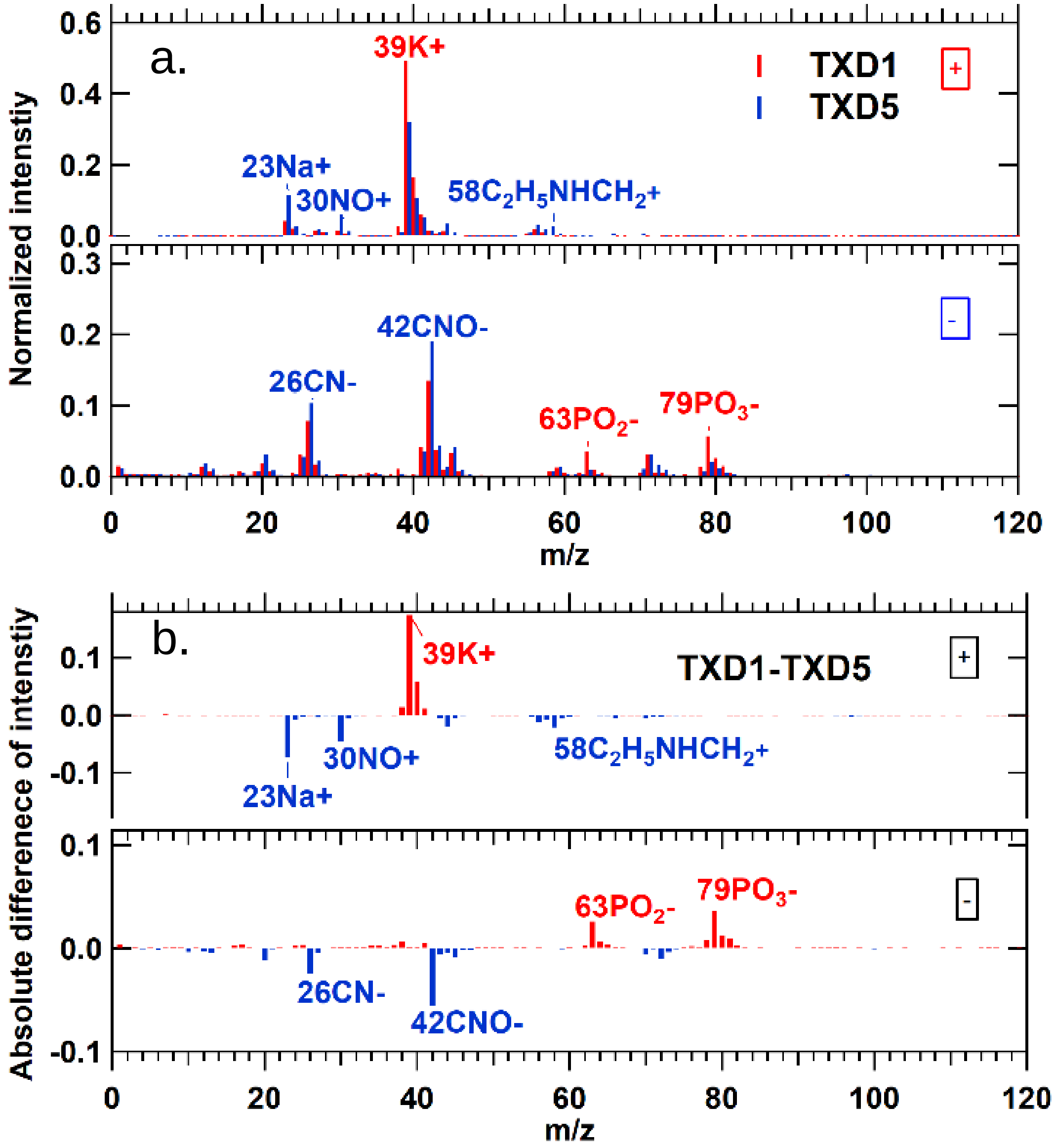

Figure ~~S2~~S1. Laboratory reference mass spectra of dry dispersed TXD01 and TXD05 particles with LAAPTOF. ~~The left panels show~~ (a) Tthe stacked averaged spectra of cations (top) and anions (bottom) found in TXD01 and TXD05. (b)~~The right panels represent~~ Tthe absolute signal difference. These mass spectra represent a compilation of > 450 of the particles for each type (TXD01: 972 and TXD05: 472). Note that each ion peak intensity is normalized to the sum of ion signals in each spectrum before further compilation.

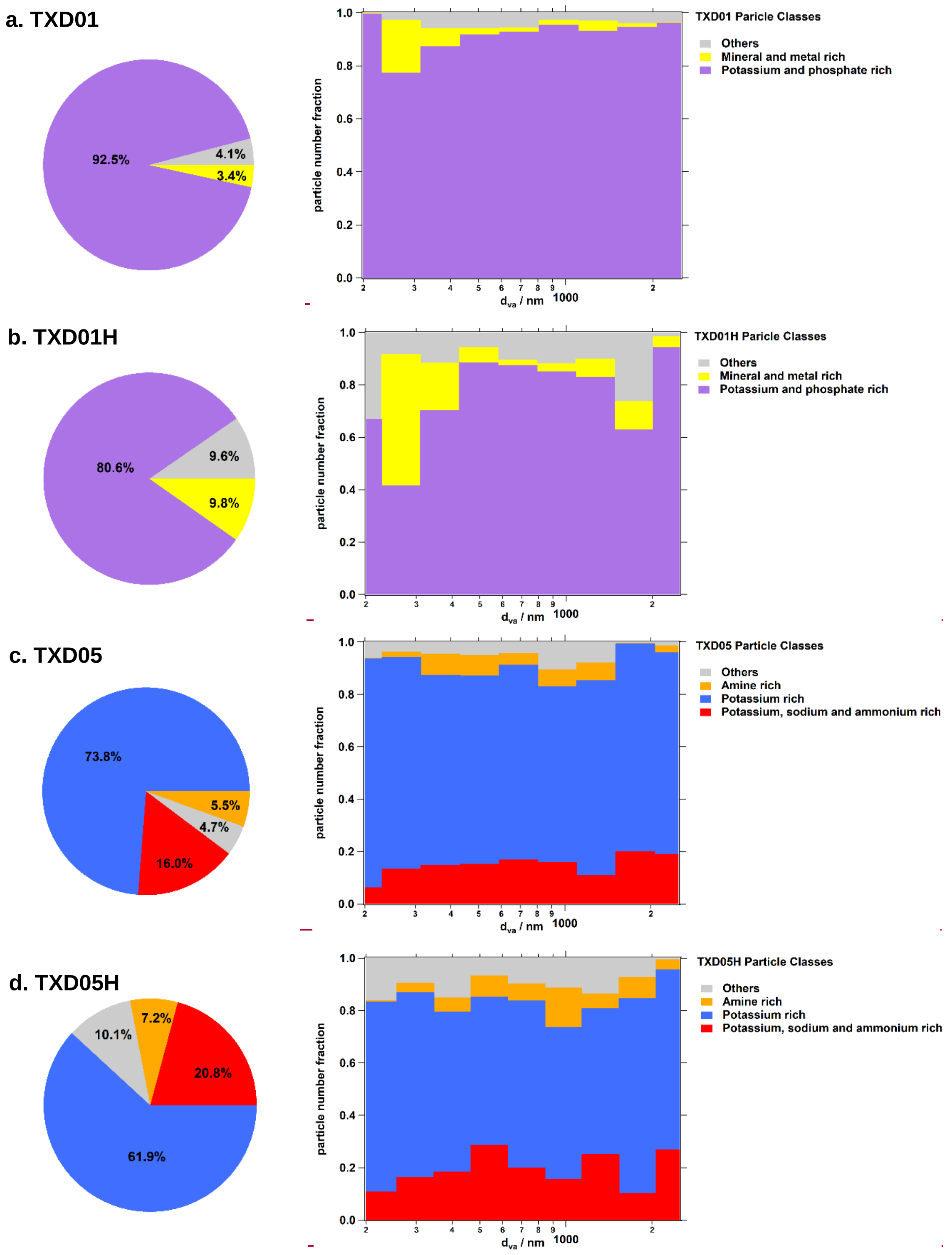
a. TXD01
92.5%
4.1%
3.4%
TXD01 Paricle Classes
Others
Mineral and metal rich
Potassium and phosphate rich
b. TXD01H
80.6%
9.6%
9.8%
TXD01H Particle Classes
Others
Mineral and metal rich
Potassium and phosphate rich
c. TXD05
73.8%
5.5%
4.7%
16.0%
TXD05 Particle Classes
Others
Amine rich
Potassium rich
Potassium, sodium and ammonium rich
d. TXD05H
7.2%
10.1%
20.8%
61.9%
TXD05H Particle Classes
Others
Amine rich
Potassium rich
Potassium, sodium and ammonium rich
particle number fraction
0.0
0.2
0.4
0.6
0.8
1.0
2
3
4
5
6
7
8
9
1000
2
d_{va} / nm

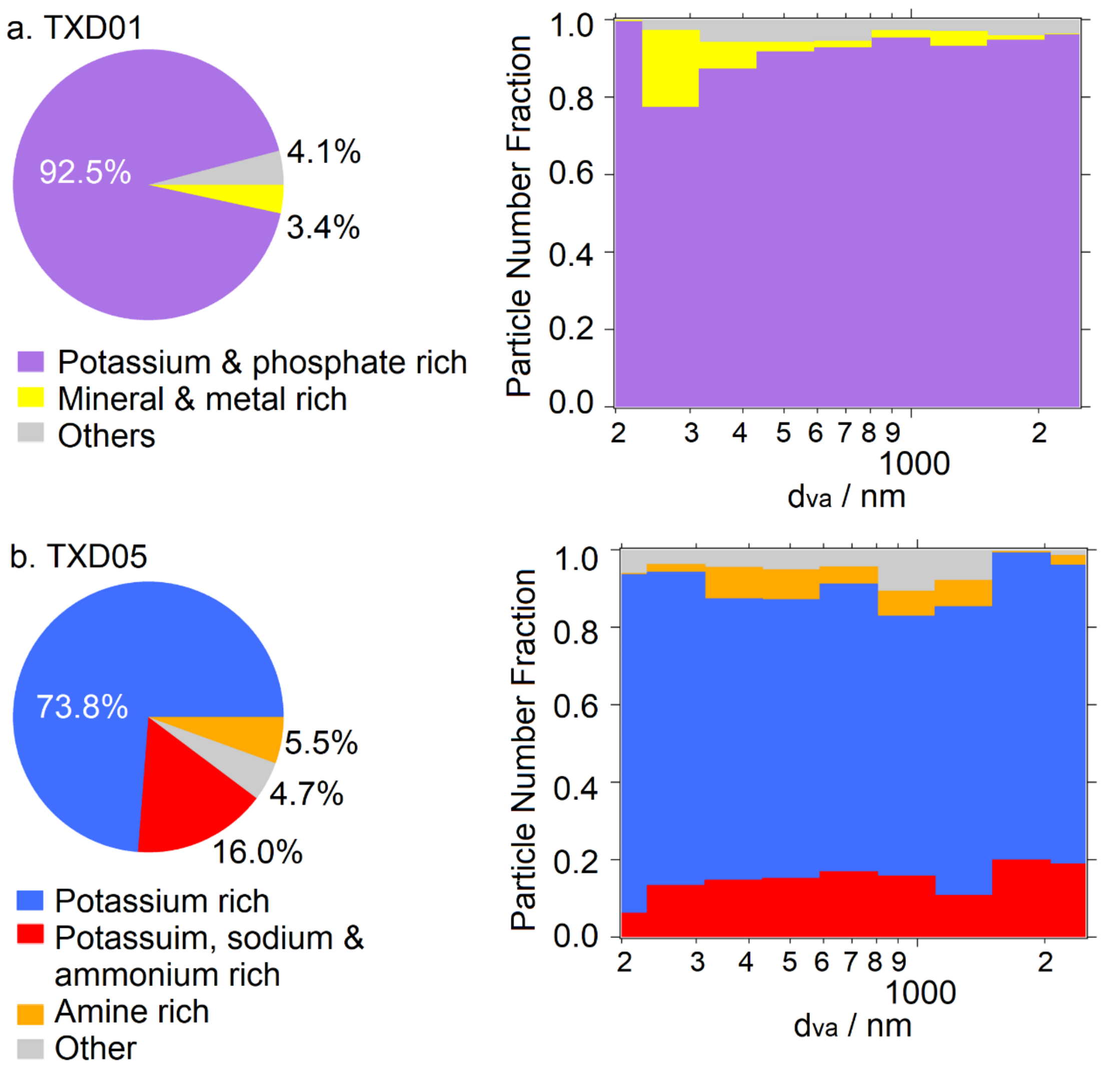

Figure ~~S3~~S2. Particle population fraction and size distribution based on clustered types, for TXD01 (a)~~, TXD01H (b),~~ and TXD05 (b~~c~~)~~, and TXD05H (d)~~. Note that the class named "others" (in grey color) is the small fraction of particles with unknown patterns. This class differs across TXD particle samples.

~~S5~~S2. Taxonomic diversity of two Texas dust samples.

~~We examined the diversity of *Archaea*, *Bacteria*, and *Fungi* in TXD01 and TXD05. Bulk samples, dry-heated bulks (100°C for 12 hours), and aerosolized particles collected on nuclepore filters were analyzed. Useful data for *Bacteria* were generated from the amplification and sequencing of the V3 – V5 region of the 16S rDNA phylogenetic marker down to the genus and species-level. The predominant phyla of *Archaea* consisted of methanogens, colonizers of the bovine rumen, as expected (Fouts et al., 2012) (**Table S2a**). The bacterial fraction of the microbiome was dominated by *Actinobacteria* (the most abundant phylum, common soil inhabitants), *Proteobacteria*, *Firmicutes* (diverse bacterial phyla with species living in the soil as well as in the bovine rumen), and *Bacteroidetes* (common members of the bovine rumen microflora) (Fouts et al., 2012; Chaucheyras-Durand and Ossa, 2014). No known IN-active bacterial species were identified in either sample (Després et al., 2012), although the genus *Pseudomonas* (containing IN-active species) was detected in low numbers (**Table S2b**). The predominant fungal taxa in our samples belong to *Pezizomycetes* (*Ascomycota*), common soil inhabitants. In this taxon, the coprophilic genus *Ascobolus* was detected in high numbers, as expected (Sarrocco, 2016). The genera *Fusarium* (*Ascomycota-Hypocreales*) and *Mortierella* (*Mucuromycota-Mortierellales*) were also detected in low numbers. These genera contain species with IN activity; however, the phylogenetic analysis did not detect any known IN-active species of these genera (**Table S2c**). Nonetheless, it is very interesting that we did not identify any known IN-active biological species in our samples.~~ **Table S1** summarizes our results of metagenomics analysis. Here we describe the methodology employed for our metagenomics analysis of sample microbiomes.

As the first step of the microbiome analysis, all reads with ambiguous bases ("N") were removed. Chimeric reads were identified and removed based on the de-novo algorithm of UCHIME (Edgar et al., 2011) as implemented in the VSEARCH package (Rognes et al., 2016). The remaining set of high-quality reads was processed using minimum entropy decomposition (MED; Eren et al., 2013 and 2015). MED provides a computationally efficient means to partition marker gene datasets into operational taxonomic units (OTUs). Each OTU represents a distinct cluster with a significant sequence divergent from any other cluster. By employing Shannon entropy, MED uses only the information-rich nucleotide positions across reads and iteratively partitions large datasets while omitting stochastic variation. The MED procedure outperforms classical identity-based clustering algorithms. Sequences can be partitioned based on relevant single nucleotide differences without being susceptible to random sequencing errors. This allows a decomposition of sequence datasets with a single nucleotide resolution. Furthermore, the MED procedure identifies and filters random "noise" in the dataset, i.e., sequences with very low abundance (less than 0.02% of the average sample size).

To assign taxonomic information to each OTU, DC-MEGABLAST alignments of cluster-representative sequences to the sequence database were performed. The most specific taxonomic assignment for each OTU was then transferred from the set of best-matching reference sequences (lowest common taxonomic unit of all the best matches). A sequence identity of 70% across at least 80% of the representative sequence was the minimal requirement for considering reference sequences. Further processing of OTUs and taxonomic assignments ~~was~~ were performed using the QIIME software package (version 1.9.1, http://qiime.org/). Abundances of bacterial taxonomic units were normalized using lineage-specific copy numbers of the relevant marker genes to improve estimates~~ (Angly, 2014)~~. Taxonomic assignments were performed using the NCBI_nt reference database (Release 2019-01-05).

Table ~~S2~~S1. An a~~A~~bundance of major orders of *Archaea* (a) Bacteria (b) and Eukaryotes (c) in dust samples TXD01 and TXD05~~ (**a**)~~. ~~Numbers indicate percentage of the OTUs for each phylum in the total archaeal microbiome. The analysis of the aerosolized TXD01 sample and of dry heat-treated bulk samples did not generate any useful data. Abundance of major bacterial and eukaryotic (incl. fungal) orders in dust samples TXD01 and TXD05 are shown in (**b**) and (**c**).~~ Numbers indicate the percentage of the OTUs for each order in the total archaeal, bacterial and eukaryotic microbiome. The analysis of the aerosolized TXD01 sample did not generate any useful archaeal data.

a. Archaea Taxonomy	~~**Aerosolized**~~ **TXD01**	~~**Aerosolized**~~ **TXD05**
Unclassified	-	0.00%
Euryarchaeota; Methanobacteria; Methanobacteriales	-	93.80%
Euryarchaeota; Methanomicrobia; Methanomicrobiales	-	0.10%
Euryarchaeota; Methanomicrobia; Methanosarcinales	-	0.00%
Euryarchaeota; Thermoplasmata; Methanomassiliicoccales	-	0.00%
Thaumarchaeota; Nitrososphaeria; Nitrososphaerales	-	6.10%

b. Bacteria Taxonomy	~~**Aerosolized**~~ **TXD01**	~~**Aerosolized**~~ **TXD05**
Unclassified	4.00%	2.60%
Actinobacteria; Acidimicrobiales	0.80%	0.20%
Actinobacteria; unclassified	3.00%	2.10%
Actinobacteria; Actinomycetales	0.20%	0.00%
Actinobacteria; Bifidobacteriales	0.00%	0.00%
Actinobacteria; Corynebacteriales	16.40%	13.70%
Actinobacteria; Frankiales	0.20%	0.00%
Actinobacteria; Geodermatophilales	0.30%	0.00%
Actinobacteria; Glycomycetales	0.20%	0.40%
Actinobacteria; Jiangellales	0.00%	0.00%
Actinobacteria; Kineosporiales	0.00%	0.00%
Actinobacteria; Micrococcales	12.30%	2.10%
Actinobacteria; Micromonosporales	0.10%	0.00%
Actinobacteria; Propionibacteriales	5.00%	0.20%
Actinobacteria; Pseudonocardiales	7.70%	39.20%
Actinobacteria; Streptomycetales	11.30%	28.60%
Actinobacteria; Streptosporangiales	2.30%	6.50%
Actinobacteria; Coriobacteriales	0.00%	0.00%
Actinobacteria; Solirubrobacterales	0.20%	0.00%
Bacteroidetes; unclassified	0.10%	0.00%
Bacteroidetes; Chitinophagales	0.30%	0.00%
Bacteroidetes; Cytophagales	0.70%	0.00%
Bacteroidetes; Flavobacteriales	4.20%	0.00%
Bacteroidetes; Saprospirales	0.10%	0.00%
Bacteroidetes; Sphingobacteriales	1.10%	0.00%
Chloroflexi; Sphaerobacterales	4.00%	1.10%
Cyanobacteria; Chroococcales	0.00%	0.00%
Fibrobacteres; Fibrobacterales	0.00%	0.00%
Firmicutes; unclassified	0.10%	0.00%
Firmicutes; Bacilli; unclassified	0.10%	0.00%
Firmicutes; Bacillales	6.10%	2.40%
Firmicutes; Lactobacillales	0.60%	0.00%
Firmicutes; Clostridiales	5.90%	0.30%
Firmicutes; Erysipelotrichales	1.00%	0.10%
Firmicutes; Acidaminococcales	0.00%	0.00%

Firmicutes; Tissierellia; unclassified	0.00%	0.00%
Firmicutes; Tissierellales	0.00%	0.00%
Gemmatimonadetes; Gemmatimonadales	0.40%	0.00%
Gemmatimonadetes; Longimicrobiales	0.00%	0.00%
Nitrospinae; Nitrospinales	0.00%	0.00%
Planctomycetes; Candidatus Brocadiales	0.00%	0.00%
Proteobacteria; unclassified	0.10%	0.00%
Proteobacteria; Alphaproteobacteria; unclassified	0.30%	0.00%
Proteobacteria; Alphaproteobacteria; Caulobacterales	0.50%	0.00%
Proteobacteria; Alphaproteobacteria; Rhizobiales	2.90%	0.00%
Proteobacteria; Alphaproteobacteria; Rhodobacterales	0.50%	0.00%
Proteobacteria; Alphaproteobacteria; Rhodospirillales	0.00%	0.00%
Proteobacteria; Alphaproteobacteria; Sphingomonadales	1.60%	0.00%
Proteobacteria; Betaproteobacteria; Burkholderiales	1.30%	0.00%
Proteobacteria; Deltaproteobacteria; Desulfuromonadales	0.00%	0.00%
Proteobacteria; Deltaproteobacteria; Myxococcales	0.00%	0.00%
Proteobacteria; Gammaproteobacteria; unclassified	0.00%	0.00%
Proteobacteria; Gammaproteobacteria; Aeromonadales	0.00%	0.00%
Proteobacteria; Gammaproteobacteria; Cardiobacteriales	0.00%	0.00%
Proteobacteria; Gammaproteobacteria; Cellvibrionales	0.40%	0.00%
Proteobacteria; Gammaproteobacteria; Chromatiales	0.00%	0.00%
Proteobacteria; Gammaproteobacteria; Enterobacterales	1.60%	0.50%
Proteobacteria; Gammaproteobacteria; Nevskiales	0.00%	0.00%
Proteobacteria; Gammaproteobacteria; Oceanospirillales	0.00%	0.00%
Proteobacteria; Gammaproteobacteria; Pseudomonadales	0.60%	0.00%
Proteobacteria; Gammaproteobacteria; Xanthomonadales	1.00%	0.00%
Proteobacteria; Bdellovibrionales	0.50%	0.00%
Rhodothermaeota; Rhodothermales	0.00%	0.00%
Spirochaetes; Spirochaetales	0.00%	0.00%
c. Eukaryotes~~ic~~ Taxonomy	**~~Aerosolized~~ TXD01**	**~~Aerosolized~~ TXD05**

Unclassified	0.30%	1.60%
Trichiida	0.00%	0.00%
Oligohymenophorea; Philasterida	0.00%	0.00%
Oligohymenophorea; Sessilida	0.00%	0.00%
Phyllopharyngea; Chlamydodontida	0.00%	0.00%
Spirotrichea; Sporadotrichida	0.00%	0.00%
Ascomycota; unclassified	1.10%	0.90%
Ascomycota; Capnodiales	0.00%	0.00%
Ascomycota; Pleosporales	0.00%	0.00%
Ascomycota; Eurotiales	1.30%	2.80%
Ascomycota; Onygenales	1.70%	5.20%
Ascomycota; Pertusariales	0.00%	0.00%
Ascomycota; Leotiomycetes; unclassified	0.10%	0.00%
Ascomycota; Rhytismatales	0.00%	0.00%
Ascomycota; Thelebolales	0.00%	0.00%
Ascomycota; Pezizales	68.00%	20.40%
Ascomycota; Saccharomycetales	0.10%	0.10%
Ascomycota; Glomerellales	0.00%	0.00%
Ascomycota; Hypocreales	16.90%	59.50%
Ascomycota; Melanosporales	0.10%	0.10%
Ascomycota; Microascales	0.60%	3.10%
Ascomycota; Sordariales	5.30%	2.80%
Basidiomycota; unclassified	0.00%	0.00%
Basidiomycota; Sporidiobolales	0.00%	0.00%
Basidiomycota; Tremellomycetes; unclassified	0.00%	0.00%
Basidiomycota; Trichosporonales	4.40%	3.30%
Basidiomycota; Wallemiales	0.00%	0.00%
Chytridiomycota; Rhizophlyctidales	0.00%	0.00%
Chytridiomycota; Spizellomycetales	0.00%	0.00%
Chytridiomycota; Neocallimastigales	0.00%	0.00%
Mucoromycota; Mortierellales	0.00%	0.00%
Mucoromycota; Mucorales	0.10%	0.20%

S3. Comparison of two immersion freezing techniques

~~As shown in **Fig. S4**, t~~The West Texas ~~Cryogenic~~ cryogenic ~~Refrigerator~~ refrigerator ~~Applied~~ applied to ~~Freezing~~ freezing ~~Test~~ test system (WT-CRAFT) system and the ~~Ice~~ ice n~~N~~ucleation s~~S~~pe~~E~~ctrometer of the Karlsruhe Institute of Technology (INSEKT) ~~measured the immersion mode freezing efficiency of a bulk test open-lot livestock facility (OLLF) material (TXD01)~~were compared using an identical sample collected at an open-lot livestock facility (OLLF). This complementary analysis was performed to indirectly validate WT-CRAFT against INSEKT measurements. The data from both techniques were analyzed and compared in terms of ambient INP concentration, n_{INP}.~~with the method described in the main manuscript **Sect. 2.4**, The comparison showed that the ice nucleation (IN)-active surface site density values as function of temperature (T), $n_{s,geo}(T)$, over -8°C > T > -21°C agreed within CI95% and ± 0.5 °C T errors. Further, both methods successfully captured a local maximum in freezing spectra shown in **Fig. S4** at around -10°C, suggesting that they are comparable immersion freezing detection techniques. We note the following two caveats: (1) the geometric specific surface area (SSA) of 4.95 m^2 g^{-1} (**Table 2**) was used to convert from n_m to $n_{s,geo}$ according to Eqns. [1] – [3] in **Sect. S4**, and (2) while the BET and geometric SSA difference is small according to **Table 2**, the BET SSA and associated IN-active surface site density values scaled to BET SSA, $n_{s,BET}$, may be more representative for a bulk TXD01 sample. According to Eqn. 4 of Hiranuma et al. (2015), the $n_{s,BET}$ value can be easily obtained by scaling n_m to BET SSA. In the case of TXD01, the difference between $n_{s,BET}$ anf $n_{s,geo}$ can be represented by the ratio of BET SSA to geometric SSA $n_{s,geo}$.~~

~~In addition to the bulk TXD01 sample, the comparability of the two immersion freezing techniques was assessed using t~~We used the field aerosol particle samples collected using polycarbonate filter samplers ~~(PFSs)~~ at OLLF-3 on July 24th~~in~~ 2019 for this comparison test (**Table 2**). A 50% split of the filter was used for each assay to measure n_{INP} as a function of temperature, $n_{INP}(T)$, by the methods described in **Sects. 2.1.3** (INSEKT) and **2.2.3** (WT-CRAFT). ~~We chose~~Using this sample for the comparison is reasonable since its ~~INP concentration,~~ n_{INP}~~,~~ spectra fall between the measured maximum and minimum $n_{INP}(T)$ in 2017-2019 even when considering 95% binomial confidence intervals (CI95%)~~bounds~~. Thus, it is representative ~~for~~ of the field OLLF $n_{INP}(T)$ data presented in this study. ~~Furthermore, with this sample, we also conducted the INSEKT wet-boiling treatment analysis.~~ **Figure ~~S5~~ S3** shows the $n_{INP}(T)$ spectra of the same sample measured by WT-CRAFT and INSEKT in the temperature~~T~~ range between -8 °C and -22.5 °C. As can be seen, both techniques successfully generated $n_{INP}(T)$ data virtually overlapping ~~and~~ within error bars.~~,~~ ~~only a~~At temperature~~T~~ < -22°C, WT-CRAFT measures lower values. The two methods correlate well with each other, with the Pearson correlation coefficient (r) of 0.90 ($n_{INP,INSEKT}$ = (2.12~~13~~ × $n_{INP,WT\text{-}CRAFT}$) – 11.23~~10~~). ~~The comparison of non-heated vs. wet-boiled $n_{INP,INSEKT}$ data for the overlapping T ranges showed negligible difference between $n_{INP,non\text{-}heated}$ and $n_{INP,wet\text{-}boiled}$. The correlation plot of non-heated vs. wet-boiled (**Fig. S5b**) indicates no difference within CI95% uncertainties [r = 0.97; $n_{INP,wet\text{-}boiled}$ = (1.0849 × $n_{INP,non\text{-}heated}$) + 7.1958], suggesting heat resistivity of OLLF-INPs collected on this PFS sample.~~

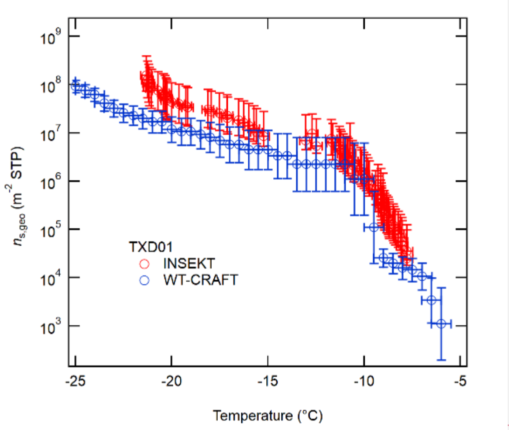

~~**Figure S4**. Immersion freezing $n_{\mathrm{s,geo}}$(*T*) spectra of the bulk TXD01 sample measured by KIT-INSEKT and WT-CRAFT for their compatibility test.~~

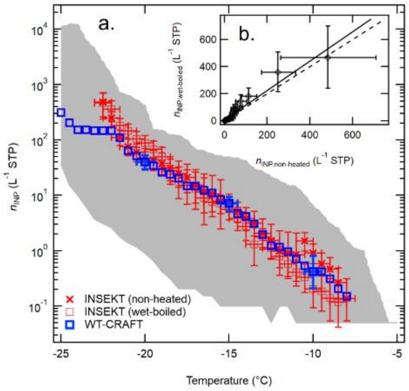

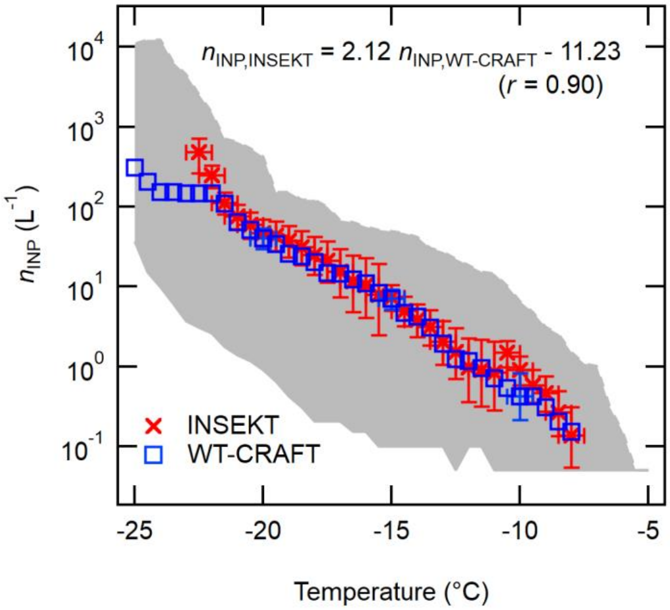

Figure ~~S5~~S3. The n_{INP}(*T*) spectra of aerosol particles collected at OLLF-3 in summer 2019, measured with WT-CRAFT (blue) and INSEKT (red)~~: a comparison of the non-heated $n_{\mathrm{INP,non\text{-}heated}}$(*T*) (red cross) to the wet-boiled $n_{\mathrm{INP,wet\text{-}boiled}}$(*T*) (red square) INSEKT measurements and non-treated WT-CRAFT measurements is shown in (a). ~~. The uncertainties in temperature~~*T*~~ and n_{INP} are ± 0.5 °C and ± CI95%, respectively. Error bars are shown at selected temperature~~*T*~~s for the WT-CRAFT data to make all data points visible. ~~The correlation of non-heated vs. wet-boiled plot for the overlapping *T* ranges from INSEKT is shown in (b). The black dashed~~

~~line represents the 1:1 curve to guide the reader's eye (i.e., no difference between $n_{\mathrm{INP,non\text{-}heated}}$ and $n_{\mathrm{INP,wet\text{-}boiled}}$). Shaded~~ The shaded area represents max – min $n_{\mathrm{INP}}(T)$ for all our OLLF samples collected in 2017 – 2019.

~~**S4.** Derivation of n_{INP}, n_{m}, and $n_{\mathrm{s,geo}}$~~

~~Here we describe the conversion procedure used to derive ambient n_{INP}, n_{m}, and $n_{\mathrm{s,geo}}$. Initially, we computed the $C_{\mathrm{INP}}(T)$ value, which is the nucleus concentration in ultrapure water suspension (L^{-1} water) at a given T as described in Vali (1971). This $C_{\mathrm{INP}}(T)$ value was calculated as a function of unfrozen fraction, $f_{unfrozen}(T)$ (i.e., the ratio of number of droplets unfrozen to the total number of droplets) as:~~

~~$$C_{INP}(T) = -\frac{\ln\left(f_{unfrozen}(T)\right)}{V_d} \qquad [1]$$~~

~~in which, V_d is the volume of the droplet (3 μL) for WT-CRAFT and sample in a well (50 μL) for INSEKT.~~

~~Next, we converted $C_{INP}(T)$ to $n_{\mathrm{INP}}(T)$: INP in the unit volume of atmospheric air at standard T and pressure (STP) conditions, which is 273.15 K and 1013 mbar. The cumulative n_{INP} per unit volume of sample air, described in the previous study DeMott et al. (2017), was then estimated as:~~

~~$$n_{INP}(T) = C_{INP}(T) \times (DF) \times \frac{V_l}{V_{air}} \qquad [2]$$~~

~~where DF is a serial dilution factor (e.g., DF = 1 or 10 or 100 and so on). The sampled air volume (V_{air}) is given in **Table 1**. The suspension volume (V_l) is optimized to achieve the detection limit of 0.05 INP L^{-1} (corresponding to the first frozen droplet).~~

~~Finally, based on Eqn. 3 of Hiranuma et al. (2015), the $n_{\mathrm{s,geo}}(T)$ and $n_{\mathrm{m}}(T)$ values can be derived as:~~

~~$$n_m(T) = \frac{n_{INP}(T)}{M_{ve}} \approx \left(\frac{S_{total}}{M_{total}}\right) n_{s,geo}(T) \qquad [3]$$~~

~~where M_{ve} is the mass of a spherical particle of volume equivalent diameter (g), and $S_{\mathrm{total}}/M_{\mathrm{total}}$ is a geometric specific surface area (Hiranuma et al., 2015). The value used for converting field $n_{\mathrm{m}}(T)$ to $n_{\mathrm{s,geo}}(T)$ data, ~ 0.4 m^2 g^{-1}, is derived from particle size distribution measurements presented in Fig. 3 of Hiranuma et al. (2011).~~

~~S6. IN parameterization~~

~~The exponential fits for T-binned $n_{s,geo}$ data of all lab and field measurements are summarized in **Table S3**. Fit parameters, computationally optimized for given the best correlation coefficient (r) for each category are provided in this table. As can be inferred from the table, the overall $\Delta\log(n_{s,geo})/\Delta T$ value is similar for all non-heated categories (0.20 – 0.42). This range of deviations is roughly similar to what we previously observed for supermicron IN-active cellulose particles (0.26 – 0.40; Hiranuma et al., 2019). Slightly higher $\Delta\log(n_{s,geo})/\Delta T$ values were observed for wet-boiled particles (0.59 – 0.61) than others may be indicative of an alternation in freezing efficiency. This parameterization offers a simple representation of supermicron-dominant INPs from OLLF, which can act as an important point source of agricultural INPs (nearly half of OLLF-INPs is supermicron in diameter; see **Sect. 3.2**) in a very simple manner. Since our immersion parameterization is solely a function of a single parameter, T, this parameterization can be easily incorporated in many model platforms in a computationally-friendly manner. Offering a universal single parameterization for soil dust-derived INPs is not the scope of this work. As OLLF represents a point source of fresh livestock-generated dust, we expect that it would have different ice nucleation efficiency than aged/weathered dusts. Individual parameterizations are useful to analyze spectra by comparing $\Delta\log(n_{s,geo})/\Delta T$ values etc. Nonetheless, our **Fig. 8** shows a comparison of our $n_{s,geo}$ data with six relevant IN parameterizations of soil/desert dust.~~

S4. Heat treatment analysis

INSEKT was also used to assess immersion freezing ability and efficiency of heated filter samples. As explained in **Sect. 2.1.3**, a series of diluted samples were examined in INSEKT. We made sure to assess overlapping T intervals in a series of measurements to see if immersion freezing spectra from multiple measurements agree within CI95%.

As for heat treatment, the suspension sample tube was immersed in boiling water (~100 °C) for 20 minutes. This temperature was chosen to denature proteinaceous INPs. The choice of 100 °C for heat treatment seems valid because proteinaceous structures will be destroyed below ~ 100 °C (Steinke et al., 2016). For example, Szyrmer and Zawadzki (1997) found some known cell-free IN-active microbes (e.g., *Fusarium* nuclei) are stable only up to 60 °C. Other than this study, IN activity by bacteria (Morris et al., 2004; Christner et al., 2008), fungi (Humphreys et al., 2001), and lichens (Henderson-Begg, et al., 2009) has been shown to be heat-sensitive irreversibly at 100 °C or below. Other soil organic components can be decomposed at temperatures between 100 °C and 300 °C (Tobo et al., 2014). Thus, subtracting heated n_{INP} or INP concentration per unit geometric particle surface area ($n_{s,geo}$) from non-heated values allows us to assess~~assessing~~ their contribution to immersion freezing. The rest of the heating procedure is adapted from Schiebel (2017). Briefly, the aerosol particle suspension (3 mL) from a non-treated stock was first transferred to a sterile falcon tube. The screw-cap was closed, such that no water was lost. Then the tube was placed together with a precisely fitting styrofoam ring in a water-filled glass beaker. The styrofoam ring ensured that the tube was floating, and all of the aerosol suspension was submerged below the water surface for best heat transfer. The beaker was placed on a stirring hot plate to boil the water.

The effect of heat treatment on our laboratory and field samples for immersion freezing, summarized in **Fig. S4**, revealed inclusion of heat-labile INPs in our laboratory samples but not in the field sample. While the effect of heat treatment is not as obvious as what was previously observed in other soil dust samples: e.g., a wheat harvest soil dust in Suski et al. (2018), the TXD01 sample showed a reduction in $n_{s,geo}$ at temperatures above -22 °C after heat treatment. At -19 °C, the heat eliminated INPs for our detection limit in this study (i.e., $n_{s,geo} \approx 5 \text{ x } 10^5$ m^{-2}). Similarly, TXD05 also exhibited a sensitivity to heat above -20 °C. Heating reduced the freezing efficiency of the TXD05 sample below our detection limit at -19 °C. From our metagenomics analysis, presented in **Sect. 3.1.4**, no known IN-active microbiomes are present in our laboratory samples, which limits the heat-labile composition to be heat sensitive organics.

In contrast, heat treatment on the field sample, collected in OLLF-3 on July 24th, 2019, did not show substantial sensitivity to heat compared to our laboratory samples. The INP concentrations are reduced in the temperature range between -10 °C and -12.5 °C, presumably due to the loss of heat-labile INPs. However, the overall heat-stable feature of this field sample suggests the presence of immersion freezing mode active heat-stable components, including non-heat-labile organics and mineral compounds. This heat-resistant feature of OLLF samples may also be due to their pre-exposure to soil temperature on average higher than ambient temperature even at a depth of 150 mm during summer (Cole et al., 2009).

Previously, Suski et al. (2018) found that heat-treatment (95 °C for 20 min) can suppress the n_{INP} of wheat harvest soil dust samples from Kansas, USA by more than two orders of magnitude at -12 °C. The authors concluded that the decomposition of IN-active heat-labile organics and bacteria is responsible for the observed n_{INP} suppression. This result is consistent with the impact of heat treatment on the IN efficiency of soil dust samples from different regions, such as the one from a lodgepole pine forest in Wyoming, USA (Hill et al., 2016; 105 °C for 20 min) and another from Central Yakutia (Conen et al., 2011; 100 °C for 10 min). Similarly, Tobo et al. (2014) found that 300 °C combustion can reduce the IN fraction of Wyoming soil dust at -24 °C by the same orders of magnitude observed by Suski et al. (2018). In contrast, Steinke et al (2016) found no notable effect of heat treatment (~ 110 °C) on the Argentinian soil dust IN efficiency at ~ -24 °C. This heat-stable nature of Argentinian soil dust may have coincided with its lack of IN-active proteins and/or heat-sensitive microbes, which aligns with the absence of known IN-active microbes in our OLLF samples. In total, our findings and the observations by Steinke et al. (2016) eliminate proteinaceous and biological ice-nucleating components as the primary source of IN abundance in air. Thus, the investigation of heat-stable organic INPs is key to further understand the properties of soil dust INPs. Future research should focus on understanding how organic composition influences atmospheric immersion freezing. Our current knowledge regarding IN-active organics is still limited.

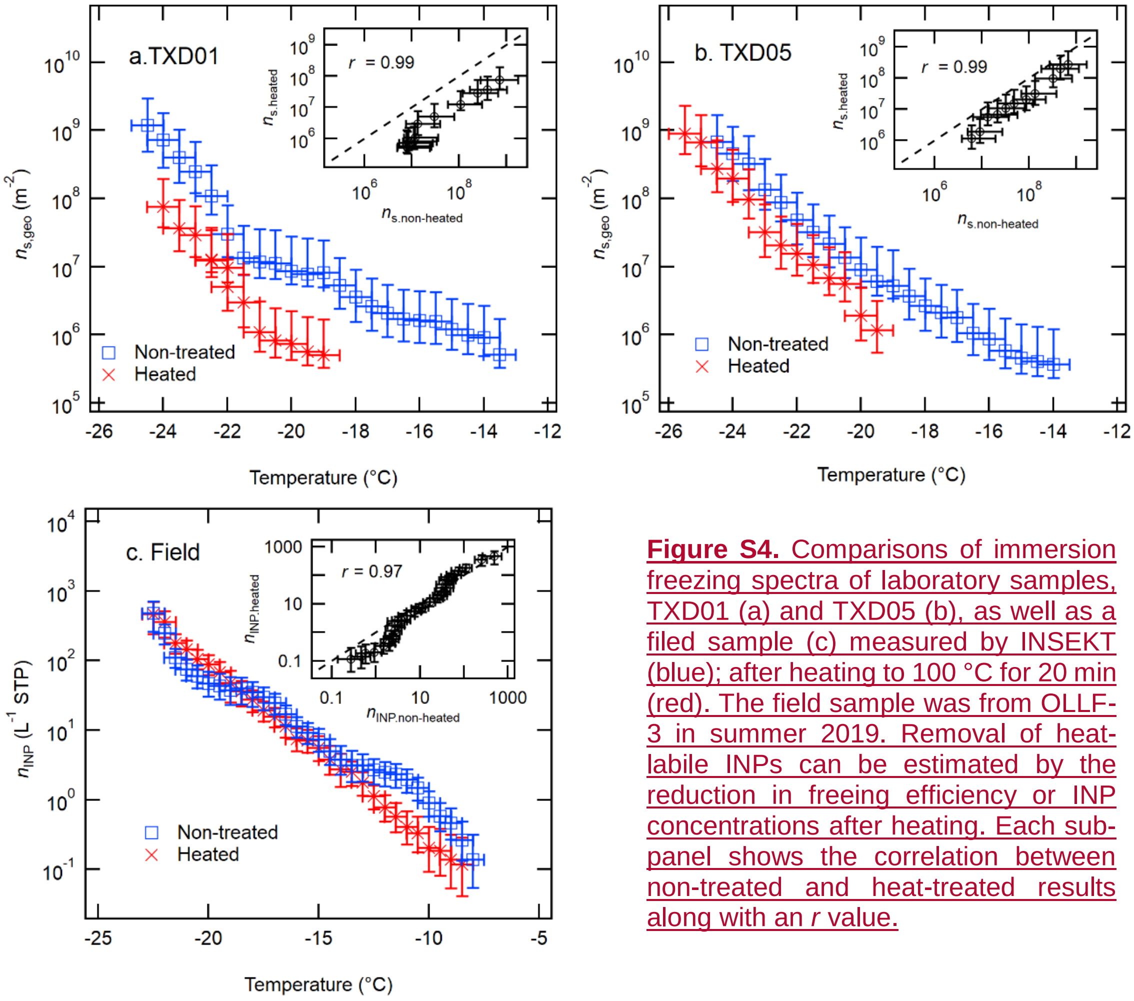

Figure S4. Comparisons of immersion freezing spectra of laboratory samples, TXD01 (a) and TXD05 (b), as well as a filed sample (c) measured by INSEKT (blue); after heating to 100 °C for 20 min (red). The field sample was from OLLF-3 in summer 2019. Removal of heat-labile INPs can be estimated by the reduction in freeing efficiency or INP concentrations after heating. Each sub-panel shows the correlation between non-treated and heat-treated results along with an *r* value.

~~3.~~S5. Estimated INPs released from an OLLF

Tapered-element oscillating microbalances (TEOMs; Thermo Scientific Inc., Model 1400ab; Patashnick and Rupprecht, 1991) were deployed at OLLF-1 to continuously monitor mass concentrations of particulate matter less than 10 µm diameter (PM_{10}). Two identical TEOMs were deployed at OLLF-1: one at the upwind edge and another at the downwind location of OLLF-1 (**Fig. 2**). With an operating flow rate of 16.7 LPM, our TEOM measured < 1 g m^{-3} of PM with a 5-min time resolution. Both TEOMs ran continuously during the entire 2016 – 2019 study period except for routine maintenance activities. The inlets of DustTrak and TEOMs were maintained at ~ 1.5 m above the ground to be consistent with our polycarbonate filter samplers. It is noteworthy that our TEOM and DustTrak PM_{10} measurements agreed within ± 40% on average.

~~Upon confirmation of the comparability between field and lab $n_{s,geo}$ values, we proceeded with~~To complement our observation, we estimated ambient INP concentration at OLLF-1~~n_{INP} estimation~~ based on our field mass concentration data, using the OLLF-1 TEOM PM_{10} data. We ~~elected~~ chose to use the OLLF-1 data due to their reasonable spatiotemporal coverage (i.e., two identical model TEOMs deployed at the downwind and upwind sites for ~~2017~~ 2016 – 2019). A summary of TEOM mass concentration data in different seasons over ~~2017~~ 2016 – 2019 is~~are~~ available in **Table ~~8~~S2**. In general, PM_{10} mass concentrations from OLLF-1 (average ± standard errors) were high in meteorological summers ($3.9 \times 10^{-7} \pm 5.6 \times 10^{-8}$ g L^{-1}) and springs ($4.5 \times 10^{-7} \pm 2.4 \times 10^{-7}$ g L^{-1}) as compared to fall ($2.4 \times 10^{-7} \pm 4.4 \times 10^{-8}$ g L^{-1}) and winter ($1.5 \times 10^{-7} \pm 5.3 \times 10^{-8}$ g L^{-1}). A similar trend was found for the upwind PM_{10} mass concentration: summer ($3.4 \times 10^{-8} \pm 9.0 \times 10^{-9}$ g L^{-1}) ≥ spring ($2.8 \times 10^{-8} \pm 9.3 \times 10^{-9}$ g L^{-1}) > fall ($1.8 \times 10^{-8} \pm 5.7 \times 10^{-9}$ g L^{-1}) ≥ winter ($1.4 \times 10^{-8} \pm 7.1 \times 10^{-10}$ g L^{-1}). But, the measured values at the upwind location are consistently an order magnitude lower than that from the downwind location.

Frequently, the observed PM_{10} concentration exceeded 10^{-7} g L^{-1}, which is consistent with previous studies (Bush et al., 2014~~; Hiranuma et al., 2011~~). On the other hand, the observed mass concentration at the upwind sites was ~~typically substantially~~ lower except for known/recorded interruptions (e.g., a tractor-trailer passing by), resulting in a transient increase in mass concentration. As the upwind n_{INP} can be considered non-negligible (see **Sect. 3.2.1**), we subtracted mass concentrations measured at a nominal upwind edge from the downwind TEOM mass concentration~~concertation~~ values to compute PM_{10} from OLLF-1. The screened TEOM data were used as ambient particle concentration data to estimate n_{INP} from an OLLF.

~~To estimate n_{INP}, we used the $n_{s,geo}$ parameterization given in **SI Sect. S6**.~~ Due to the atmospheric relevance and temperature~~T~~ coverage extending to -5 °C, we used a fit of ***Field_Median*** in **Table S3** to compute representative $n_{s,geo}$ relevant to OLLF. To convert $n_{s,geo}$ to n_{INP}, we have adapted Equations (1) – (3) in **Sect. 2.1.3** ~~in Hiranuma *et al.* (2015)~~. Briefly, the measured mass concentration, as well as field specific surface area (SSA), ~~as well as field *SSA*~~ were used to convert from $n_{s,geo}$ to n_{INP}:

$$n_{INP}(T)(L^{-1}) = n_{s,geo}(T)(m^{-2}) \times Geometric\ SSA\left(\frac{m^2}{g}\right) \times \text{Mass Conc.}\left(\frac{g}{L}\right). \qquad [S1]$$

where the geometric *SSA* value for field data is~~,~~ ~ 0.4 m^2 g^{-1}~~, is derived from particle size distribution measurements presented in Fig. 3 of Hiranuma et al. (2011)~~ (**Sect. 2.2.3**). Our assumption of n_{INP} to be linearly scaled to mass concentration is supported by the observed correlation between PM mass and n_{INP} (**Fig. 7a**).

Table ~~8~~ S2 also summarizes the TEOM ~~mass concentrations and~~ estimated annual and seasonal n_{INP} ~~in different seasons over~~from ~~2017~~ 2016 to~~–~~ 2019. ~~In general, PM_{10} mass concentrations from OLLF-1 (average ± standard errors) were high in meteorological summers ($3.9 \times 10^{-7} \pm 5.6 \times 10^{-8}$ g L^{-1}) and springs ($4.5 \times 10^{-7} \pm 2.4 \times 10^{-7}$ g L^{-1}) as compared to fall ($2.4 \times 10^{-7} \pm 4.4 \times 10^{-8}$ g L^{-1}) and winter ($1.5 \times 10^{-7} \pm 5.3 \times 10^{-8}$ g L^{-1}). A similar trend was found for the upwind PM_{10} mass concentration: summer ($3.4 \times 10^{-8} \pm 9.0 \times 10^{-9}$ g L^{-1}) ≥ spring ($2.8 \times 10^{-8} \pm 9.3 \times 10^{-9}$ g L^{-1}) > fall ($1.8 \times 10^{-8} \pm 5.7 \times 10^{-9}$ g L^{-1}) ≥ winter ($1.4 \times 10^{-8} \pm 7.1 \times 10^{-10}$ g L^{-1}). But, the measured values at the upwind location are consistently an order magnitude lower than that from the downwind location.~~ On average, the estimated mean n_{INP} values at -15, -20, and -25 °C in 2016 – 2019 were estimated as 46.8 (±25.3 seasonal standard deviation; same hereafter), 288.1 (± 156.1), and 5,250.9 (± 2,845.6) L^{-1}, respectively. In addition, the median n_{INP} at -15, -20, and -25 °C in 2016

– 2019 were estimated as 14.7 (± 9.2), 90.9 (± 56.4), and 1,656.3 (± 1,028.1) L^{-1}, respectively. As our n_{INP} is linearly scaled to mass concentration (Eqn. S1), estimated n_{INP} showed a similar seasonal variability as seen in mass concentration. For instance, at -20 °C, the cumulative n_{INP} averages for each meteorological season over three years from 2016 to 2019 ~~2016 – 2019~~ were estimated as follows: spring (315.4 ± 164.9 L^{-1}) ≥ summer (270.4 ± 39.0 L^{-1}) > fall (165.1 ± 30.8 L^{-1}) ≥ winter (106.9 ± 36.8 L^{-1}). The observed high n_{INP} values were expected for such ~~a~~ high PM$_{10}$ mass concentrations emitted from the cattle feedlot~~feedyard~~, which represent an important point source of agricultural aerosol particle emission. However, we reemphasize that the IN efficiency of OLLF aerosol particles is ~~somehow~~ similar to other agricultural aerosol particles found in previous studies as shown~~discussed~~ in ~~**Sect. 3.2 (**~~**Fig. ~~8~~4**~~)~~.

Figure ~~9~~ S5 displays the TEOM mass concentration time series over ~~2017~~ 2016 – 2019 as well as cumulative n_{INP} estimated at temperature~~*T*~~s of -15 °C, -20 °C, and -25 °C. The background mass concentration measured at the upwind location (1.7 × 10^{-8} to 2.6 × 10^{-8} g L^{-1}) is shown with a red dashed line in **Fig. ~~9a~~ S5a** and subtracted from the downwind data. The resulting OLLF mass concentration was on average ~~is~~ 4.12 × 10^{-7} ± 2.96 × 10^{-9} g L^{-1} (or 411.57 ± 2.96 µg m^{-3}). Annual averages of OLLF mass concentrations are indicated with a blue dashed line in **Fig. ~~9a~~S5a**. On average, the downwind concentration exhibited higher mass concentration by more than an order of magnitude. This result implies a constant high particle load from the OLLF, which was also seen by a previous study at the same OLLF (Hiranuma et al., 2011). Seasonal variation is also seen in **Fig. ~~9a~~S5a,** as the annual peak of mass concentration (> 10^{-5} g L^{-1}) coincided with summer in each case.

Figure ~~9b~~ S5b shows associated n_{INP} estimations. ~~As seen in **Fig. 9b**,~~ The average estimated INPs at three different temperature~~*T*~~s, -15 °C, -20 °C, and -25 °C, are shown as a gray dashed line, black dashed line, and black solid line, respectively. Our results show that the aerosol particles downwind of a feedlot contain several thousand INPs L^{-1} (median = 1,656 L^{-1}; average = 5,251 L^{-1}) at standard temperature~~*T*~~ and pressure (STP) at -25 °C, which is three orders of magnitude higher than typical ambient n_{INP} from continental sources as reported in DeMott et al. (2010). ~~–~~More discussion of OLLF n_{INP} in comparison with previous studies is provided in **Sect. 3.2.3~~6~~**. We note that our estimation of *n*INP is limited at the source location. Further understanding of OLLF-derived INPs in the atmosphere will require future research in the dust generation mechanisms in association with local dynamics and thermodynamics, vertical distribution of OLLF dust, and their fate in the atmosphere.

~~Our lab and field measurements-based parameterizations open up further study opportunities to incorporate supermicron INPs from agricultural source in the atmospheric modeling simulation and may provide a hint to reveal the identity of INPs at relatively high *T*s (> -15 ºC). Note that the existence of supermicron particles at cloud altitudes is especially non-negligible when we consider atmospheric immersion freezing, which initiates on the surface of a few in a million particles.~~

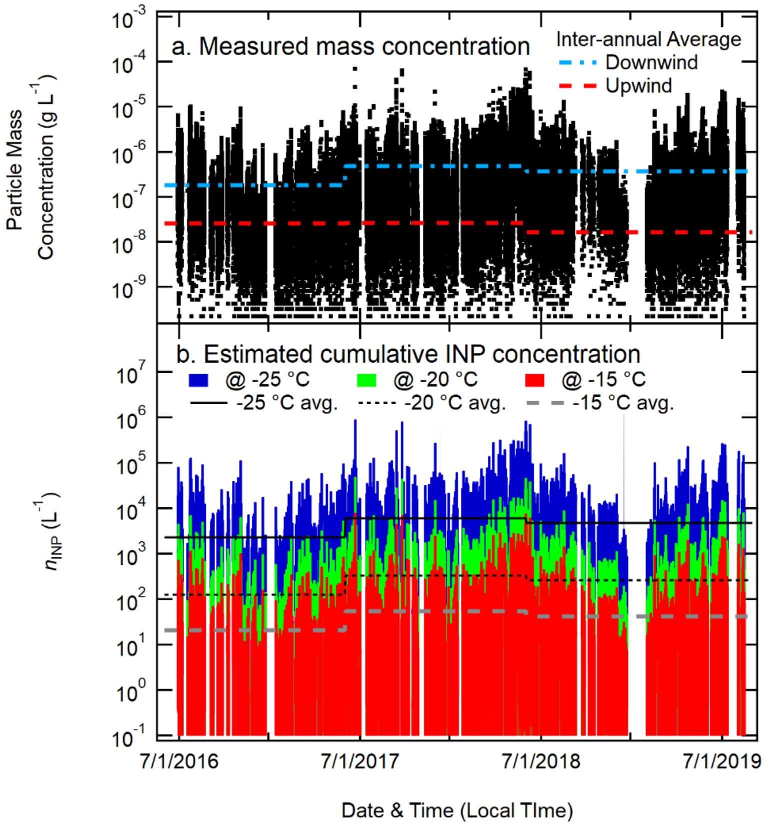

Figure S5~~**Figure 9**~~. OLLF INP concentrations. Time-series plot of TEOM mass concentration measured at the downwind side of OLLF-1 (a) and cumulative n_{INP} estimated at temperatures of -15 °C, -20 °C, and -25 °C (b). In Panel a, inter-annual average mass concentrations of aerosol particles from OLLF (blue dashed line) and upwind (red dashed line) are shown (numbers adapted from **Table ~~8~~S2**). In Panel b, likewise, inter-annual average n_{INP} estimated at -15, -20, and -25 °C (reported in **Table ~~8~~S2**) are also shown. Meteorological summer in Texas is used for the beginning and ending time~~-~~stamps of each year.

~~Table 8~~Table S2. Inter-annual and seasonal PM$_{10}$ mass concentrations from OLLF-1 as well as estimated n_{INP}.

	PM$_{10}$ Mass Concentration (g L^{-1})		Estimated $n_{\mathrm{INP}}(T)$ (L^{-1})		
	*OLLF	Upwind	T = -15 °C	T = -20 °C	T = -25 °C
2016 – 2017	**1.8E-07**	**2.6E-08**	**20.7**	**127.5**	**2323.4**
Summer	3.7E-07	5.2E-08	42.3	260.5	4747.7
Fall	1.6E-07	2.8E-08	18.1	111.7	2036.3
Winter	6.3E-08	1.5E-08	7.2	44.2	806.2
Spring	1.6E-07	2.1E-08	17.7	108.9	1985.5
2017 – 2018	**4.8E-07**	**2.6E-08**	**54.6**	**336.4**	**6133.0**
Summer	3.0E-07	2.3E-08	33.8	208.5	3801.1
Fall	3.1E-07	1.9E-08	35.4	218.2	3978.3
Winter	2.5E-07	1.3E-08	27.9	171.7	3129.6
Spring	9.2E-07	4.6E-08	104.1	641.3	11690.9
2018 – 2019	**3.7E-07**	**1.7E-08**	**42.3**	**260.7**	**4752.5**
Summer	4.9E-07	2.6E-08	55.6	342.3	6240.6
Fall	2.4E-07	7.9E-09	26.8	165.3	3013.0
Winter	1.5E-07	1.3E-08	17.0	104.8	1910.2
Spring	2.8E-07	1.6E-08	31.8	195.8	3570.0

*Upwind concentration is subtracted.

Table S3. OLLF-INP parameterization: List of exponential fit parameters to the $n_{s,geo}$ for temperature~~T~~-binned ensemble datasets of lab study as well as field study. The datasets are fitted in the log space. The ~~correlation coefficient,~~ r value~~,~~ ~~correlation coefficient, r,~~ for each fit is also shown. All $n_{s,geo}$ values are in m^{-2}. temperature~~T~~ is in °C. Note the fifth-order polynomial fit function is sensitive for all decimals shown here. To reproduce the fitted curves, we needed to include all decimals.

Fitted dataset: Sample ID (INSEKT sample type)	Fitted T range	Fit Parameters $n_{s,geo}(T) = \exp(a + b \cdot T + c \cdot T^2 + d \cdot T^3 + e \cdot T^4 + f \cdot T^5]$							
		a (m^{-2})	b (m^{-2} °C^{-1})	c (m^{-2} °C^{-2})	d (m^{-2} °C^{-3})	e (m^{-2} °C^{-4})	f (m^{-2} °C^{-5})	r	Δlog ($n_{s,geo}$)/ΔT
~~TXD01 (bulk)~~	~~-29˚C < T < -7.5˚C~~	~~-10.419739559253788~~	~~-4.736514708000364~~	~~-0.19248508975777787~~	~~0.0025143767156404874~~	~~0.0002817257460974357~~	~~3.66476024299544e-06~~	~~0.99~~	~~0.28~~
~~TXD01H (bulk)~~	~~-28.5˚C < T < -7.5˚C~~	~~-22.02476692454698~~	~~-8.027234773393355~~	~~-0.5620907167927012~~	~~-0.016652073879196847~~	~~-0.00016994936493112665~~	~~-1.2200599889511637e-07~~	~~0.99~~	~~0.26~~
TXD01 (filter)	-29˚C < T < -13.5˚C	-649.609266142404~~4~~	-166.17848015453 7~~06~~	-16.331424541701 3~~84~~	-0.785403143752226	-0.01845636506788 16~~9~~	-0.00017023048008878~~034~~	0.99	0.41
~~TXD01H (filter, dry-heated)~~	~~-28.5˚C < T < -12˚C~~	~~17.885511152572057~~	~~-1.8325915290723702~~	~~-0.5650878320173172~~	~~-0.04817379804678202~~	~~-0.0016235221213422987~~	~~-1.973016312032128e-05~~	~~0.97~~	~~0.35~~
~~TXD01H (filter, wet-boiled)~~	~~-28.5˚C < T < -19˚C~~	~~-28412.092220119186~~	~~-6043.63511549024~~	~~-511.44780894398167~~	~~-21.530974485881597~~	~~-0.4508541686398098~~	~~-0.003757133824947974~~	~~0.99~~	~~0.59~~
~~TXD05 (bulk)~~	~~-28.5˚C < T < -10˚C~~	~~-50.023271755289954~~	~~-16.04573078900857~~	~~-1.6173561828000045~~	~~-0.08074357074021918~~	~~-0.0019357893701810924~~	~~-1.8076791589170566e-05~~	~~0.64~~	~~0.35~~
~~TXD05H (bulk)~~	~~-27˚C < T < -9.5˚C~~	~~-28.41132102063094~~	~~-9.820913042395558~~	~~-0.9094936795258034~~	~~-0.03972654718668897~~	~~-0.0007636244274088211~~	~~-5.200001963207848e-06~~	~~0.99~~	~~0.33~~
TXD05 (filter)	-28.5˚C < T < -14˚C	-313.3058252180446	-75.912698717769	-6.9043325932941 1~~35~~	-0.30470826275283 3~~64~~	-0.00646068282529837~~2~~	-5.27553644987649~~44~~e-05	0.62	0.42
~~TXD05H (filter, dry-heated)~~	~~-27˚C < T < -14˚C~~	~~-452.01181238097746~~	~~-117.32306672273883~~	~~-11.762368934161058~~	~~-0.5836182871815891~~	~~-0.014288215373972207~~	~~-0.0001386700575218297~~	~~0.97~~	~~0.41~~
~~TXD05H (filter, wet-boiled)~~	~~-27˚C < T < -19.5˚C~~	~~41020.3220707645~~	~~9026.327490224949~~	~~791.3895483931685~~	~~34.55111220994813~~	~~0.7512394301270052~~	~~0.00650767203399298~~	~~0.97~~	~~0.61~~
Field_ Median	-25˚C < T < -5˚C	-29.647010567958~~052~~	-16.3170583864393~~28~~	-2.30949598965458~~2~~	-0.1625704680712~~0043~~	-0.005523933523123 53~~8~~	-7.23939690197926e-05	0.94	0.52
~~Field_Max~~	~~-25˚C < T < -5˚C~~	~~-33.22332405003339~~	~~-17.91894068815357~~	~~-2.537870078194984~~	~~-0.17808422538269214~~	~~-0.006028509490726683~~	~~-7.87080475404568e-05~~	~~0.93~~	~~0.53~~
~~Field_Min~~	~~-25˚C < T < -5˚C~~	~~-3.6982332795064234~~	~~-5.347998607534987~~	~~-0.6782792077804785~~	~~-0.04122346827949928~~	~~-0.0011424218790211352~~	~~-1.193966078225184e-05~~	~~0.99~~	~~0.44~~

S6. List of abbreviations

- AIDA: aerosol interaction and dynamics in the atmosphere
- APS: aerosol particle sizer
- BET: Brunauer-Emmett-Teller
- CI95%: 95% confidence intervals
- $C_{\mathrm{INP}}(T)$: nucleus concentration in ultrapure water suspension
- CPC: condensation particle counter
- DF: dilution factor
- DFPC: dynamic filter processing chamber
- D_{ve}: volume equivalent diameter
- $f_{unfrozen}(T)$: ratio of the number of droplets unfrozen to the total number of droplets
- ICR: ice crystal residual
- IN: ice nucleation
- INP: ice-nucleating particle
- INSEKT: IN spectrometer of the Karlsruhe Institute of Technology
- LAAPTOF: laser ablation aerosol particle time-of-flight mass spectrometer
- MED: minimum entropy decomposition
- M_{ve}: mass of a spherical particle of volume equivalent diameter
- $n_{\mathrm{INP}}(T)$: INP concentration per unit standard air volume as a function of temperature
- $n_{\mathrm{m}}(T)$: INP concentration per unit particle mass as a function of temperature
- $n_{\mathrm{s,geo}}(T)$: INP concentration per unit geometric particle surface area as a function of temperature
- O14: O'Sullivan *et al*. (2014)
- OLLF: open-lot livestock facility
- OTU: operational taxonomic unit
- PFS: polycarbonate filter sampler
- PM: particulate matter
- PM_x = particulate matter smaller than x μm in diameter
- r: correlation coefficient
- RH: relative humidity
- S16: Steinke *et al*. (2016)
- S20: Steinke et al. (2020)
- SI: Supplemental Information
- SMPS: scanning mobility particle sizer
- SSA: specific surface area
- $S_{\mathrm{total}}/M_{\mathrm{total}}$: geometric specific surface area
- STP: standard temperature and pressure
- Su18: Suski et al. (2018)
- T14: Tobo et al. (2014)
- TEOM: tapered-element oscillating microbalance
- U17: Ullrich *et al*. (2017)
- V_{air}: sampled air volume
- V_d: volume of the sample in a well
- V_{l}: suspension liquid volume
- WT-CRAFT: West Texas cryogenic refrigerator applied to freezing test system

SI References

- ~~S. Angelino, D. T. Suess, K. A. Prather, Formation of aerosol particles from reactions of secondary and tertiary alkylamines: Characterization by aerosol time-of-flight mass spectrometry. *Environ. Sci. Technol*. **35**, 3130–3138 (2001).~~
- ~~S. Benz et al., *T*-dependent rate measurements of homogeneousice nucleation in cloud droplets using a large atmospheric simulation chamber. *J. Photoch. Photobio*. A. **176**, 208–217 (2005).~~
- ~~J. E. Boulter et al. Design and performance of a pumped counterflow virtual impactor. *Aerosol. Sci. Technol*. **40**, 969–976 (2006).~~
- ~~F. Chaucheyras-Durand, F. Ossa, REVIEW: The rumen microbiome: Composition, abundance, diversity, and new investigative tools. *The Professional Animal Scientist*. **30**, 1–12 (2014).~~
- ~~P. J. DeMott et al., Comparative measurements of ambient atmospheric concentrations of ice nucleating particles using multiple immersion freezing methods and a continuous flow diffusion chamber. *Atmos. Chem. Phys*. **17**, 11227–11245 (2017).~~
- ~~V. R. Després et al., Primary biological aerosols in the atmosphere: A review of observations and relevance. *Tellus B*. **64**, 15598, https://doi.org/10.3402/tellusb.v64i0.15598 (2012).~~
- ~~D. E. Fouts et al., Next generation sequencing to define prokaryotic and fungal diversity in the bovine rumen. *PLoS One*. **7**, e48289, https://doi.org/10.1371/journal.pone.0048289 (2012).~~
- ~~N. Hiranuma, S. D. Brooks, J. Gramann, B. W. Auvermann, High concentrations of coarse particles emitted from a cattle feeding operation. *Atmos. Chem. Phys.* **11**, 8809–8823 (2011).~~
- ~~N. Hiranuma et al., A comprehensive laboratory study on the immersion freezing behavior of illite NX particles: a comparison of 17 ice nucleation measurement techniques. *Atmos. Chem. Phys.* **15**, 2489–2518 (2015).~~
- ~~N. Hiranuma et al., Development and characterization of an ice-selecting pumped counterflow virtual impactor (IS-PCVI) to study ice crystal residuals. *Atmos. Meas. Tech*. **9**, 3817–3836 (2016).~~
- ~~N. Hiranuma et al., A comprehensive characterization of ice nucleation by three different types of cellulose particles immersed in water. *Atmos. Chem. Phys*. **19**, 4823–4849 (2019).~~
- ~~D. M. Murphy et al., Single-particle mass spectrometry of tropospheric aerosol particles. *J. Geophys. Res.-Atmos*. **111**, D23S32, https://doi.org/10.1029/2006JD007340 (2006).~~
- ~~National Research Council. “Minerals” in *Nutrient Requirements of Beef Cattle: Seventh Revised Edition: Update 2000* (The National Academies Press, 2000), pp. 54–69.~~
- ~~R. Ocsay, I. Salma, W. Wang, W. Maenhaut, Characterization and diurnal variation of size-resolved inorganic water soluble ions at a rural background site. *J. Environ. Monitor.* **8**, 300–306 (2006).~~
- ~~K. A. Pratt, L. E. Hatch, K. A. Prather, Seasonal volatility dependence of ambient particle phase amines. *Environ. Sci. Technol*. **43**, 5276–5281 (2009).~~
- ~~S. Sarrocco, Dung-inhabiting fungi: a potential reservoir of novel secondary metabolites for the control of plant pathogens. *Pest. Manag. Sci*. **72**, 643–652 (2016).~~
- ~~T. Schiebel, Ice nucleation activity of soil dust aerosols. Thesis, Karlsruhe Institute of Technology, https://doi.org/10.5445/IR/1000076327 (20 October 2017).~~
- ~~S. Schmidt et al., Online single particle analysis of ice particle residuals from mountain-top mixed-phase clouds using laboratory derived particle type assignment. *Atmos. Chem. Phys.* **17**, 575–594 (2017).~~
- ~~J. Schneider et al., Mass-spectrometric identification of primary biological particle markers and application to pristine submicron aerosol measurements in Amazonia. *Atmos. Chem. Phys.* **11**, 11415–11429 (2011).~~

- ~~X. Shen et al., Laser ablation aerosol particle time-of-flight mass spectrometer (LAAPTOF): Performance, reference spectra and classification of atmospheric samples. *Atmos. Meas. Tech*. **11**, 2325–2343 (2018).~~
- ~~X. Shen et al., Understanding of atmospheric aerosol particles with improved particle identification and quantification by single particle mass spectrometry. *Atmos. Meas. Tech*. **12**, 2219–2240 (2019).~~
- ~~P. J. Silva, R. A. Carlin, K. A. Prather, Single particle analysis of suspended soil dust from Southern California. *Atmos. Environ*. **34**, 1811–1820 (2000).~~
- ~~G. Vali, Quantitative evaluation of experimental results on the heterogeneous freezing nucleation of supercooled liquids. *J. Atmos. Sci.* **28**, 402–409 (1971).~~
- ~~M. A. Zawadowicz, K. D. Froyd, D. Murphy, D. J. Cziczo, Improved identification of primary biological aerosol particles using single particle mass spectrometry. *Atmos. Chem. Phys*. **17**, 7193–7212 (2017).~~

S. Angelino et al., Formation of aerosol particles from reactions of secondary and tertiary alkylamines: Characterization by aerosol time-of-flight mass spectrometry. *Environ. Sci. Technol*. **35**, 3130–3138 (2001).

J. Bush et al., Increasing stocking density reduces emissions of fugitive dust from cattle feedyards. *Applied Engineering in Agriculture* **30**, 815–824 (2014).

B. C. Christner et al., Ubiquity of biological ice nucleators in snowfall. *Science* **319**, 1214, https://doi.org/10.1126/science.1149757 (2008).

N. A. Cole et al., Chemical composition of pen surface layers of beef cattle feedyards. *Professional Animal Scientist* **25**, 541–552 (2009).

F. Conen et al., Biological residues define the ice nucleation properties of soil dust. *Atmos. Chem. Phys*. **11**, 9643–9648 (2011).

P. J. DeMott et al., Predicting global atmospheric ice nuclei distributions and their impacts on climate. *Proc. Natl. Acad. Sci. U.S.A.* **107,** 11217–11222 (2010).

R. C. Edgar et al., UCHIME improves sensitivity and speed of chimera detection. *Bioinformatics* **27**, 2194–2200 (2011).

A. M. Eren et al., Oligotyping: differentiating between closely related microbial taxa using 16s rRNA gene data. *Methods, Ecol. Evol*. **4**, 1111–1119 (2013).

A. M. Eren et al., Minimum entropy decomposition: Unsupervised oligotyping for sensitive partitioning of high-throughput marker gene sequences. *The ISME Journal* **9**, 968–979 (2015).

S. K. Henderson-Begg et al., Terrestrial and airborne non-bacterial ice nuclei. *Atmosph. Sci. Lett*. **10**, 215–219 (2009).

T. C. J. Hill et al., Sources of organic ice nucleating particles in soils. *Atmos. Chem. Phys*. **16**, 7195–7211 (2016).

N. Hiranuma et al., High concentrations of coarse particles emitted from a cattle feeding operation. *Atmos. Chem. Phys.* **11**, 8809–8823 (2011).

T. L. Humphreys et al., Sensitivity of Partially Purified Ice Nucleation Activity of Fusarium acuminatum SRSF 616. *Curr. Microbiol*. **42**, 330–338 (2001).

C. E. Morris et al., Ice nucleation active bacteria and their potential role in precipitation. *J. Phys. IV France* **121**, 87–103 (2004).

D. M. Murphy et al., Single-particle mass spectrometry of tropospheric aerosol particles. *J. Geophys. Res.-Atmos*. **111**, D23S32, https://doi.org/10.1029/2006JD007340 (2006).

National Research Council, “Minerals” in *Nutrient Requirements of Beef Cattle: Seventh Revised Edition: Update 2000* (The National Academies Press). pp. 54–69 (2000).

R. Ocsay et al., Characterization and diurnal variation of size-resolved inorganic water soluble ions at a rural background site. *J. Environ. Monitor.* **8**, 300–306 (2006).

D. O'Sullivan et al., Ice nucleation by fertile soil dusts: relative importance of mineral and biogenic components. *Atmos. Chem. Phys*. **14**, 1853–1867 (2014).

H. Patashnick, and E. G. Rupprecht, Continuous PM-10 measurements using the tapered element oscillating microbalance. *Journal of the Air and Waste Management Association* **41**, 1079–1083 (1991).

K. A. Pratt et al., Seasonal volatility dependence of ambient particle phase amines. *Environ. Sci. Technol*. **43**, 5276–5281 (2009).

T. Rognes et al., VSEARCH: a versatile open source tool for metagenomics. *Peer J*. **4**, e2584, https://doi.org/10.7717/peerj.2584 (2016).

T. Schiebel, Ice nucleation activity of soil dust aerosols. Thesis, Karlsruhe Institute of Technology, 131 pp., https://doi.org/10.5445/IR/1000076327 (20 October 2017).

S. Schmidt et al., Online single particle analysis of ice particle residuals from mountain-top mixed-phase clouds using laboratory derived particle type assignment. *Atmos. Chem. Phys.* **17**, 575–594 (2017).

J. Schneider et al., Mass-spectrometric identification of primary biological particle markers and application to pristine submicron aerosol measurements in Amazonia. *Atmos. Chem. Phys.* **11**, 11415–11429 (2011).

X. Shen et al., Laser ablation aerosol particle time-of-flight mass spectrometer (LAAPTOF): Performance, reference spectra and classification of atmospheric samples. *Atmos. Meas. Tech*. **11**, 2325–2343 (2018).

X. Shen et al., Understanding of atmospheric aerosol particles with improved particle identification and quantification by single particle mass spectrometry. *Atmos. Meas. Tech*. **12**, 2219–2240 (2019).

P. J. Silva et al., Single particle analysis of suspended soil dust from Southern California. *Atmos. Environ*. **34**, 1811–1820 (2000).

I. Steinke et al., Ice nucleation activity of agricultural soil dust aerosols from Mongolia, Argentina, and Germany. *J. Geophys. Res.-Atmos*. **121**, 13559–13576 (2016).

I. Steinke et al., Complex plant-derived organic aerosol as ice-nucleating particles – more than the sums of their parts? *Atmos. Chem. Phys.* **20**, 11387–11397 (2020).

K. J. Suski et al., Agricultural harvesting emissions of ice-nucleating particles. *Atmos. Chem. Phys*. **18**, 13755–13771 (2018).

W. Szyrmer, and I. Zawadzki, Biogenic and anthropogenic sources of ice-forming nuclei: A review. *Bull. Am. Meteorol. Soc*. **78**, 209–228 (1997).

Y. Tobo et al., Organic matter matters for ice nuclei of agricultural soil origin. *Atmos. Chem. Phys*. **14**, 8521–8531 (2014).

R. Ullrich et al., A new icenucleation active site parameterization for desert dust and soot. *J. Atmos. Sci*. **74**, 699–717 (2017).

M. A. Zawadowicz et al., Improved identification of primary biological aerosol particles using single particle mass spectrometry. *Atmos. Chem. Phys*. **17**, 7193–7212 (2017).